Probing Hidden Monopole Dark Matter through Axion Portal Coupling

アクシオンポータルによる隠れたモノポール暗黒物質の探究

Thesis for the Degree of Doctor of Philosophy

Ho Shu-Yu

Department of Physics, Tohoku University

Advisor : Prof. Fuminobu Takahashi

Submitted : 08/12/2020

TOHOKU UNIVERSITY

GPPU GRADUATE PROGRAM ON PHYSICS FOR THE UNIVERSE

宇宙創成物理学
国際共同大学院

Abstract

In this thesis, we explore the monopole dark matter (DM) emerging from a spontaneous breakdown of non-Abelian gauge symmetry in the hidden sector. We focus on a scenario where this hidden monopole DM was produced as a topological defect during a second-order phase transition in the early era of the universe. It is known that the direct detection search for such monopole DM is formidable due to its feeble interactions with the standard model particles in the minimal form. In our framework, we then introduce an axion-like particle (ALP), a, connecting the hidden monopole DM and the standard model particles, and examine the current limits and the future prospects from DM direct detection searches and beam-dump experiments. We find two parameter regions around $(m_a/\mathrm{MeV}, f_a/\mathrm{GeV}) = \mathcal{O}(10, 10^5)$ and $\mathcal{O}(100, 10^4)$ where the hidden monopole DM and the ALP are respectively within the reach of the future experiments such as PICO-500 and SHiP. We also point out that the hidden photons mainly produced by the decay of ALP contribute to dark radiation with $\Delta N_{\mathrm{eff}} \simeq 0.6$ which can relax the tension for the recent measurements of the Hubble parameter H_0.

Keywords : Hidden monopole dark matter, Axion-like particle, Direct detection searches, Beam-dump experiments, H_0 tension.

List of Publications

- Hidden Monopole Dark Matter via Axion Portal and its Implications for Direct Detection Search, Beam-Dump experiments, and the H_0 tension,
  Ryuji Daido (Tohoku U.), Shu-Yu Ho (Tohoku U.), Fuminobu Takahashi (Tohoku U.),
  JHEP 01 (2020) 185, arXiv : 1909.03627 [hep-ph].

- Relaxing the Cosmological Moduli Problem by Low-scale Inflation,
  Shu-Yu Ho (Tohoku U.), Fuminobu Takahashi (Tohoku U.), Wen Yin (KAIST),
  JHEP 1904 (2019) 149, arXiv : 1901.01240 [hep-ph].

- Cosmological Adiabatic Conversion between the QCD axion and ALP Dark Matter,
  Shu-Yu Ho (Tohoku U.), Ken'ichi Saikawa (Max Planck Inst.),
  Fuminobu Takahashi (Tohoku U.),
  JCAP 1810 (2018) no.10, 042, arXiv : 1806.09551 [hep-ph].

∗ This thesis is based on the above publications, mainly the first one.

Contents

List of Figures

List of Tables

Chapter 0

Overview of the Thesis

0.1 Motivation

The standard model (SM) of particle physics is a marvelously successful theory describing almost all the experiments in a very high precision. Nonetheless, in cosmology, there are still some mysteries that are not revealed in the SM. Dark matter (DM) is one of the palpable evidence of physics beyond the SM. It makes up about a quarter of the present energy budget of the universe. It is also known to play a crucial role in structure formation. However, what DM is made of remains one of the great enigmas in particle physics and cosmology.

One of the peculiar properties of DM is its stability. Its lifetime must be at least an order of magnitude longer than the present age of the universe. The stability of DM may be ensured by symmetries. For instance, in the WIMP scenario, the DM is usually stabilized by discrete symmetries. However, it is believed that no global symmetry can exist in a theory of quantum gravity. On the other hand, the DM may be stable due to its longevity. For example, the QCD axion and axion-like particles are in such a category. Also, it is possible that the stability of DM is achieved by an unbroken gauge symmetry. One such example is a magnetic monopole in the hidden sector,[1] which is the main interest of this thesis.

A magnetic monopole is a topological defect which arises associated with the spontaneous breaking of a gauge symmetry $\mathcal{G}$ down to $\mathcal{H}$ with a non-trivial $\pi_2(\mathcal{G}/\mathcal{H})$. The simplest example is the ′t Hooft-Polyakov monopole [1,2] with $\mathcal{G} = \mathrm{SU}(2)$ and $\mathcal{H} = \mathrm{U}(1)$, and it is the magnetic charge under the U(1) gauge symmetry that makes the magnetic monopole absolutely stable. If there exists a hidden sector which includes such a gauge symmetry and its subsequent spontaneous breaking allows a monopole solution. Then, hidden monopoles are necessarily created at the phase transition and contribute to DM.

The hidden monopole is a feasible DM candidate. However, it is formidable to search

[1] A hidden sector (sometimes it is also called the dark sector) is a sector containing some hypothetical particles which is weakly coupled to or completely decoupled from the SM sector.

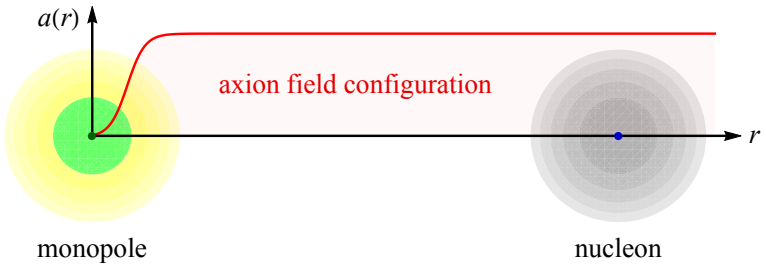

Figure 1: The field configuration of the axion around the monopole.

for it directly by experiments since its couplings to the SM particles are weak. In fact, in the minimal form of the hidden monopole DM model, it is totally decoupled from the SM sector at a renormalizable level. The setup can be extended to couple the monopole to the SM sector through the Higgs, vector, or axion portal coupling. Actually, the Higgs portal coupling was assumed in Refs. [3, 4] in order to keep the hidden sector in thermal equilibrium with the SM plasma. The monopole can interact with the nucleon via the Higgs portal coupling. However, the expected monopole-nucleon scattering cross-section is far below the sensitivities of any DM direct detection experiments in the foreseeable future. On the other hand, the hidden monopole acquires a tiny electric charge through the vector portal coupling. The mini-charged DM is stringently constrained by various experiments and observations [5]. We will come back to these possibilities later in this thesis. Our main focus is the axion portal coupling. By solving the equation of motion of a massive axion, $a(r)$, with the Witten effect [6], we find the field configuration of the axion around the hidden monopole and compute the monopole-nucleon spin-dependent elastic scattering cross-section, see Fig. 1. Furthermore, axions can be probed by beam-dump experiments such as SHiP. As we shall see later, we find two parameter regions with the axion mass and decay constant given by $(m_a/\mathrm{MeV}, f_a/\mathrm{GeV}) = \mathcal{O}(10, 10^5)$ and $\mathcal{O}(100, 10^4)$, where the hidden monopole DM and the axion are within the reach of the DM direct searches and the beam-dump experiments, respectively.

0.2 Organization

The structure of this thesis is as follows. In Ch. 1, we briefly review the SM, modern cosmology, and some unsolved problems in Sec. 1.1, and mention a couple of appealing DM candidates in Sec. 1.2. In Ch. 2, we introduce the ′t Hooft-Polyakov model and the Witten effect in Sec. 2.1, and discuss the production mechanism of the hidden monopole DM and possible portal couplings to detect them in Sec. 2.2 and Sec. 2.3. In Ch. 3, we show how to calculate the scattering cross-section of monopole and nucleon via axion portal coupling and then compare with the limits from the DM direct searches. In Ch. 4, we employ our results to the beam-dump experiments and the other constraints. A conclusion is given in Ch. 5. Some cumbersome derivations are presented in the appendices.

Chapter 1

Introduction

1.1 Description of the Universe

It goes without saying that the SM of particle physics is a remarkable theory as it precisely describes the microscopic world, while the discovery of the Higgs boson at the Large Hadron Collider (LHC) was a tremendous triumph of the SM [7, 8]. On the other hand, with the unprecedented precision measurements of the anisotropies of the cosmic microwave background (CMB) [9], the ΛCDM model in the cosmology is widely accepted as a successful theory describing the universe. However, there are still thorny problems and issues that cannot be explained well by the SM. In the following, we will first give a brief introduction of the SM, ΛCDM model, and some unsolved problems, and then discuss one of the problems, DM, in the second part of this chapter.

1.1.1 The Standard Model of Particle Physics

The SM of particle physics is based on the gauge theory with the symmetry group $\mathcal{G}_{\rm SM} = \mathrm{SU}(3)_C \otimes \mathrm{SU}(2)_L \otimes \mathrm{U}(1)_Y$ plus spontaneous symmetry breaking, which gives the masses of the elementary particles and the fundamental interactions between them. In this model, we have three generations of spin 1/2 matter fields, quarks $(u, d), (c, s), (t, b)$ and leptons $(e, \nu_e), (\mu, \nu_\mu), (\tau, \nu_\tau)$, and their forces are carried by spin 1 particles called gauge bosons. The quarks and leptons have the weak and electromagnetic interactions, which are carried by massive vector bosons $W^\pm$ and Z^0, and by photon γ, respectively. The quarks also have the strong interaction, which is carried by gluons G. In addition to these interactions, there is a gravitational force as well. However, it is not formulated as part of the SM, and no one has discovered the graviton yet. Nevertheless, its classical counterpart, gravitational waves, was detected by LIGO and Virgo collaboration [10]. To explain the masses of the SM particles, we also introduce a spin 0 scalar field H called the Higgs field. The gauge representation assignments of the SM fields are summarized

Table 1.1: The gauge representation assignments of the SM fields, here we only show one generation of the matter fields for simplicity, and the subscripts L and R are chiralities.

	$Q_L = \begin{pmatrix} u_L \\ d_L \end{pmatrix}$	u_R	d_R	$E_L = \begin{pmatrix} \nu_{eL} \\ e_L \end{pmatrix}$	e_R	G	W	B	$H = \begin{pmatrix} \phi^+ \\ \phi^0 \end{pmatrix}$
$\mathrm{SU(3)_C}$	**3**	**3**	**3**	**1**	**1**	**8**	**1**	**1**	**1**
$\mathrm{SU(2)}_L$	**2**	**1**	**1**	**2**	**1**	**1**	**3**	**1**	**2**
$\mathrm{U(1)}_Y$	1/3	4/3	−2/3	−1	−2	0	0	0	1

in Tab. 1.1, where G, W, and B are gauge bosons of the gauge group $\mathrm{SU(3)_C}, \mathrm{SU(2)}_L$, and $\mathrm{U(1)}_Y$, respectively, and the electric charge Q of a particle is defined by its third component of weak isospin T_3 and hypercharge Y via the relation $Q = T_3 + Y/2$.

Before the electroweak symmetry breaking, all the SM fermions and gauge bosons are massless. When the temperature of the universe falls below the electroweak scale, the vacuum expectation value of the Higgs field $\langle H \rangle$ starts to develop a non-zero value and gradually reaches to the present value $v \simeq 246\,\mathrm{GeV}$. At the same time, the symmetry group $\mathcal{G}_{\mathrm{SM}}$ breaks down to $\mathrm{SU(3)_C} \otimes \mathrm{U(1)_{EM}}$, where EM refers to the electromagnetic interaction. In the Higgs vacuum state, three degrees of freedom (Goldstone bosons) of the Higgs doublet are absorbed by $W^\pm$ and Z^0 gauge bosons to form their longitudinal components, then they become massive, while γ remains massless corresponding to the unbroken $\mathrm{U(1)_{EM}}$ symmetry. On the other hand, the SM fermions acquire their masses through the Yukawa couplings to the Higgs field, and the Higgs boson obtains the mass via its self-interaction. The above phenomenon is known as the Higgs mechanism [11–13].

The SM also provides the source of CP-violation observed in kaon decays [14]. When we make a unitary transformation for the quark flavor eigenstates into the quark mass eigenstates (the eigenstates where the mass matrices of quark are diagonal) in the SM Lagrangian, there is a product of two unitary matrices which cannot be removed in the quark-W boson interactions. This product of the two unitary matrices is the celebrated Cabibbo-Kobayashi-Maskawa (CKM) matrix [15]. In the case of two families of quarks, the elements in the CKM matrix are real numbers. However, if the families of quarks is greater than two, the elements of the CKM matrix are complex numbers. For instance, in the SM with three families of quarks, the CKM matrix can be parameterized by three angles and one CP-violating complex phase angle. In the lepton sector, there is no such matrix as neutrinos are assumed to be massless in the SM. However, the phenomena of neutrino oscillations show that they have small masses. To describe the neutrino mixing and CP-violation, a matrix similar to the CKM matrix is introduced, which is called the Pontecorvo-Maki-Nakagawa-Sakata matrix [16, 17]. On the other hand, there is another source of CP-violation in the strong interaction. We will discuss it in the later section.

1.1.2 The Modern Cosmology : ΛCDM model

From the large scale observations of the universe, the spatial distribution of matter such as galaxies or clusters of galaxies is homogeneous and isotropic on average. Given the assumption of homogeneity and isotropy of space, one can describe the universe by the so-called Friedmann-Lemaître-Robertson-Walker (FLRW) metric given as

$$ds^2 \;=\; dt^2 - R(t)^2\left[\frac{dr^2}{1-kr^2} + r^2\big(d\theta^2 + \sin^2\theta\, d\phi^2\big)\right] \;, \tag{1.1}$$

where $R(t)$ represents the scale factor that depends on the cosmic time t, (r, θ, ϕ) is the spherical coordinate, and k is the spatial curvature which is positive, zero, and negative in open, flat, and closed universe, respectively.

The expansion of the universe is governed by the Einstein field equations

$$\mathcal{R}_{\mu\nu} - \frac{1}{2} g_{\mu\nu}\mathcal{R} \;=\; 8\pi G_{\rm N}\mathcal{T}_{\mu\nu} \;, \tag{1.2}$$

where $\mathcal{R}_{\mu\nu}$ is the Ricci curvature tensor, $\mathcal{R} = g^{\mu\nu}\mathcal{R}_{\mu\nu}$ is the Ricci scalar, $G_{\rm N}$ is the Newton's gravitational constant, and $\mathcal{T}_{\mu\nu}$ is the energy momentum tensor. The assumption of the isotropy imposes that one can always choose a coordinate system in which $\mathcal{T}_{\mu\nu}$ is diagonal and its spatial components are equal. On the other hand, the homogeneity requires that the components of $\mathcal{T}_{\mu\nu}$ only depend on the time in the same coordinate system. These facts suggest that one can express $\mathcal{T}_{\mu\nu}$ in the form of the ideal (perfect) fluid with the energy density $\rho = \rho(t)$ and pressure $P = P(t)$ as

$$\mathcal{T}_{\mu\nu} \;=\; \mathrm{diag}\big(\rho, P, P, P\big) \;, \tag{1.3}$$

and from the first law of thermodynamic $dE = -PdV$ (assume the universe is flat and expands adiabatically), we have $d(\rho R^3) = -PdR^3$, or

$$\dot{\rho} \;=\; -\frac{3\dot{R}}{R}\big(\rho + P\big) \;. \tag{1.4}$$

The energy density and pressure of an ideal fluid are related by the equation of state $\omega = P/\rho$, where we take ω time-independent for simplicity. Through this relation, one can find $\rho \propto R^{-3(1+\omega)}$. With Eqs. (1.1) and (1.3), the temporal component $(\mu, \nu) = (0, 0)$ of the Einstein field equations gives the Friedmann equation

$$H^2 + \frac{k}{R^2} \;=\; \frac{8\pi G_{\rm N}}{3}\rho \;, \tag{1.5}$$

here $H = \dot{R}/R$ is the Hubble parameter, and the spatial component $(\mu, \nu) = (j, j)$ gives

$$\frac{\ddot{R}}{R} \;=\; -\frac{4\pi G_{\rm N}}{3}\big(\rho + 3P\big) \;, \tag{1.6}$$

which is called the acceleration equation. Note that (1.5) has been used in deriving (1.6).

Based on the cosmological observations, it is known that our universe is filled with radiation (γ), matter (m), and the cosmological constant (Λ). The equations of state and behaviors of energy density for these components are summarized below

$$\begin{cases} \text{Radiation} & \omega = 1/3 \,, & \rho_\gamma \propto R^{-4} \\ \text{Matter} & \omega = 0 \,, & \rho_{\rm m} \propto R^{-3} \\ \text{Cosmological constant} & \omega = -1 \,, & \rho_\Lambda \propto \text{constant} \end{cases} .$$

From the acceleration equation, it is easy to see that the radiation and matter decelerate the expansion of the universe ($\ddot{R} < 0, P > 0$), and the cosmological constant accelerates the expansion of the universe ($\ddot{R} > 0, P < 0$). If the universe is flat and dominated by one of these components, then one can find the behaviors of the scale factor by using the Friedmann equation as

$$\begin{cases} \text{Radiation-dominated epoch} & R \propto t^{1/2} \,, & H = 1/(2t) \\ \text{Matter-dominated epoch} & R \propto t^{2/3} \,, & H = 2/(3t) \\ \text{Cosmological constant-dominated epoch} & R \propto e^{Ht} \,, & H = \left(8\pi G_{\rm N}\rho_\Lambda/3\right)^{1/2} \end{cases} ,$$

where the behaviors of the Hubble parameter are also shown. Now, gathering these three contributions, the Friedmann equation is written by

$$H^2 + \frac{k}{R^2} = \frac{8\pi G_{\rm N}}{3}\left(\rho_{\gamma,0}R^{-4} + \rho_{{\rm m},0}R^{-3} + \rho_{\Lambda,0}\right) , \tag{1.7}$$

where $\rho_{\gamma,0}, \rho_{{\rm m},0}$, and $\rho_{\Lambda,0}$ are the energy densities at the present time t_0 with $R(t_0) = 1$. It is convenient to express Eq. (1.7) in terms of the density parameters defined by

$$\Omega_\gamma \equiv \frac{\rho_{\gamma,0}}{\rho_{{\rm c},0}} \,, \quad \Omega_{\rm m} \equiv \frac{\rho_{{\rm m},0}}{\rho_{{\rm c},0}} \,, \quad \Omega_\Lambda \equiv \frac{\rho_{\Lambda,0}}{\rho_{{\rm c},0}} \,, \quad \Omega_k \equiv -\frac{k}{H_0^2} \,, \tag{1.8}$$

where $\rho_{{\rm c},0} \equiv 3H_0^2/(8\pi G_{\rm N})$ is the critical energy density today with $H_0 \simeq 70\,\text{km/sec/Mpc}$ being the Hubble constant. Then, with these definitions, Eq. (1.7) becomes

$$\frac{H^2}{H_0^2} = \Omega_\gamma R^{-4} + \Omega_{\rm m} R^{-3} + \Omega_k R^{-2} + \Omega_\Lambda \,, \tag{1.9}$$

which determines the evolution of the universe. From the latest CMB data measured by the Planck satellite, the density parameters are estimated as [9, 18]

$$\Omega_\gamma \simeq 5.44 \times 10^{-5} \,, \quad \Omega_{\rm m} \simeq 0.315^{+0.007}_{-0.007} \,, \quad \Omega_\Lambda \simeq 0.685^{+0.007}_{-0.007} \,, \quad \Omega_k \simeq 0.001^{+0.002}_{-0.002} \,, \tag{1.10}$$

which indicates that our universe is almost flat. As we will discuss later, the matter consists of the ordinary matter and cold dark matter (CDM). The cosmological model containing the Λ, CDM, and the ordinary matter is known as the ΛCDM model, which is an economical model consistent with most of the observations in the universe.

1.1.3 Thermodynamics of the Universe

In the early era of the universe, the SM particles are in thermal equilibrium with the common temperature T (conventionally, we adopt the temperature of photons). As the temperature decreases, the interaction rates of some of the SM particles become smaller than the expansion rate of the universe and then they decouple from the thermal bath. For instance, the interaction rates of the SM neutrinos with the thermal bath become equal to the Hubble expansion rate at the temperature of about 1 MeV. After that, the SM neutrinos evolve with their own temperature T_ν. In the following, we will show how to estimate the relation of T and T_ν by using the thermodynamics of the universe.

The energy density ρ and entropy density s of the universe are mainly contributed by relativistic particles. One can express them in terms of the photon temperature T as [19]

$$\rho(T) = \frac{\pi^2}{30} g_{*\rho}(T) T^4 , \quad s(T) = \frac{2\pi^2}{45} g_{*s}(T) T^3 , \tag{1.11}$$

with $g_{*\rho}$ (g_{*s}) being the effective relativistic energy (entropy) degrees of freedom given by

$$g_{*\rho}(T) = \sum_{m_X \ll T} C_X g_X \left(\frac{T_X}{T}\right)^4 , \quad g_{*s}(T) = \sum_{m_X \ll T} C_X g_X \left(\frac{T_X}{T}\right)^3 , \tag{1.12}$$

where the summation is over all relativistic degrees of freedom, m_X, T_X and g_X are the mass, temperatue and internal degrees of freedom of particle species X, respectively, and $C_X = 1$ for bosons and $C_X = 7/8$ for fermions. With Eq. (1.11), the Friedmann equation of the flat universe in the radiation-dominated era is written as

$$H^2 = \frac{4\pi^3 g_{*\rho}(T)}{45} \frac{T^4}{m_{\rm Pl}^2} , \tag{1.13}$$

where $m_{\rm Pl} = G_{\rm N}^{-1/2} = 1.22 \times 10^{19}\,\text{GeV}$ is the Planck mass, and $T \propto H^{1/2} \propto t^{-1/2}$ provided that $g_{*\rho}(T) \simeq$ constant (this is true if the temperature of the universe is high enough).

At the temperatures before the neutrino decoupling ($T_{\text{dec},\nu} \simeq 1\,\text{MeV}$), the relativistic particles are $\gamma, e^\pm, \nu$ and $\bar{\nu}$, and $e^\pm$ become non-relativisitc after $T_{\text{dec},\nu}$. Utilizing Eq. (1.4) and the second law of thermodynamics, one can show that $d(sR^3) = 0$, thus

$$s_\nu(T_1 > T_{\nu,\text{dec}}) R(t_1)^3 = s_\nu(T_\nu < T_{\nu,\text{dec}}) R(t_2)^3 , \tag{1.14}$$

$$s_{\gamma+e^\pm}(T_1 > T_{\nu,\text{dec}}) R(t_1)^3 = s_\gamma(T < T_{\nu,\text{dec}}) R(t_2)^3 , \tag{1.15}$$

where t_1 is the time before $T_{\nu,\text{dec}}$ at which $\gamma, e^\pm, \nu$ and $\bar{\nu}$ have the same temperature T_1, and t_2 is the time after $T_{\nu,\text{dec}}$ at which the neutrinos (photons) have temperature T_ν (T). With Eqs. (1.11), (1.14) and (1.15), it follows that

$$\frac{g_{*s,\nu}(T_1 > T_{\nu,\text{dec}}) T_1^3}{g_{*s,\gamma+e^\pm}(T_1 > T_{\nu,\text{dec}}) T_1^3} = \frac{g_{*s,\nu}(T_\nu < T_{\nu,\text{dec}}) T_\nu^3}{g_{*s,\gamma}(T < T_{\nu,\text{dec}}) T^3} , \tag{1.16}$$

where $g_{*s,\nu}(T_1 > T_{\nu,\mathrm{dec}}) = g_{*s,\nu}(T_\nu < T_{\nu,\mathrm{dec}}) = 21/4$, $g_{*s,\gamma+e^\pm}(T_1 > T_{\nu,\mathrm{dec}}) = 11/2$, and $g_{*s,\gamma}(T < T_{\nu,\mathrm{dec}}) = 2$. Plugging these numbers into Eq. (1.16), we find

$$\frac{T_\nu}{T} = \left(\frac{4}{11}\right)^{1/3} . \tag{1.17}$$

With this result, the effective relativistic energy degrees of freedom today is estimated as

$$g_{*\rho,0} = 2 + \frac{7}{8} \times 2 \times N_{\mathrm{eff}} \left(\frac{T_\nu}{T}\right)^4 = 2 + \frac{7}{4} N_{\mathrm{eff}} \left(\frac{4}{11}\right)^{4/3} , \tag{1.18}$$

where N_{eff} is defined as the effective number of neutrino species. The SM model predicts $N_{\mathrm{eff}} = 3.045$ [20], thus $g_{*\rho,0} \simeq 3.38$. Any deviation of N_{eff} from the SM value would bring a hint for the physics beyond the SM. Suppose there exists a hidden sector which has a portal coupling to the SM sector and assume that the hidden sector is always in thermal equilibrium and has at least one relativistic degrees of freedom characterized the hidden temperature T_{H}. Then, from Eqs. (1.11) and (1.18), we deduce

$$\Delta N_{\mathrm{eff}}(T) = \frac{4}{7} \left(\frac{T}{T_\nu}\right)^4 \Delta g_{*\rho}(T) , \tag{1.19}$$

with

$$\Delta g_{*\rho}(T) = \sum_{m_{\mathrm{H}} \ll T} C_{\mathrm{H}} g_{\mathrm{H}} \left(\frac{T_{\mathrm{H}}}{T}\right)^4 = \sum_{m_{\mathrm{H}} \ll T} C_{\mathrm{H}} g_{\mathrm{H}} \left[\frac{g_{*s,\mathrm{H}}(T_{\mathrm{H,dec}})}{g_{*s,\mathrm{H}}(T_{\mathrm{H}})} \frac{g_{*s,\mathrm{SM}}(T)}{g_{*s,\mathrm{SM}}(T_{\mathrm{H,dec}})}\right]^{4/3} , \tag{1.20}$$

where the summation is over all the relativistic degrees of freedom in the hidden sector, and $T_{\mathrm{H,dec}} > T_{\nu,\mathrm{dec}}$ is the temperature at which the hidden sector decoupled from the SM sector. Usually, $\Delta N_{\mathrm{eff}}(T)$ is estimated around $T \simeq T_{\nu,\mathrm{dec}} \simeq 1\,\mathrm{MeV}$ or below. Considering an example where the hidden sector has N_g gauge bosons, N_f chiral fermions, and N_{GB} Goldstone bosons which remain relativistic until the recombination epoch and decouple from the SM sector at the same time, then, from Eqs. (1.19) and (1.20), we have

$$\Delta N_{\mathrm{eff}}(T_{\nu,\mathrm{dec}}) = \left(\frac{8}{7} N_g + N_f + \frac{4}{7} N_{\mathrm{GB}}\right) \left[\frac{g_{*s,\mathrm{SM}}(T_{\nu,\mathrm{dec}})}{g_{*s,\mathrm{SM}}(T_{\mathrm{H,dec}})}\right]^{4/3} . \tag{1.21}$$

1.1.4 Unsolved Problems

The SM of particle physics and ΛCDM model can well describe a lot of phenomena of the subatomic world and the universe, respectively. The marriage of particle physics and cosmology can even let us understand the thermal history of the universe. Nevertheless, there are still some puzzles in the universe, and the SM provides no satisfactory answers to them. Here we enumerate and introduce some of the unsolved problems with possible solutions succinctly in the following.

• **Dark Matter** : The mass-to-light ratio of the cluster galaxies and the anomalous behavior of the galaxy rotation curves indicate that the universe is full of some invisible substance called dark matter (DM). One of the ways to estimate the current DM density is to use the CMB temperature and polarization anisotropies. The latest analysis gives $\Omega_{\rm DM} \simeq 0.26$ which is roughly five times larger than the present density of the ordinary matter (or baryonic matter) $\Omega_{\rm b} \simeq 0.05$ determined by big bang nucleosynthesis (BBN) and CMB [18]. Although the evidence of DM is overwhelming, there is no DM candidate in the SM. The cosmological observations show that DM should be cold or warm (non-relativistic) at the structure formation epoch, electrically neutral (or mini-charged), non-baryonic matter, and stable or with a lifetime much longer than the age of the universe. The discrepancy between N-body simulations and the structure of observed galactic halos also suggests that DM may possess sizable self-interactions. A bunch of DM models have been proposed in the past. We will discuss them in the next section.

• **Neutrino Mass** : The phenomenon of neutrino oscillations indicates that the SM neutrinos have small but non-negligible masses, which is inconsistent with the SM due to the absence of the right-handed neutrinos. Nevertheless, if the SM neutrino is Majorana particle (a fermion that is its own anti-particle) rather than Dirac particle, then its mass can be generated via a dimensional-5 operator (also called the Weinberg operator) as

$$\mathcal{O}_5 \propto \frac{1}{\Lambda_{\rm NP}} \left(\overline{E_L^{\rm c}} \widetilde{H}^*\right) \left(\widetilde{H}^\dagger E_L\right) + \text{h.c.} \ , \tag{1.22}$$

where $\Lambda_{\rm NP}$ is an energy scale of new physics, the superscript c is the charge conjugation, and $\widetilde{H} = i\sigma_2 H^*$ with σ_2 being the second Pauli matrix. Notice that this operator violates the lepton number by two units, $\Delta L = 2$. After the electroweak symmetry breaking, the Majorana neutrino mass is given by $m_\nu \sim v^2/\Lambda_{\rm NP}$, then $m_\nu \lesssim 0.1\,\text{eV}$ if $\Lambda_{\rm NP} \gtrsim 10^{15}\,\text{GeV}$. The SM neutrinos with the masses suppressed by the high energy scale of new physics is known as the seesaw mechanism [21].

• **Baryon Asymmetry** : The Dirac equation predicts that every fermion has its own anti-particle. Thus, one can expect that the Big Bang of the universe produced an equal amount of matter and anti-matter at the very beginning. Subsequently, the matter and anti-matter annihilate with each other into photons or other light particles. As a result, the universe would be flooded with radiation. However, it contradicts with our universe since the matter density dominates over the radiation density by the observations, while there is almost no anti-matter (it can only be created in cosmic rays or particle colliders). The up-to-date analysis of BBN and CMB show that the baryon-to-photon ratio [18]

$$\eta = \left.\frac{n_B - n_{\bar{B}}}{n_\gamma}\right|_{\rm today} \simeq 6 \times 10^{-10} \ , \tag{1.23}$$

where n_B ($n_{\overline{B}}$) and n_γ are the number densities of baryons (anti-baryons) and photons, respectively. One may think that this baryon asymmetry is merely an initial condition of

the universe. Even so, any pre-existing asymmetries before the period of inflation would be diluted by this exponential expansion of the universe.

A dynamical mechanism to generate the baryon asymmetry in the early universe is the so-called baryogenesis. One of the criteria (known as the Sakharov's conditions [22]) to accomplish successful baryogenesis is the existence of CP violation. However, the CP violation in the SM is insufficient to reach the required value of η [23–25] and the electroweak baryogenesis is failed in the framework of the SM [26]. Leptogenesis is an alternative way to generate matter-anti-matter asymmetry [27,28]. Through the sphaleron processes [29], an imbalance of the number of leptons and anti-leptons can transfer to an imbalance of the number of baryons and anti-baryons. A model with the Majorana neutrino mass terms mentioned above can accommodate a leptogenesis due to the lepton number violations.

• **The Strong CP problem** : As we already mentioned that CP is not a conserved quantity in nature. Therefore, it is allowed to construct a Lagrangian which violates CP symmetry. The theta term in quantum chromodynamics (QCD) is one of the examples which does not preserve CP symmetry, and it takes the form as

$$\mathcal{L}_{\rm QCD} = \bar{\theta}\frac{\alpha_s}{16\pi}\epsilon^{\mu\nu\rho\sigma}G^b_{\mu\nu}G^b_{\rho\sigma} \ , \tag{1.24}$$

where $\bar{\theta}$ is a dimensionless parameter, α_s is the strong fine structure constant, $G^b_{\mu\nu}$ is the gluon field strength tensor with a color index b, and $\epsilon^{\mu\nu\rho\sigma}$ is the anti-symmetric tensor with $\epsilon^{0123} = +1$. Notice that in the physical basis where all the quark masses are real, $\bar{\theta} = \theta_{\rm QCD} + \theta_{\rm weak}$ with $\theta_{\rm weak} = \arg\big(\Pi_q m_q\big)$. In this expression, the first term comes from the strong interaction and the second term comes form the electroweak interaction.

The magnitude of $\bar{\theta}$ is expected to be order one according to the Dirac naturalness. However, the measurements of the neutron electric dipole moment cap $|\bar{\theta}| < 10^{-10}$ [30]. The strong CP problem is why $\bar{\theta}$, coming from entirely different physics is so small.

The PQ (Peccei-Quinn) mechanism is one of the attractive solutions which can solve the strong CP problem [31,32], in which the vacuum expectation value of the QCD axion drives the value of $\bar{\theta}$ to zero dynamically, while it can act as DM as well. We will discuss the QCD axion in more detail in the next section.

• **Cosmological constant** : As we can see from (1.10), most of the energy budget of the universe is contributed by the cosmological constant, which has a negative pressure to push the universe outwards against the gravity of the matter. The cosmological constant is a vacuum energy density of empty space, and it is related to the notion of dark energy (or quintessence). However, the form of dark energy is left unknown.

From (1.8) and (1.10), one can estimate the energy density of the cosmological constant as $\rho_\Lambda = \Omega_\Lambda \rho_{\rm c,0} \sim 10^{-47}\,{\rm GeV}^4$. On the other hand, the Higgs condensation in the SM predicts the vacuum energy density to be about $\rho_{\rm vac} \sim \upsilon^4 \sim 10^9\,{\rm GeV}^4$, which is 56 orders of magnitude bigger than ρ_Λ. Without the fine-tuning, this huge hierarchy between ρ_Λ and $\rho_{\rm vac}$ is known as the cosmological constant problem.

1.2 Dark Matter Candidates

A variety of DM candidates have been proposed in the literature such as primordial black holes, massive compact halo objects, axions, weakly interacting massive particles, strongly interacting massive particles, sterile neutrinos, hidden photons, asymmetric DM, topological defects, and fuzzy DM, and so on. In the following, we will first introduce two of the papular DM candidates, weakly interacting massive particles and axions, and discuss some of the other possible DM candidates in the end of this section.

1.2.1 Weakly Interacting Massive Particles

By definition, weakly interacting massive particles (WIMP) are theoretical particles with the adequately large masses and with the couplings as weak as the weak strength. If a WIMP is stable on a cosmological time scale, then it can serve as a DM candidate. The WIMP can be thermally produced in the early universe after inflation. At high temperatures, the WIMP is in thermal equilibrium with other particles. As the universe cools down, at a certain time point, the interaction rates of WIMP and other particles become comparable to the expansion rate of the universe. Then, the WIMP is chemically decoupled (freeze-out) from the thermal bath while its comoving number density approaches a constant amount, see Fig. 1.1 for the demostration of the freeze-out mechanism.

To evaluate the current abundance of a WIMP DM, we have to solve the Boltzmann equation for the DM number density $n_{\rm DM}$, which can be written as

$$\frac{dn_{\rm DM}}{dt} + 3Hn_{\rm DM} \;=\; -\langle\sigma_{\rm ann}v_{\rm rel}\rangle_{\rm eff}\left[n_{\rm DM}^2 - \left(n_{\rm DM}^{\rm eq}\right)^2\right] \,, \tag{1.25}$$

where $\langle\sigma_{\rm ann}v_{\rm rel}\rangle_{\rm eff}$ is the thermal-averaged value of the effective annihilation cross-section times the relative speed of a DM pair, and $n_{\rm DM}^{\rm eq}$ is the equilibrium number density of DM. With the expression of $\langle\sigma_{\rm ann}v_{\rm rel}\rangle_{\rm eff}$, one can solve this Boltzmann equation numerically. However, the relic density of WIMP DM can be estimated approximately by the following relation [18, 19]

$$\Omega_{\rm WIMP}h^2 \;\simeq\; \frac{3\times10^{-27}\,{\rm cm}^3/{\rm s}}{\langle\sigma_{\rm ann}v_{\rm rel}\rangle_{\rm eff}} \;\simeq\; \frac{0.1\,{\rm pb}}{\langle\sigma_{\rm ann}v_{\rm rel}\rangle_{\rm eff}} \,, \tag{1.26}$$

where $h \simeq 0.7$ is the normalized Hubble constant, while the freeze-out temperature of DM is $T_f \simeq m_{\rm WIMP}/25$ with $m_{\rm WIMP}$ being the mass of WIMP DM. This implies that at freeze-out the WIMP DM is non-relativistic. Now, let us parametrize

$$\langle\sigma_{\rm ann}v_{\rm rel}\rangle_{\rm eff} \;=\; \frac{\alpha_{\rm ann}^2}{m_{\rm WIMP}^2} \,, \tag{1.27}$$

and take $\alpha_{\rm ann} \sim \alpha_{\rm weak} \sim 1/30$ and $m_{\rm WIMP}$ from a sub-GeV to TeV scale, where $\alpha_{\rm ann}$ is the coupling strength of the DM annihilation processes. Then, from (1.26), the correct order of relic density of DM can be obtained. This is called the WIMP miracle.

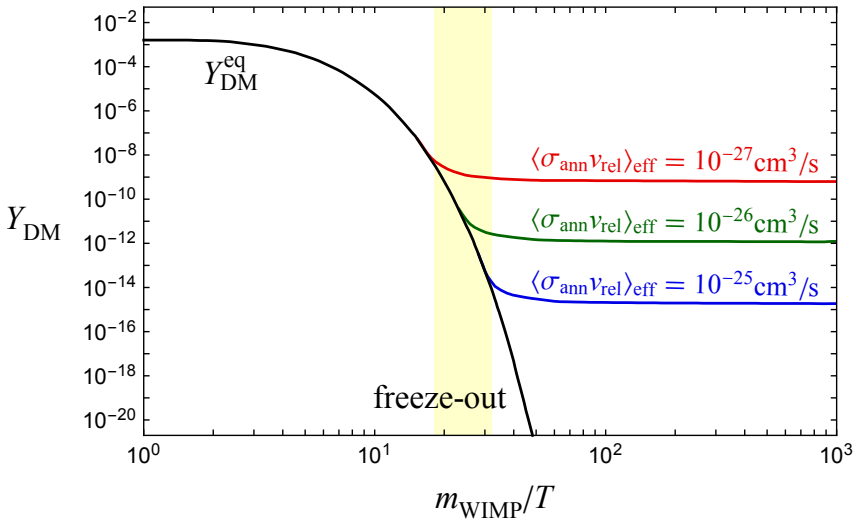

Figure 1.1: A demonstration of chemical freeze-out of WIMP DM with different values of $\langle\sigma_{\rm ann}v_{\rm rel}\rangle_{\rm eff}$, where $Y_{\rm DM} = n_{\rm DM}/s$ ($Y^{\rm eq}_{\rm DM} = n^{\rm eq}_{\rm DM}/s$) is the actual (equilibrium) comoving number denisty of DM, and the yellow shaded region is the freeze-out zone of WIMP DM.

A number of well-motivated WIMP DM models have been postulated. For example, the lightest R-odd superparticle in supersymmetric models with R-parity [33], the lightest T-odd particle in the little Higgs models with T-parity [34], and the lightest Kaluza-Klein particle with KK-parity in universal extra dimension [35], and so on.

Many underground experiments have been and are being performed to hunt WIMP DM directly. Most of these searches look for the recoil signal of nuclei induced by the elastic scattering of a WIMP DM off a nucleon. The r.m.s velocity of DM with respect to the center of our galaxy is expected to a few hundred kilometers per second at the location of our solar system, typically, around 220 km/s with density 0.3 GeV/cm^3. With these velocities, the nuclear recoil energy is of the order of 1 to 100 keV assuming that the WIMP mass is within the range of few GeV to few TeV.

Unveiling the spin of DM is one of the tasks of these underground experiments since DM could be a scalar boson, a vector boson, a Dirac fermion, a Majorana fermion, even a Rarita-Schwinger fermion. Based on the spin of WIMP DM, the elastic scattering cross-section of WIMP and nucleon can be distinguished into *spin-independent* (SI) couplings and *spin-dependent* (SD) couplings. The SI cross-sections are proportional to A^2, where A is the atomic mass number of the target material, e.g. Ge to Xe. On the other hand, the SD cross-sections are proportional to the nuclear spin factor $J(J+1)$, e.g. ^{19}F and ^{23}Na, etc. In Fig. 1.2, we present some of the calculated exclusion curves for SI WIMP-nucleon and SD WIMP-proton elastic scattering cross-sections as a function of WIMP mass at 90 % C.L. [36]. Besides these experiments, there are other searches using the annual forward-backward asymmetry of the nuclear recoil direction from the revolution of the earth around the sun such as DAMA/NaI and DAMA/LIBRA.

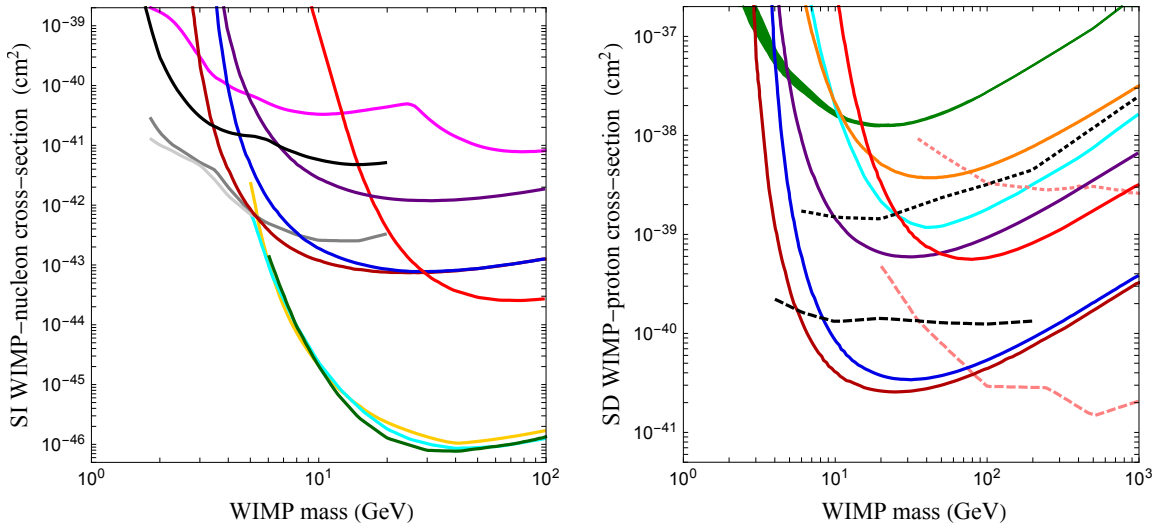

Figure 1.2: The 90% C.L. limits on the SI WIMP-nucleon and SD WIMP-proton elastic scattering cross-sections, where the color representatives are, PICO-60 C_3F_8 complete exposure (maroon), PICO-60 C_3F_8 first blind exposure (blue), PICO-60 CF_3I (red), PICO-2L (purple), DarkSide-50 low-mass (gray), LUX (yellow), XENON1T (green), PICASSO (green band), CRESST-II (magenta), CDMS-lite (black), SIMPLE (orange), PandaX-II (cyan), IceCube (dashed and dotted pink), and SuperK (dashed and dotted black) [36].

1.2.2 The QCD Axion and Axion-Like Particles

The QCD axion, ϕ, is a pseudo-Nambu-Goldstone boson associated with the spontaneous breakdown of a global axial U(1) Peccei-Quinn (PQ) symmetry [31, 32, 37, 38]. At energies below the scale of the PQ symmetry breaking and above that of the QCD phase transition, it couples to gluons through the following effective interaction

$$\mathcal{L}_{\phi gg} = \frac{\alpha_s}{8\pi}\frac{\phi}{f_\phi}G^b_{\mu\nu}\widetilde{G}^{b\mu\nu} \ , \tag{1.28}$$

where f_ϕ the axion decay constant, and $\widetilde{G}^{b\mu\nu} = \frac{1}{2}\epsilon^{\mu\nu\rho\sigma}G^b_{\rho\sigma}$ the dual tensor of $G^{b\mu\nu}$. Due to the existence of this interaction, the topological fluctuations of the gluon fields induce the following cosine-type potential for the QCD axion field at the high temperature as

$$V_{\rm QCD}(\phi) \simeq \chi(T)\left[1-\cos\left(\frac{\phi}{f_\phi}\right)\right] \ , \tag{1.29}$$

where $\chi(T)$ is the topological susceptibility, which is a function of the temperature T of background radiations. In particular, $\chi(T)$ takes some finite values at low temperatures, while it goes to zero at temperatures much higher than the QCD confinement scale. At low temperatures, the QCD axion potential has a minimum at $\bar{\theta} = \langle\phi\rangle/f_\phi = 0$ (here we have redefined the QCD axion field, $\phi \to \phi - \bar{\theta}f_\phi$), which provides a dynamical solution to the strong CP problem, where $\langle\phi\rangle$ is the vacuum expectation value of the QCD axion.

By expanding the QCD axion potential (1.29) around the minimum, one can obtain the mass of the QCD axion given by

$$m_\phi^2(T) \,=\, \frac{\chi(T)}{f_\phi^2} \,, \tag{1.30}$$

which also depends on the background temperature T. Here we model the temperature dependence of the QCD axion mass as a power-law function

$$m_\phi(T) \,\simeq\, \begin{cases} \dfrac{\sqrt{\chi_0}}{f_\phi}\left(\dfrac{T_{\rm QCD}}{T}\right)^n & T \,>\, T_{\rm QCD} \\ m_\phi \equiv m_\phi(T \to 0) & T \,<\, T_{\rm QCD} \end{cases} \,, \tag{1.31}$$

where χ_0 is evaluated by lattice QCD and the parameters $T_{\rm QCD}$ and n are chosen such that they reproduce the correct order of $m_\phi(T)$ and that the value of $m_\phi(T)$ is matched with the zero temperature value m_ϕ at $T = T_{\rm QCD}$. The latest lattice QCD computations give $n = 4.08$ [39–43]. On the other hand, a more recent detailed analysis suggests the following numerical result on the zero temperature mass of the QCD axion [44]

$$m_\phi \,=\, 5.70(7)\,\mu{\rm eV}\left(\frac{10^{12}\,{\rm GeV}}{f_\phi}\right) \,. \tag{1.32}$$

The QCD axion is produced (non-thermally) in the early era of the universe via the realignment mechanism [45–47]. If the QCD axion takes a spatially uniform initial value, $\phi_0 = f_\phi \vartheta_0$, throughout the observable universe,[1] it starts to oscillate about the minimum of the potential when its mass $m_\phi(T)$ becomes comparable to the Hubble friction term $H(T)$. Such a coherently oscillating axion field can behave as CDM in the universe, see Fig. 1.3 as an illustration. The relic abundance of the QCD axion DM, Ω_ϕ, estimated by the realignment mechanism in the regime $|\vartheta_0| \ll \pi$ reads [54]

$$\Omega_\phi h^2 \,\simeq\, 0.14\,\vartheta_0^2\left(\frac{f_\phi}{10^{12}\,{\rm GeV}}\right)^{1.17} \,, \tag{1.33}$$

which holds for $f_\phi \lesssim 3 \times 10^{17}\,{\rm GeV}$ corresponding to the circumstance where the QCD axion begins to oscillate before $m_\phi(T)$ reaches the zero temperature value. In addition, the lower bound on $f_\phi \gtrsim 4 \times 10^8\,{\rm GeV}$ ensures the stability of the QCD axion DM on a cosmological time scale [55–57]. Note that when the initial angle ϑ_0 becomes sufficiently large, namely $\vartheta_0 \simeq \mathcal{O}(1)$, the anharmonic effect which leads to the enhancement of the QCD axion abundance must be taken into account [58].

[1] This is guaranteed if the PQ symmetry was broken before inflation and never restored afterward, however, it does not hold if the PQ symmetry was restored and got spontaneously broken after inflation. In the latter case, we must take account of the effect of the collapse of strings and domain walls rather than the realignment mechanism [48–53].

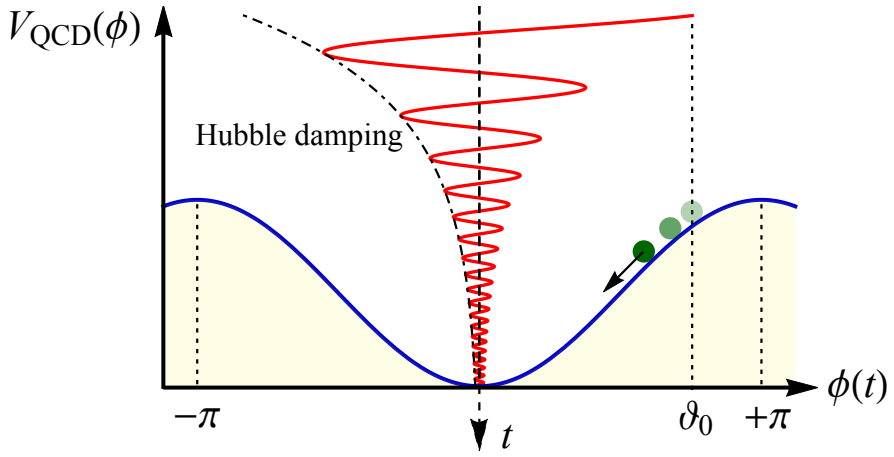

Figure 1.3: The realignment mechanism for the QCD axion, where the red twisty curve is the trajectory of the QCD axion (green ones) oscillating on the potential (blue curve), and ϑ_0 is the initial value of the QCD axion field. The trajectory of the QCD axion can be obtained by solving the equation of motion, $\ddot{\phi} + 3H(T)\dot{\phi} + m_\phi^2(T)\phi = 0$.

The descriptions on the QCD axion above can be generalized in some fundamental frameworks like string theory or supersymmetry. For example, in the context of string axiverse [59–61] or axion landscape [62, 63], there appear ubiquitous axion-like particles (ALPs). However, in contrast to the QCD axion, ALPs generally do not acquire a mass from the non-perturbative effects of QCD as they are not necessary to have couplings to gluons. Instead, their masses may originate from other high energy theories (e.g. hidden confining gauge interactions [64]).

The ALPs can also be produced in the early universe via the realignment mechanism and they can account for CDM for certain values of the parameters [65, 66]. Considering an ALP field, φ, with a mass m_φ and a decay constant f_φ, then, the relic abundance of the ALP from realignment mechanism is estimated as [66]

$$\Omega_\varphi h^2 \simeq 0.3\,\vartheta_{\varphi,0}^2 \left(\frac{m_\varphi}{1\,\mathrm{eV}}\right)^{1/2} \left(\frac{f_\varphi}{10^{12}\,\mathrm{GeV}}\right)^2 , \tag{1.34}$$

where $\vartheta_{\varphi,0}$ is an initial angle of the ALP field. Note that, unlike the QCD axion, the ALP mass is assumed to be constant in temperature and independent of the decay constant, which explains the different powers of the decay constants in Eqs. (1.33) and (1.34).

The experimental investigations of the QCD axion and ALPs rely on their couplings to the visible particles. These couplings are suppressed by the axion decay constants. For instance, the couplings of the QCD axion and an ALP to photons are given by

$$\mathcal{L}_{\phi\gamma\gamma} = -\frac{g_{\phi\gamma\gamma}}{4}\phi F_{\mu\nu}\widetilde{F}^{\mu\nu} , \quad \mathcal{L}_{\varphi\gamma\gamma} = -\frac{g_{\varphi\gamma\gamma}}{4}\varphi F_{\mu\nu}\widetilde{F}^{\mu\nu} , \tag{1.35}$$

where $F_{\mu\nu}$ is the electromagnetic field strength tensor and $\widetilde{F}_{\mu\nu}$ being its dual tensor, and

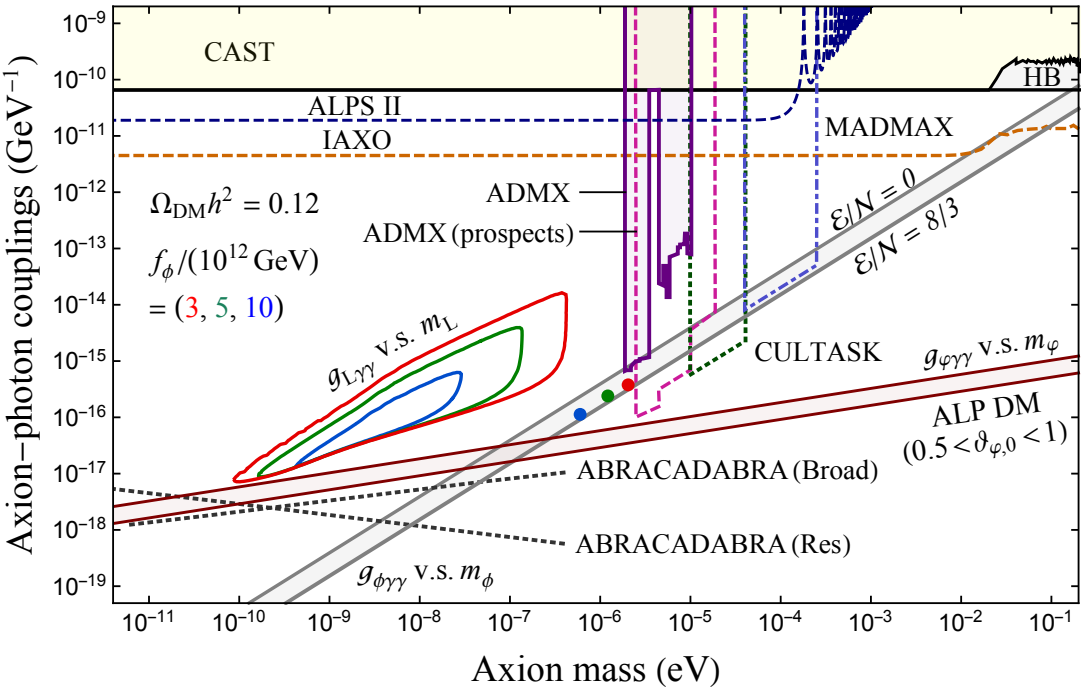

Figure 1.4: The various experimental and astrophysical constraints on the axion-photon coupling as a function of the axion mass, where we show the current bounds by ADMX [67–69] and CAST [70] along with the future sensitivities by ADMX (prospects) [71], CULTASK [72], MADMAX [73], ABRACADABRA [74], ALPS II [75] and IAXO [76]. The limit from the studies of the horizontal branch (HB) stars is displayed as well [77]. For a comparison, we show in the brown diagonal band the ALP-photon coupling $g_{\varphi\gamma\gamma}$ with $C_{\varphi\gamma} = 1$, and in the gray solid diagonal lines the QCD axion-photon coupling $g_{\phi\gamma\gamma}$ with $\mathcal{E}/\mathcal{N} = 0$ for the KSVZ model [78, 79] and $\mathcal{E}/\mathcal{N} = 8/3$ for the DFSZ model [80, 81]. Note that the color dots represent the QCD axion DM with $f_\phi = (3, 5, 10) \times 10^{12}\,{\rm GeV}$, and the abundance of ALP (1.34) explains DM for the initial angle between 0.5 and 1.

the coupling coefficients $g_{\phi\gamma\gamma}$ and $g_{\varphi\gamma\gamma}$ read

$$g_{\phi\gamma\gamma} = \frac{\alpha}{2\pi f_\phi}\left[-1.92(4) + \frac{\mathcal{E}}{\mathcal{N}}\right], \quad g_{\varphi\gamma\gamma} = \frac{\alpha}{2\pi f_\varphi} C_{\varphi\gamma}\,. \tag{1.36}$$

with $\alpha = e^2/(4\pi)$ being the fine structure constant. The square bracket in $g_{\phi\gamma\gamma}$ contains a model-independent contribution from the mixing with mesons (the first term) and a model-dependent contribution (the second term) given by the electromagnetic anomaly $\mathcal{E}$ and the color anomaly $\mathcal{N}$ of the PQ symmetry. On the other hand, the coefficient $C_{\varphi\gamma}$ in $g_{\varphi\gamma\gamma}$ only includes a model-dependent contribution. The presence of photon coupling provides a promising way for various direct detections of the QCD axion DM and ALP DM. We show in Fig. 1.4 some of the ongoing and prospective axion-search experiments utilizing the axion-photon coupling.

The ALP can have some cosmological applications. For example, it has been studied in Ref. [82] that the abundance of the QCD axion can be suppressed by the mass ratio m_φ/m_ϕ if there exists a nonzero mass mixing between the QCD axion and the ALP. As a consequence, the axion-photon coupling ($g_{\mathrm{L}\gamma\gamma}$) for the light mass eigenstate (m_{L}) can be enhanced by a few orders of magnitude (see the color solid contours in Fig. 1.4), which is advantageous for the future ALP and axion-search experiments. However, if the mass of an axion is too light and with too large initial amplitude, then it may be stable on a cosmological time scale and contributes too much energy density to the observed DM abundance. This is known as the cosmological moduli problem. Interestingly, this moduli problem can be relaxed by low-scale inflation provided that the field values of the axion follows the Bunch-Davies distribution peaked at the potential minima, see Ref. [83] for more discussions of cosmological and astrophysical constraints on this scenario.

1.2.3 Other Possible Candidates

In addition to WIMP and axions, physicists have come up with other possible entities as DM constituent, which may have different mass scales than WIMP and axions. Based on the observations, the possible mass scale of DM spreads over a very wide range from $10^{-22}\,\mathrm{eV}$ to $10^{58}\,\mathrm{GeV}$, where the lower limit is due to the quantum effects and the upper limit is due to the tidal disruption of DM halos around the structures. Let us introduce some of the DM paradigms different from WIMP and axions in a nutshell as follows.

• **Strongly Interacting Massive Particles** : Like the WIMP, strongly interacting massive particles (SIMP) are thermal relics produced via the freeze-out mechanism in the early universe. But, unlike the WIMP DM, the number of SIMP DM is cannibalized by itself mainly through 3 to 2 annihilation processes rather than 2 to 2 annihilation processes, see the middle Feynman diagram in Fig. 1.5. Now, similar to the WIMP DM, one can calculate the current relic abundance of a SIMP DM by solving the Boltzmann equation for the DM number density, which is given by [84]

$$\frac{dn_{\mathrm{DM}}}{dt} + 3Hn_{\mathrm{DM}} \;=\; -\langle\sigma_{3\to2}v_{\mathrm{rel}}^2\rangle_{\mathrm{eff}}\left(n_{\mathrm{DM}}^3 - n_{\mathrm{DM}}^2 n_{\mathrm{DM}}^{\mathrm{eq}}\right)\,, \tag{1.37}$$

where $\langle\sigma_{3\to2}v_{\mathrm{rel}}^2\rangle_{\mathrm{eff}}$ is the thermal-averaged value of the effective cross-section of a 3 to 2 annihilation process. The approximate formula of the relic density of SIMP DM can be derived by using the method analog to the case of WIMP DM, the result is given by [85]

$$\Omega_{\mathrm{SIMP}}h^2 \;\simeq\; 1.73\times10^{-5}\left(\frac{m_{\mathrm{SIMP}}}{40\,\mathrm{MeV}}\right)^{-1}\left[\frac{\langle\sigma_{3\to2}v_{\mathrm{rel}}^2\rangle_{\mathrm{eff}}}{\mathrm{MeV}^{-5}}\right]^{-1/2}\,, \tag{1.38}$$

where m_{SIMP} is the mass of SIMP DM. Notice that the relic abundance of SMIP DM depends not only on the effective cross-section but also on the mass of SIMP DM. The

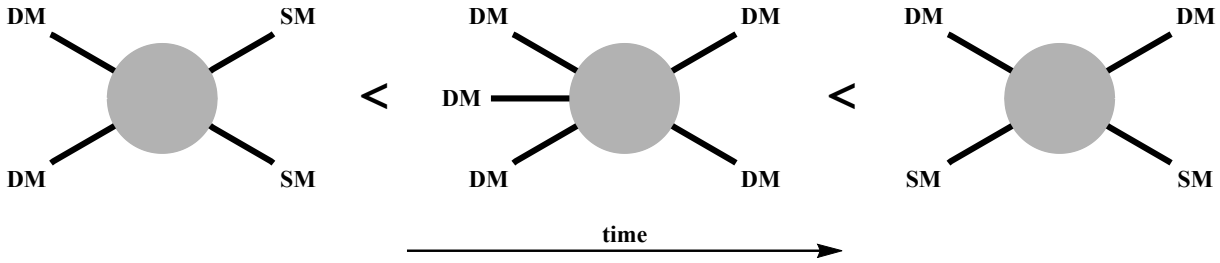

Figure 1.5: The diagrammatic demonstration of the SIMP condition, where the right, middle and left panels are the Feynman diagrams for 2 to 2 annihilation process, 3 to 2 annihilation process, and kinetic scattering process of SIMP DM, respectively.

effective annihilation cross-section in Eq. (1.37) or (1.38) can be parameterized as

$$\langle \sigma_{3\to 2} v_{\rm rel}^2 \rangle_{\rm eff} \;=\; \frac{\alpha_{3\to 2}^3}{m_{\rm SIMP}^5} \;, \tag{1.39}$$

where $\alpha_{3\to 2}$ is the effective coupling of DM in the 3 to 2 annihilation process. Plugging (1.39) into (1.38), and taking $\alpha_{3\to 2} \sim 1$ and $m_{\rm SIMP}$ from an MeV to sub-GeV scale, one can obtain the correct magnitude of the DM relic abundance. Clearly, the *strongly* in the acronym of SIMP means that the effective couplings $\alpha_{3\to 2}$ are much larger than the effective couplings $\alpha_{\rm ann}$ in the WIMP scenario. With this advantage, the SIMP DM can have sizable self-interactions which may resolve some astrophysical tensions such as the core-versus-cusp and too-big-to-fail problems.

To have a successful realization of the SIMP paradigm, one has to require that the interacting rates of 3 to 2 annihilation processes are much bigger than the ones of 2 to 2 annihilation processes. On the other hand, to prevent the heat up of SIMP DM due to 3 to 2 processes, the interacting rates of 3 to 2 annihilation processes must be smaller than the ones of the kinetic scattering between the SIMP DM and the SM particles. This is called the SIMP condition [84], see Fig. 1.5 for a diagrammatic demonstration.

• **Asymmetric DM** : As mentioned in the previous section, the relic density of DM is about five times larger than the baryonic matter, $\Omega_{\rm DM}/\Omega_{\rm b} \simeq 5$. Since the production mechanisms of DM and the baryon asymmetry may have different origins, it might be possible that this ratio is an initial condition of the universe or is set by the anthropic principle. However, if the relic abundance of DM is produced in the same manner as the baryon asymmetry, namely $n_{\rm DM} - n_{\overline{\rm DM}} \sim n_B - n_{\overline{B}}$, then the mass densities of DM and the baryonic matter can be connected to each other [86–88]. It follows that

$$\frac{\rho_{\rm DM}}{\rho_{\rm b}} \;\simeq\; \frac{m_{\rm ADM}}{m_p} \frac{n_{\rm DM} - n_{\overline{\rm DM}}}{n_B - n_{\overline{B}}} \;\simeq\; \frac{m_{\rm ADM}}{m_p} \;\simeq\; 5 \;, \tag{1.40}$$

where $m_{\rm ADM}$ is the mass of asymmetric DM, and $m_p \simeq 1\,{\rm GeV}$ being the mass of proton. Therefore, $m_{\rm ADM} \simeq 5 m_p \simeq 5\,{\rm GeV}$ which is the typical mass scale of asymmetric DM.

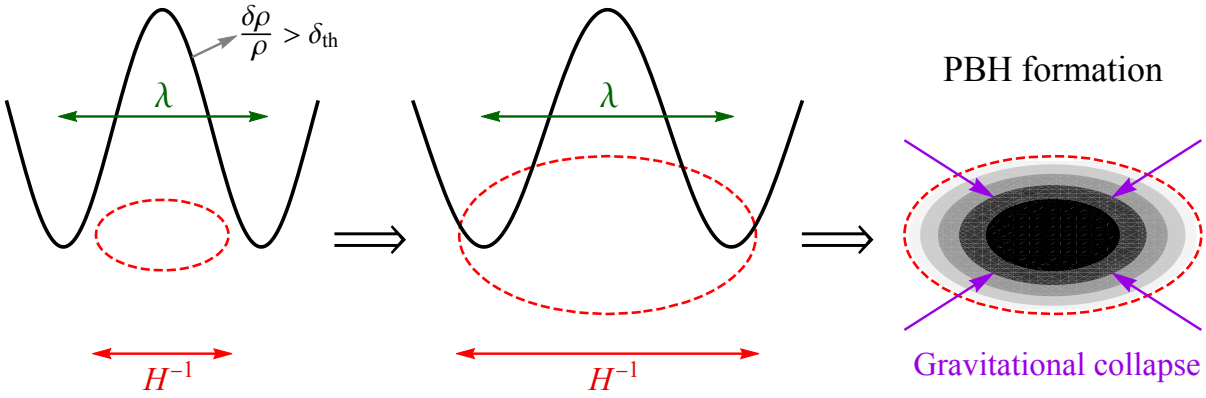

Figure 1.6: The illustration of a PBH formation, where λ is the spatial wavelength of density fluctuation, H^{-1} is the size of the Hubble horizon, $\delta\rho/\rho$ is the density contrast, and $\delta_{\rm th} \simeq 0.4$ is the threshold of $\delta\rho/\rho$ to form a PBH [91]. For demonstration purpose, we describe the universe in 2d space, where the red dashed oval represents the Hubble horizon and the black shaded region represents the PBH. Note that the crests (troughs) of the solid curve line indicate the underdense (overdense) regions of density fluctuation.

• **Primordial Black Holes** : Primordial black holes (PBHs) are formed at the very early time of the universe (at the radiation-dominated epoch) through the gravitational collapse in the overdense regions of density fluctuation [89, 90]. The formation of a PBH can be seen in Fig. 1.6. When the spatial wavelength λ of density fluctuation is longer than the size of horizon H^{-1}, nothing happens to the fluctuation due to the causality. Since λ and H^{-1} increase as the universe expands, while the former one grows slower than the latter one. Hence, λ becomes equal to H^{-1} at a certain point. Then, once the fluctuation enters the horizon, a black hole is formed by the gravitational collapse if the density perturbation $\delta\rho$ is large enough to against the pressure by the radiation.

Since a PBH is formed in the radiatio-dominated era and at the scale of the Hubble horizon, its mass is then roughly equal to the total energy of radiation contained within the horizon. Thus, we have

$$m_{\rm PBH} \simeq \frac{4\pi}{3} H(T)^{-3} \rho(T) \simeq 2 \times 10^5 M_\odot \left(\frac{t}{1\,{\rm sec}} \right) , \tag{1.41}$$

where $M_\odot \simeq 1.989 \times 10^{33}\,{\rm g} \simeq 1.116 \times 10^{57}\,{\rm GeV}$ is the solar mass. Here we have used Eqs. (1.11) and (1.13), and the relation between the cosmic time and the temperature at the radiation-dominated epoch, $t \simeq 0.301 g_{*\rho}(T)^{-1/2} m_{\rm Pl}/T^2$ for deriving (1.41). Hence, PBHs can have a wide mass range depending on their formation time.

PBHs are non-baryonic, long-lived, and non-relativistic objects. Therefore, they are plausible CDM candidates. Moreover, the PBHs with a mass larger than about $10^3 M_\odot$ can be the seeds of the supermassive black holes ($\sim 10^9 M_\odot$) as they cannot be explained by the astrophysical mechanisms. However, PBHs can evaporate via thermal emission

like the stellar black holes. Thus, for PBHs to be a dominant component of DM, one has to require that the mass of PBHs $m_{\rm PBH} \gtrsim 10^{15}\,{\rm g} \simeq 5\times 10^{-19} M_\odot$ [92]. Otherwise, it would have dissipated by present due to the Hawking radiation. On the other hand, the abundance of PBHs is tightly constrained by various cosmological and astrophysical observations because of their evaporation and gravitational lensing effects. For example, it has been analyzed in Ref. [93] that only the PBHs with the mass from $10^{17}\,{\rm g}$ to $10^{20}\,{\rm g}$ can have a significant contribution to DM ($\Omega_{\rm PBH}/\Omega_{\rm DM} \gtrsim 0.1$).

• **Fuzzy DM** : Fuzzy DM (FDM) or quantum wave DM has drawn an attention in recent years [94]. In this scenario, DM is composed of extraordinarily light bosons with a particle mass of order $m_{\rm FDM} \sim 10^{-22}\,{\rm eV}$. Then, the de Broglie wavelength of FDM is

$$\frac{\lambda_{\rm FDM}}{2\pi} = \frac{\hbar}{m_{\rm FDM} v} \simeq 2\,{\rm kpc}\left(\frac{m_{\rm FDM}}{10^{-22}\,{\rm eV}}\right)^{-1}\left(\frac{v}{10\,{\rm km\cdot sec^{-1}}}\right)^{-1}. \tag{1.42}$$

The DM with wavelength in such an astronomical scale may suppress the formation of small-scale structures, which can address some astrophysical issues such as the missing satellites problem or the core-versus-cusp problem, etc.

• **Topological Defects** : Topological defects (TD) occur when two adjacent regions in different phases cannot be transited smoothly between each other, which are common objects in various fields of physics such as condensed matter physics, atomic physic, and cosmology, etc. Mathematically, when a symmetry group $\mathcal{G}$ spontaneously breaks down to its subgroup $\mathcal{H}$, there is a vacuum manifold $\mathcal{M}$ which is homeomorphic to the coset space $\mathcal{G}/\mathcal{H}$. Then, the homotopy groups of $\mathcal{M}$ can determine which kind of TD appeared in the theory. In other words, the configuration of TD corresponds to a non-trivial $\pi_{\rm N}(\mathcal{M})$, where $\pi_{\rm N}$ is the N-th homotopy group. In general, $\pi_{\rm N}(\mathcal{M}) \neq 0$ gives to a $(2-{\rm N})$-dimensional TD. For example, we have domain walls, cosmic strings, and magnetic monopoles if $\pi_0(S^0) = \mathbb{Z}$, $\pi_1(S^1) = \mathbb{Z}$, and $\pi_2(S^2) = \mathbb{Z}$, respectively.

Now, let us discuss the necessary conditions for the existence of magnetic monopoles in a gauge theory with the Higgs mechanism. If a gauge group $\mathcal{G}$ is semi-simple,[2] and its subgroup $\mathcal{H}$ contains one U(1) group, then $\pi_2(\mathcal{M}) = \mathbb{Z}$, thus magnetic monopoles exist. In the SM, $G_{\rm SM}$ is not semi-simple, $\pi_2(\mathcal{M}) = 0$, no magnetic monopoles exist. On the other hand, in grand unified theories (GUTs), say SU(5), magnetic monopoles can exist since SU(5) is semi-simple and it breaks down at low energies to ${\rm SU(3)_C}\otimes{\rm U(1)_{EM}}$.

Magnetic monopole is a good DM candidate since it is stabilized by the topological property and it can be created naturally in the early universe during a phase transition. The production of magnetic monopoles is shown in Fig. 1.7. Before the phase transition, the field configuration is trivial and magnetic monopoles do not exist. During the phase transition, the field configuration is correlated inside a Hubble patch but uncorrelated with other Hubble patches, then the monopole structure appears. This is known as the

[2] A semi-simple group is a group that contains no non-trivial Abelian subgroups.

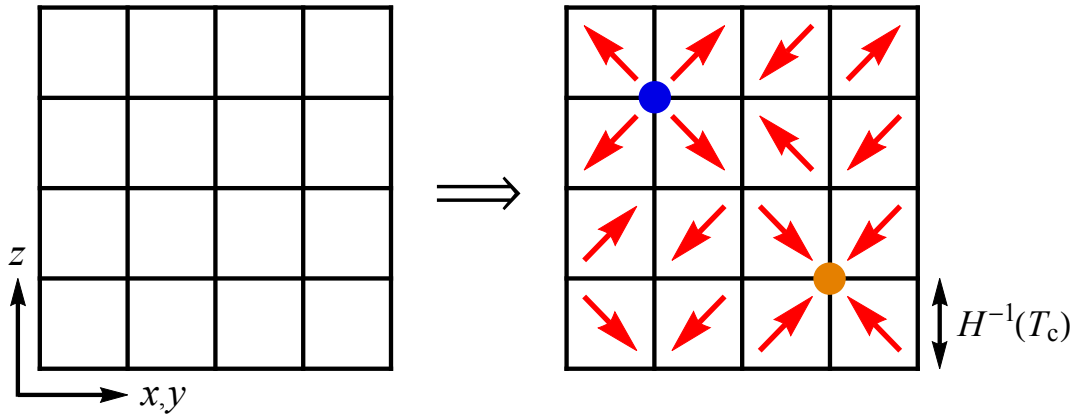

Figure 1.7: The production of magnetic monopoles by the Kibble mechanism, where the left (right) panel is the unbroken (broken) phase of the universe before (after) the phase transition. The red arrow represents the field orientation in each Hubble region, and the blue (orange) solid point represents a magnetic monopole (an anti-monopole).

Kibble machanism [95]. Now, assuming at least one magnetic monopole is produced in a Hubble volume during a phase transition, $n_{\rm M} \sim H(T_{\rm c})^3$. Then, the energy density of magnetic monopoles today is estimated as

$$\Omega_{\rm M} h^2 \simeq 10^{17} \left(\frac{m_{\rm M}}{10^{16}\,{\rm GeV}} \right) \left(\frac{T_{\rm c}}{10^{16}\,{\rm GeV}} \right)^3 \left[\frac{g_{*\rho}(T_{\rm c})}{100} \right]^{1/2} , \tag{1.43}$$

where $m_{\rm M}$ is the mass of magnetic monopole, $T_{\rm c}$ is the critical temperature at which the phase transition occurs, and $10^{16}\,{\rm GeV}$ is the typical energy scale of GUTs. Therefore, if the magnetic monopole is originated from GUTs, then its adundance would exceed the current relic adundance of DM by 17 orders of magnitude. Such superheavy monopoles is precisely the monopole problem in cosmology.

1.2.4 ′t Hooft-Polyakov Monopole as DM Candidate

In this thesis, we will explore another type of magnetic monopole, ′t Hooft-Polyakov monopole, in the hidden sector. In this model, they consider the gauge field theory with $\mathcal{G} = {\rm SU}(2) \simeq {\rm SO}(3)$, which is spontaneously broken down to $\mathcal{H} = {\rm U}(1) \simeq {\rm SO}(2)$ via the Higgs mechanism. Now, since every rotation in 3d space by SO(3) group is one to one correspondence to a point on a 2d space sphere with a rotation by SO(2) group, then taking the quotient of SO(3) by these latter rotations removes that degree of freedom. Thus, we have the coset space ${\rm SO}(3)/{\rm SO}(2) \simeq S^2$, and $\pi_2[{\rm SO}(3)/{\rm SO}(2)] = \pi_2(S^2) = \mathbb{Z}$ entails the existence of the monopole solution. Intriguingly, it turns out that the hidden monopole in the ′t Hooft-Polyakov model can be a suitable DM candidate by using the Kibble-Zurek mechanism. We will study in more detail in the following chapters.

Chapter 2

Hidden Monopole Dark Matter

It was pointed out by ′t Hooft and Polyakov independently that a magnetic monopole can necessarily appear when a non-Abelian gauge symmetry is spontaneously broken via the Higgs mechanism [1, 2]. It can serve as a promising DM candidate if the symmetry is in the hidden sector [3, 4]. In this chapter, we first present a pedagogical review of the ′t Hooft-Polyakov model [96–98], then we discuss the production mechanism of the hidden monopole DM and estimate its relic abundance in the last part of this chapter.

2.1 ′t Hooft-Polyakov Monopole

2.1.1 The Lagrangian Density

The simplest model containing a hidden monopole M is an $\mathrm{SU}(2)_{\mathrm{H}}$ gauge theory with gauge fields $\boldsymbol{A}^{\mu}_{\mathrm{H}} = \left(A^{\mu}_{\mathrm{H}1}, A^{\mu}_{\mathrm{H}2}, A^{\mu}_{\mathrm{H}3}\right)^{\mathrm{T}}$ coupled to an isovector scalar field $\boldsymbol{\phi} = (\phi_1, \phi_2, \phi_3)^{\mathrm{T}}$, where the H subscript denotes *hidden*. The Lagrangian density is given by

$$\mathcal{L}_{\mathrm{H}} = -\frac{1}{4}\boldsymbol{F}^{\mu\nu}_{\mathrm{H}} \cdot \boldsymbol{F}_{\mathrm{H}\mu\nu} + \frac{1}{2}\mathcal{D}^{\mu}\boldsymbol{\phi} \cdot \mathcal{D}_{\mu}\boldsymbol{\phi} - \mathcal{V}(\phi) \,, \tag{2.1}$$

where $\boldsymbol{F}^{\mu\nu}_{\mathrm{H}} = \partial^{\mu}\boldsymbol{A}^{\nu}_{\mathrm{H}} - \partial^{\nu}\boldsymbol{A}^{\mu}_{\mathrm{H}} + e_{\mathrm{H}}\boldsymbol{A}^{\mu}_{\mathrm{H}} \times \boldsymbol{A}^{\nu}_{\mathrm{H}}$ is the gauge field strength tensor with $e_{\mathrm{H}} > 0$ being the hidden gauge coupling constant, and $\mathcal{D}^{\mu}\boldsymbol{\phi} = \partial^{\mu}\boldsymbol{\phi} + e_{\mathrm{H}}\boldsymbol{A}^{\mu}_{\mathrm{H}} \times \boldsymbol{\phi}$ is the covariant derivative. Notice that $\cdot$ and $\times$ here are the dot and cross products in the isospin space. The potential of the isovector scalar field is

$$\mathcal{V}(\phi) = \frac{1}{4}\lambda_{\phi}\left(\phi^2 - \upsilon^2_{\mathrm{H}}\right)^2 \,, \quad \phi = \sqrt{\boldsymbol{\phi} \cdot \boldsymbol{\phi}} \,, \tag{2.2}$$

where $\lambda_{\phi} > 0$ is the quartic coupling, and $\upsilon_{\mathrm{H}} = \langle\phi\rangle$ is the vacuum expectation value of $\boldsymbol{\phi}$ at which the potential is minimized.

Now, let us take the third component of $\boldsymbol{\phi}$ developes the vacuum expectation value, $\langle\boldsymbol{\phi}\rangle = \left(0, 0, \upsilon_{\mathrm{H}}\right)$, without loss of generality, then the $\mathrm{SU}(2)_{\mathrm{H}}$ gauge symmetry is spontaneous broken down to $\mathrm{U}(1)_{\mathrm{H}}$ gauge symmetry which corresponds to rotations about the

3-axis. By expanding the Lagrangian density around the true vacuum state and in the unitary gauge, $\boldsymbol{\phi} \to \big(0, 0, \upsilon_{\rm H} + \phi_3\big)$, we obtain the particle spectrum including a massless hidden photon $\gamma_{\rm H}$, two massive hidden vector bosons $W^{\pm}_{\rm H}$, and a massive hidden scalar φ. Their masses can be extracted from the quadratic terms of the Lagrangian density as

$$\begin{aligned}
\frac{1}{2}\mathcal{D}^{\mu}\boldsymbol{\phi}\cdot\mathcal{D}_{\mu}\boldsymbol{\phi} \;&\supset\; \frac{1}{2}e_{\rm H}^2\big(\boldsymbol{A}^{\mu}_{\rm H}\times\boldsymbol{\phi}\big)\cdot\big(\boldsymbol{A}_{{\rm H}\mu}\times\boldsymbol{\phi}\big) \\
&=\; \frac{1}{2}e_{\rm H}^2\Big[\big(\boldsymbol{A}^{\mu}_{\rm H}\cdot\boldsymbol{A}_{{\rm H}\mu}\big)\big(\boldsymbol{\phi}\cdot\boldsymbol{\phi}\big) - \big(\boldsymbol{A}^{\mu}_{\rm H}\cdot\boldsymbol{\phi}\big)\big(\boldsymbol{A}_{{\rm H}\mu}\cdot\boldsymbol{\phi}\big)\Big] \\
&=\; \frac{1}{2}e_{\rm H}^2\big(\upsilon_{\rm H}+\phi_3\big)^2\big(A^{\mu}_{\rm H1}A_{{\rm H1}\mu} + A^{\mu}_{\rm H2}A_{{\rm H2}\mu}\big) \\
&\supset\; m^2_{W_{\rm H}}W^{+\mu}_{\rm H}W^{-}_{{\rm H}\mu}\;, \\
\mathcal{V}(\phi) \;&=\; \frac{1}{4}\lambda_{\phi}\Big[\big(\upsilon_{\rm H}+\phi_3\big)^2 - \upsilon_{\rm H}^2\Big]^2 \;\supset\; \frac{1}{2}m^2_{\varphi}\varphi^2\;,
\end{aligned} \tag{2.3}$$

where the hidden vector fields $W^{\pm}_{\rm H}$ and $\gamma_{\rm H}$, and the hidden scalar field φ are defined as

$$W^{\pm\mu}_{\rm H} \equiv \frac{1}{\sqrt{2}}\big(A^{\mu}_{\rm H1} \mp iA^{\mu}_{\rm H2}\big)\;, \quad A^{\mu}_{\rm H} \equiv A^{\mu}_{\rm H3}\;, \quad \varphi \equiv \phi_3\;, \tag{2.4}$$

and the corresponding masses are given by

$$m_{W_{\rm H}} = e_{\rm H}\upsilon_{\rm H}\;, \quad m_{\gamma_{\rm H}} = 0\;, \quad m_{\varphi} = \sqrt{2\lambda_{\phi}}\,\upsilon_{\rm H}\;. \tag{2.5}$$

On the other hand, their hidden charges can be read off from the coupling to the hidden photon, e.g. see Eq. (D.1). Apparently, the hidden massive vector bosons $W^{\pm}_{\rm H}$ has hidden charge $\pm e_{\rm H}$, and others are neutral under $\mathrm{U}(1)_{\rm H}$.

The equations of motion for the hidden gauge field and the hidden scalar field can be derived by using the Euler-Lagrange equations as

$$\partial_{\mu}\left(\frac{\partial\mathcal{L}_{\rm H}}{\partial\big(\partial_{\mu}\boldsymbol{A}_{{\rm H}\nu}\big)}\right) = \frac{\partial\mathcal{L}_{\rm H}}{\partial\boldsymbol{A}_{{\rm H}\nu}}\;, \quad \partial_{\mu}\left(\frac{\partial\mathcal{L}_{\rm H}}{\partial\big(\partial_{\mu}\boldsymbol{\phi}\big)}\right) = \frac{\partial\mathcal{L}_{\rm H}}{\partial\boldsymbol{\phi}}\;. \tag{2.6}$$

After some long algebra (see appendix A.1 for the calculations), one can obtain

$$\mathcal{D}_{\mu}\boldsymbol{F}^{\mu\nu}_{\rm H} + e_{\rm H}\boldsymbol{\phi}\times\mathcal{D}^{\nu}\boldsymbol{\phi} = 0\;, \quad \mathcal{D}_{\mu}\mathcal{D}^{\mu}\boldsymbol{\phi} + \lambda_{\phi}\big(\phi^2 - \upsilon_{\rm H}^2\big)\boldsymbol{\phi} = 0\;. \tag{2.7}$$

Besides, the Bianchi identity yields one more equation of motion as

$$\mathcal{D}_{\mu}\widetilde{\boldsymbol{F}}^{\mu\nu}_{\rm H} = 0\;, \quad \widetilde{\boldsymbol{F}}^{\mu\nu}_{\rm H} = \frac{1}{2}\epsilon^{\mu\nu\rho\sigma}\boldsymbol{F}_{{\rm H}\rho\sigma}\;. \tag{2.8}$$

It is also useful to find out the total energy density of the model. First, the canonically conjugate momenta to the hidden gauge field and the hidden scalar field gives

$$\boldsymbol{E}^{j}_{\rm H} \equiv \frac{\partial\mathcal{L}_{\rm H}}{\partial\big(\partial_0\boldsymbol{A}_{{\rm H}j}\big)} = \boldsymbol{F}^{j0}_{\rm H}\;, \quad \boldsymbol{\Pi} \equiv \frac{\partial\mathcal{L}_{\rm H}}{\partial\big(\mathcal{D}_0\boldsymbol{\phi}\big)} = \mathcal{D}^0\boldsymbol{\phi}\;, \tag{2.9}$$

where $\boldsymbol{E}^j_{\rm H}$ is the hidden electric field, and the hidden magnetic field is defined as

$$\boldsymbol{B}^j_{\rm H} \equiv \frac{1}{2}\epsilon_{jkl}\boldsymbol{F}^{kl}_{\rm H} \ . \tag{2.10}$$

Then, the total energy density is written as

$$\mathcal{H}_{\rm M} = \frac{1}{2}\boldsymbol{E}^j_{\rm H}\cdot\boldsymbol{E}^j_{\rm H} + \frac{1}{2}\boldsymbol{B}^j_{\rm H}\cdot\boldsymbol{B}^j_{\rm H} + \frac{1}{2}\boldsymbol{\Pi}\cdot\boldsymbol{\Pi} + \frac{1}{2}\mathcal{D}^j\boldsymbol{\phi}\cdot\mathcal{D}^j\boldsymbol{\phi} + \mathcal{V}(\phi) \ , \tag{2.11}$$

which can be applied to estimate the mass of the hidden monopole. Before that, let us first discuss how the hidden monopole solution emerges from this gauge theory.

2.1.2 Hidden Monopole Solution

In this section, we will show how the magnetic monopole can arise from the $\mathrm{SU}(2)_{\rm H}$ gauge theory with a isovector scalar. In short, it is a static solution of the equations of motion (2.6) with finite energy field configuration. The ansatz was first given by ′t Hooft and Polyakov, and it has the following asymptotic forms at spatial infinity ($r \to \infty$) as

$$\phi_a = \upsilon_{\rm H}\frac{r^a}{r} \ , \quad A^j_{{\rm H}a} = -\epsilon_{ajk}\frac{r^k}{e_{\rm H}r^2} \ , \quad A^0_{{\rm H}a} = 0 \ , \tag{2.12}$$

where the spatial coordinates $r^a \equiv x_a$, and note that these expressions have a mixture between the isospin index $a = (1,2,3)$ and the space indices $j,k = (1,2,3)$. One can check that the asymptotic forms (2.12) satisfy (2.7). For instance,

$$\mathcal{D}^0\phi_a = \partial^0\phi_a + e_{\rm H}\epsilon_{abc}A^0_{{\rm H}b}\phi_c = 0 \tag{2.13}$$

$$\begin{aligned}\mathcal{D}^j\phi_a &= \partial^j\phi_a + e_{\rm H}\epsilon_{abc}A^j_{{\rm H}b}\phi_c = \upsilon_{\rm H}\partial^j\left(\frac{r^a}{r}\right) - e_{\rm H}\epsilon_{abc}\left(\epsilon_{bjk}\frac{r^k}{e_{\rm H}r^2}\right)\left(\upsilon_{\rm H}\frac{r^c}{r}\right) \\ &= \upsilon_{\rm H}\left(\frac{\delta_j{}^a}{r} - \frac{r_j r^a}{r^3}\right) + \upsilon_{\rm H}\left(\delta_{aj}\delta_{ck} - \delta_{ak}\delta_{cj}\right)\frac{r^k r^c}{r^3} = 0 \ .\end{aligned} \tag{2.14}$$

It follows that the second equation of motion in (2.7) is satisfied since

$$\mathcal{D}^\mu\boldsymbol{\phi} = 0 \ , \quad \phi^2 = \upsilon^2_{\rm H} \ . \tag{2.15}$$

In particular, we call (2.15) the *scalar vacuum* configuration. One can confirm that the first equation of motion in (2.7) is fulfilled with (2.12) as well (see appendix A.1).

It is known that a vector particle remains massless if it is associated with a rotation (unbroken $\mathrm{U}(1)_{\rm H} \simeq \mathrm{SO}(2)_{\rm H}$ in this model) which leaves $\boldsymbol{\phi}$ unchanged. Therefore, one can define the electromagnetic potential by projecting $\boldsymbol{A}^\mu_{\rm H}$ onto $\boldsymbol{\phi}$ in the scalar vacuum as

$$A^\mu_{\rm H} \equiv \frac{1}{\upsilon_{\rm H}}\boldsymbol{\phi}\cdot\boldsymbol{A}^\mu_{\rm H} \ , \tag{2.16}$$

from which the hidden electromagnetic tensor is identified with

$$F_{\rm H}^{\mu\nu} \equiv \frac{1}{\upsilon_{\rm H}} \boldsymbol{\phi} \cdot \boldsymbol{F}_{\rm H}^{\mu\nu} \ . \tag{2.17}$$

Let us check that (2.17) satisfies Maxwell's equations. In the scalar vacuum, we have

$$\boldsymbol{A}_{\rm H}^{\mu} \times \boldsymbol{\phi} \ = \ -\frac{1}{e_{\rm H}} \partial^{\mu} \boldsymbol{\phi} \ . \tag{2.18}$$

Taking the cross product with $\boldsymbol{\phi}$ on the both sides of (2.18), we get

$$\boldsymbol{A}_{\rm H}^{\mu} \ = \ \frac{1}{\upsilon_{\rm H}} A_{\rm H}^{\mu} \boldsymbol{\phi} - \frac{1}{e_{\rm H} \upsilon_{\rm H}^2} \big(\boldsymbol{\phi} \times \partial^{\mu} \boldsymbol{\phi} \big) \ , \tag{2.19}$$

where we have used the definition in (2.16). Substituting (2.19) into $\boldsymbol{F}_{\rm H}^{\mu\nu}$, we arrive at

$$\boldsymbol{F}_{\rm H}^{\mu\nu} \ = \ \frac{1}{\upsilon_{\rm H}} \boldsymbol{\phi} F_{\rm H}^{\mu\nu} \ , \quad F_{\rm H}^{\mu\nu} \ = \ \partial^{\mu} A_{\rm H}^{\nu} - \partial^{\nu} A_{\rm H}^{\mu} - \frac{1}{e_{\rm H} \upsilon_{\rm H}^3} \Big[\boldsymbol{\phi} \cdot \big(\partial^{\mu} \boldsymbol{\phi} \times \partial^{\nu} \boldsymbol{\phi} \big) \Big] \ , \tag{2.20}$$

where the identification (2.17) has been used (see appendix A.2 for the derivation). Using the equation of motion (2.7) in the scalar vacuum and (2.20), one can readily show that

$$\begin{aligned} \mathcal{D}_{\mu} \boldsymbol{F}_{\rm H}^{\mu\nu} \ &= \ \partial_{\mu} \boldsymbol{F}_{\rm H}^{\mu\nu} + e_{\rm H} \boldsymbol{A}_{{\rm H}\mu} \times \boldsymbol{F}_{\rm H}^{\mu\nu} \ = \ \frac{1}{\upsilon_{\rm H}} \partial_{\mu} \big(\boldsymbol{\phi} F_{\rm H}^{\mu\nu} \big) + e_{\rm H} \boldsymbol{A}_{{\rm H}\mu} \times \frac{1}{\upsilon_{\rm H}} \boldsymbol{\phi} F_{\rm H}^{\mu\nu} \\ &= \ \frac{1}{\upsilon_{\rm H}} \big(F_{\rm H}^{\mu\nu} \mathcal{D}_{\mu} \boldsymbol{\phi} + \boldsymbol{\phi} \partial_{\mu} F_{\rm H}^{\mu\nu} \big) \ = \ \frac{1}{\upsilon_{\rm H}} \boldsymbol{\phi} \partial_{\mu} F_{\rm H}^{\mu\nu} \ = \ 0 \ , \end{aligned} \tag{2.21}$$

it follows that $\partial_{\mu} F_{\rm H}^{\mu\nu} = 0$. Similarly, Eq. (2.8) leads to $\partial_{\mu} \widetilde{F}_{\rm H}^{\mu\nu} = 0$.

We have demonstrated that the definition of the electromagnetic tensor (2.17) does satisfy Maxwell's equations. Now, let us plug the asymptotic forms (2.12) into (2.16) and (2.20), we find $A_{\rm H}^{\mu} = 0$, and

$$F_{\rm H}^{j0} \ = \ -\frac{1}{e_{\rm H} \upsilon_{\rm H}^3} \Big[\boldsymbol{\phi} \cdot \big(\partial^{j} \boldsymbol{\phi} \times \partial^{0} \boldsymbol{\phi} \big) \Big] \ = \ 0 \ , \tag{2.22}$$

$$\begin{aligned} F_{\rm H}^{jk} \ &= \ -\frac{1}{e_{\rm H} \upsilon_{\rm H}^3} \Big[\boldsymbol{\phi} \cdot \big(\partial^{j} \boldsymbol{\phi} \times \partial^{k} \boldsymbol{\phi} \big) \Big] \ = \ -\frac{1}{e_{\rm H} \upsilon_{\rm H}^3} \epsilon_{abc} \phi_a \partial^{j} \phi_b \partial^{k} \phi_c \\ &= \ -\frac{1}{e_{\rm H}} \epsilon_{abc} \frac{r^a}{r} \left(\frac{\delta_j{}^b}{r} - \frac{r_j r^b}{r^3} \right) \left(\frac{\delta_k{}^c}{r} - \frac{r_k r^c}{r^3} \right) \ = \ -\frac{1}{e_{\rm H}} \epsilon_{jka} \frac{r^a}{r^3} \ . \end{aligned} \tag{2.23}$$

Thus, using the definition of electromagnetic fields in the strength tensors, $F_{\rm H}^{j0} = E_{\rm H}^{j}$ and $F_{\rm H}^{jk} = -\epsilon_{jkl} B_{\rm H}^{l}$, we obtain no electric field ($\boldsymbol{E}_{\rm H} = 0$) but a radial magnetic field as

$$\boldsymbol{B}_{\rm H}(r) \ = \ \frac{\boldsymbol{r}}{e_{\rm H} r^3} \ , \tag{2.24}$$

which is essentially induced by the isovector scalar field, see Eq. (2.23). We sketch this magnetic monopole solution in Fig. 2.1.

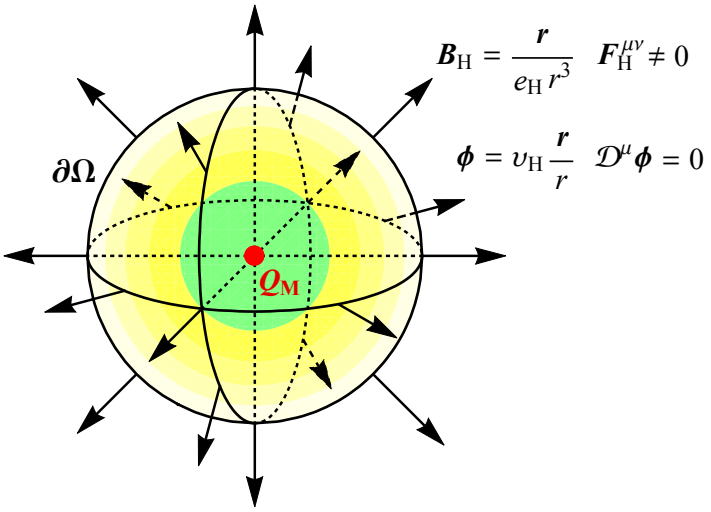

Figure 2.1: The ′t Hooft-Polyakov monopole constituted by the gauge field and the scalar field, where the isospace vector is aligned with the position vector.

With the magnetic field given in (2.24), we can find the hidden magnetic charge $Q_{\rm M}$ concentrated near the origin by measuring the magnetic flux $\Phi_{\rm B}$ through a closed surface $\partial\Omega$ in the scalar vacuum as

$$Q_{\rm M} \,=\, \Phi_{\rm B} \,=\, \oint_{\partial\Omega} \boldsymbol{B}_{\rm H} \cdot d\boldsymbol{S} \,=\, \oint_{\partial\Omega} \frac{r}{e_{\rm H} r^3} \big(r^2 d\Omega\big) \,=\, \frac{4\pi}{e_{\rm H}} \,. \tag{2.25}$$

This magnetic charge is topologically stable since it is invaraint under arbitrary deformations of $\boldsymbol{\phi}$. One can prove this statement by taking the variation of $Q_{\rm M}$ in (2.25). First, the magnetic charge can be written as

$$Q_{\rm M} \,=\, -\frac{1}{2 e_{\rm H} v_{\rm H}^3} \oint_{\partial\Omega} \epsilon_{jkl} \Big[\boldsymbol{\phi} \cdot \big(\partial^k \boldsymbol{\phi} \times \partial^l \boldsymbol{\phi}\big)\Big] dS^j \,, \tag{2.26}$$

here we have used the relations in (2.10) and (2.23). Next, we can show that

$$\epsilon_{jkl}\, \delta\Big[\boldsymbol{\phi} \cdot \big(\partial^k \boldsymbol{\phi} \times \partial^l \boldsymbol{\phi}\big)\Big] \,=\, 3\epsilon_{jkl} \Big[\delta\boldsymbol{\phi} \cdot \big(\partial^k \boldsymbol{\phi} \times \partial^l \boldsymbol{\phi}\big)\Big] + 2\epsilon_{jkl}\, \partial^k \Big[\boldsymbol{\phi} \cdot \big(\delta\boldsymbol{\phi} \times \partial^l \boldsymbol{\phi}\big)\Big] \,, \tag{2.27}$$

where $\delta\boldsymbol{\phi}$ is any deformation of $\boldsymbol{\phi}$. Note that the second term vanishes due to the Stokes' theorem in the case of an enclosing surface. On the other hand, $\partial^k \boldsymbol{\phi} \times \partial^l \boldsymbol{\phi}$ points in the same direction of $\boldsymbol{\phi}$ since $\partial^{k,l}\boldsymbol{\phi}$ is perpendicular to $\boldsymbol{\phi}$ (also see (A.15)), then, we have

$$\delta\boldsymbol{\phi} \cdot \big(\partial^k \boldsymbol{\phi} \times \partial^l \boldsymbol{\phi}\big) \;\propto\; \boldsymbol{\phi} \cdot \delta\boldsymbol{\phi} \;\propto\; \delta\big(\boldsymbol{\phi} \cdot \boldsymbol{\phi}\big) \,=\, 0 \,. \tag{2.28}$$

Therefore, the variation of the hidden magnetic charge

$$\delta Q_{\rm M} \,\propto\, \epsilon_{jkl}\, \delta\Big[\boldsymbol{\phi} \cdot \big(\partial^k \boldsymbol{\phi} \times \partial^l \boldsymbol{\phi}\big)\Big] \,=\, 0 \,, \tag{2.29}$$

which implies that the monopole can be a DM candidate due to its topological stability.

2.1.3 The Mass of Hidden Monopole

The classical mass of the hidden monopole is contributed by the total energy density of the gauge field and scalar field system. From Eq. (2.11), we have

$$m_{\rm M} = \int d^3x \left[\frac{1}{2} \boldsymbol{E}^j_{\rm H} \cdot \boldsymbol{E}^j_{\rm H} + \frac{1}{2} \boldsymbol{B}^j_{\rm H} \cdot \boldsymbol{B}^j_{\rm H} + \frac{1}{2} \boldsymbol{\Pi} \cdot \boldsymbol{\Pi} + \frac{1}{2} \mathcal{D}^j \boldsymbol{\phi} \cdot \mathcal{D}^j \boldsymbol{\phi} + \mathcal{V}(\phi) \right] . \tag{2.30}$$

In the static solution, we have $\boldsymbol{\Pi} = \mathcal{D}^0 \boldsymbol{\phi} = \partial^0 \boldsymbol{\phi} + e_{\rm H} \boldsymbol{A}^0_{\rm H} \times \boldsymbol{\phi} = 0$, and for simplicity, we further take $\mathcal{V}(\phi) \to 0$. Then, Eq. (2.30) reduces to

$$m_{\rm M} = \frac{1}{2} \int d^3x \left(\boldsymbol{E}^j_{\rm H} \cdot \boldsymbol{E}^j_{\rm H} + \boldsymbol{B}^j_{\rm H} \cdot \boldsymbol{B}^j_{\rm H} + \mathcal{D}^j \boldsymbol{\phi} \cdot \mathcal{D}^j \boldsymbol{\phi} \right) , \tag{2.31}$$

here we keep the energy density stored in the hidden electric field, and the reason will be clear in the next section. Note that the spatial integral (2.31) exists, and this is because $\mathcal{D}^j \boldsymbol{\phi} \to 0$ and $\int d^3x \, \boldsymbol{B}^j_{\rm H} \cdot \boldsymbol{B}^j_{\rm H} \propto \int dr \, r^{-2} \to 0$ at large values of r. Hence, the asymptotic solutions (2.12) do exhibit the field configuration with finite energy.

Now, let us rearrange (2.31) as

$$\begin{aligned} m_{\rm M} = {} & \frac{1}{2} \int d^3x \left(\left| \boldsymbol{E}^j_{\rm H} - \mathcal{D}^j \boldsymbol{\phi} \sin\Theta \right|^2 + \left| \boldsymbol{B}^j_{\rm H} - \mathcal{D}^j \boldsymbol{\phi} \cos\Theta \right|^2 \right) , \\ & + \sin\Theta \int d^3x \, \boldsymbol{E}^j_{\rm H} \cdot \mathcal{D}^j \boldsymbol{\phi} + \cos\Theta \int d^3x \, \boldsymbol{B}^j_{\rm H} \cdot \mathcal{D}^j \boldsymbol{\phi} \\ & \geqslant \sin\Theta \int d^3x \, \boldsymbol{E}^j_{\rm H} \cdot \mathcal{D}^j \boldsymbol{\phi} + \cos\Theta \int d^3x \, \boldsymbol{B}^j_{\rm H} \cdot \mathcal{D}^j \boldsymbol{\phi} , \end{aligned} \tag{2.32}$$

where Θ is an angular parameter and $|\boldsymbol{V}^j|^2 = \boldsymbol{V}^j \cdot \boldsymbol{V}^j$ is a shorthand definition. Then,

$$\begin{aligned} \boldsymbol{B}^j_{\rm H} \cdot \mathcal{D}^j \boldsymbol{\phi} &= \boldsymbol{B}^j_{\rm H} \cdot \partial^j \boldsymbol{\phi} + e_{\rm H} \boldsymbol{B}^j_{\rm H} \cdot \left(\boldsymbol{A}^j_{\rm H} \times \boldsymbol{\phi} \right) \\ &= \partial^j \left(\boldsymbol{\phi} \cdot \boldsymbol{B}^j_{\rm H} \right) - \boldsymbol{\phi} \cdot \left(\partial^j \boldsymbol{B}^j_{\rm H} + e_{\rm H} \boldsymbol{A}^j_{\rm H} \times \boldsymbol{B}^j_{\rm H} \right) \\ &= \partial^j \left(\boldsymbol{\phi} \cdot \boldsymbol{B}^j_{\rm H} \right) - \boldsymbol{\phi} \cdot \mathcal{D}^j \boldsymbol{B}^j_{\rm H} \\ &= \partial^j \left(\boldsymbol{\phi} \cdot \boldsymbol{B}^j_{\rm H} \right) - \boldsymbol{\phi} \cdot \frac{1}{2} \epsilon_{0jkl} \mathcal{D}^j \boldsymbol{F}^{kl} \\ &= \partial^j \left(\boldsymbol{\phi} \cdot \boldsymbol{B}^j_{\rm H} \right) \end{aligned} \tag{2.33}$$

here we have used (2.10) and the Bianchi identity. It follows that

$$\int d^3x \, \boldsymbol{B}^j_{\rm H} \cdot \mathcal{D}^j \boldsymbol{\phi} = \int d^3x \, \partial^j \left(\boldsymbol{\phi} \cdot \boldsymbol{B}^j_{\rm H} \right) = \oint_{\partial\Omega} \left(\boldsymbol{\phi} \cdot \boldsymbol{B}^j_{\rm H} \right) dS^j , \tag{2.34}$$

where we have applied the Green's theorem and evaluated the surface integral at infinity. Using Eqs. (2.10) and (2.20), one can find out in the scalar vacuum

$$\boldsymbol{\phi} \cdot \boldsymbol{B}^j_{\rm H} = \boldsymbol{\phi} \cdot \frac{1}{2} \epsilon_{jkl} \boldsymbol{F}^{kl}_{\rm H} = \boldsymbol{\phi} \cdot \frac{1}{2} \epsilon_{jkl} \left(\frac{1}{\upsilon_{\rm H}} \boldsymbol{\phi} F^{kl}_{\rm H} \right) = \upsilon_{\rm H} \left(\frac{1}{2} \epsilon_{jkl} F^{kl}_{\rm H} \right) = \upsilon_{\rm H} B^j_{\rm H} . \tag{2.35}$$

As a consequence, we have

$$\int d^3x\, \boldsymbol{B}^j_{\rm H} \cdot \mathcal{D}^j \boldsymbol{\phi} \;=\; \upsilon_{\rm H} \oint_{\partial\Omega} \boldsymbol{B}_{\rm H} \cdot d\boldsymbol{S} \;=\; \upsilon_{\rm H} Q_{\rm M} \;. \tag{2.36}$$

Similarly, using the equation of motion in Eq. (2.7), we have

$$\int d^3x\, \boldsymbol{E}^j_{\rm H} \cdot \mathcal{D}^j \boldsymbol{\phi} \;=\; \upsilon_{\rm H} \oint_{\partial\Omega} \boldsymbol{E}_{\rm H} \cdot d\boldsymbol{S} \;=\; \upsilon_{\rm H} Q_{\rm E} \;. \tag{2.37}$$

Substituting Eqs. (2.36) and (2.37) into Eq. (2.32), we obtain

$$m_{\rm M} \;\geqslant\; \upsilon_{\rm H}\big(Q_{\rm E}\sin\Theta + Q_{\rm M}\cos\Theta\big) \;. \tag{2.38}$$

The most severe bound of the monopole mass occurs when the right-hand side of (2.38) reaches its maximum value. This is the so-called Bogomol′nyi bound [99] and is given by

$$m_{\rm M} \;\geqslant\; \upsilon_{\rm H}\sqrt{Q^2_{\rm E} + Q^2_{\rm M}} \;. \tag{2.39}$$

For the ′t Hooft-Polyakov monopole, the Bogomol′nyi bound is then

$$m_{\rm M} \;\geqslant\; \frac{4\pi\upsilon_{\rm H}}{e_{\rm H}} \;. \tag{2.40}$$

In this thesis, we will use this bound as the mass of the hidden monopole for simplicity. Notice that the equality in (2.40) holds when the conditions $V(\phi) = 0$ and $\boldsymbol{B}^j_{\rm H} = \mathcal{D}^j\boldsymbol{\phi}$ are satisfied, see Eq. (2.32). For the former condition, we have two possibilities, $\lambda_\phi = 0$ or $\phi^2 = \upsilon^2_{\rm H}$ in the entire space. However, the latter one leads no magentic field since

$$B^j_{\rm H} \;\propto\; \boldsymbol{\phi}\cdot\boldsymbol{B}^j_{\rm H} \;=\; \boldsymbol{\phi}\cdot\mathcal{D}^j\boldsymbol{\phi} \;=\; \boldsymbol{\phi}\cdot\partial^j\boldsymbol{\phi} + e_{\rm H}\boldsymbol{\phi}\cdot\big(\boldsymbol{A}^j_{\rm H}\times\boldsymbol{\phi}\big) \;=\; 0 \;. \tag{2.41}$$

Therefore, we require that $\lambda_\phi \to 0$ and maintain $\phi^2 = \upsilon^2_{\rm H}$ only at spatial infinity. This is known as the Bogomol′nyi-Prasad-Sommerfield (BPS) limit [99, 100]. The dependence of the monopole mass on the non-zero λ_ϕ is discussed in appendix B.

2.1.4 The Witten Effect

In the previous section, we retain the electric field when estimating the monopole mass, and drop it at the end since the ′t Hooft-Polyakov monopole carries no electric field. However, if CP is not a conserved quantity, then, the electric field can be induced via a CP-violating term. This is named as the Witten effect [6].

To see how the hidden monopole acquires a non-zero electric charge, let us consider the following CP-violating $\theta_{\rm H}$-term in the hidden sector as

$$\mathcal{L}_\theta \;=\; \theta_{\rm H}\frac{e^2_{\rm H}}{32\pi^2}F^{\mu\nu}_{\rm H}\widetilde{F}_{{\rm H}\mu\nu} \;, \tag{2.42}$$

where $\theta_{\rm H}$ is a constant, $F_{\rm H}^{\mu\nu} = \partial^\mu A_{\rm H3}^\nu - \partial^\nu A_{\rm H3}^\mu$ is the field strength tensor of the hidden photon, and $\widetilde{F}_{\rm H}^{\mu\nu}$ is its dual tensor. We will promote $\theta_{\rm H}$ to a dynamical variable, the axion, in the next chapter. Since the $\theta_{\rm H}$-term can be rewritten as a total derivative, it does not affect the equations of motion, and one usually discards such kind term. However, in the presence of the monopole, it has a physical effect. In other words, the monopole acquires an electric charge proportional to $\theta_{\rm H}$, in addition to the magnetic charge. As a result, the monoploe becomes a dyon [101] possessing both electric charge and magnetic charge.

To derive the explicit form of the electric charge of the hidden monopole, let us start with the equations of motion of the hidden electromagnetism,

$$\partial_\mu F_{\rm H}^{\mu\nu} = \frac{e_{\rm H}^2}{8\pi^2}\partial_\mu\big(\theta_{\rm H}\widetilde{F}_{\rm H}^{\mu\nu}\big) \ , \quad \partial_\mu \widetilde{F}^{\mu\nu} = j_{\rm M}^\nu \ , \tag{2.43}$$

where $j_{\rm M}^\mu = (\rho_{\rm M}, \boldsymbol{J}_{\rm M})$ is the magnetic 4-current density. Again, by expressing the strength tensor in terms of the electric and magnetic field as $F_{\rm H}^{j0} = E_{\rm H}^j$ and $F_{\rm H}^{jk} = -\epsilon_{jkl}B_{\rm H}^l$, we obtain the modified Maxwell's equations as

$$\nabla\cdot\boldsymbol{E}_{\rm H} = \frac{e_{\rm H}^2}{8\pi^2}\nabla\cdot\big(\theta_{\rm H}\boldsymbol{B}_{\rm H}\big) \ , \quad \nabla\cdot\boldsymbol{B}_{\rm H} = \rho_{\rm M} \ . \tag{2.44}$$

Suppose that there exists a monopole at the origin with a magnetic charge $Q_{\rm M}$. When measured far from the origin, the magnetic field induced by the monopole is

$$\boldsymbol{B}_{\rm H}(r) = \frac{Q_{\rm M}}{4\pi}\frac{\hat{\boldsymbol{r}}}{r^2} \ , \tag{2.45}$$

where $\hat{\boldsymbol{r}}$ is the unit vector along the radial direction. Here we have assumed that the core radius of the monopole is negligibly small compared to r (see appendix B). Matching with (2.44), one can see that a non-zero hidden electric field is generated around the monopole at a sufficiently large r as

$$\boldsymbol{E}_{\rm H}(r) = \frac{Q_{\rm E}}{4\pi}\frac{\hat{\boldsymbol{r}}}{r^2} \quad \text{with} \quad Q_{\rm E} = \frac{e_{\rm H}^2}{8\pi^2}\theta_{\rm H}Q_{\rm M} = \frac{e_{\rm H}\theta_{\rm H}}{2\pi} \ . \tag{2.46}$$

Therefore, the hidden monopole acquires a nonzero hidden electric charge.[1] Notice that anti-monopoles $\overline{\rm M}$ have the opposite hidden electric charges. We summarize the particle spectrum of the $'$t Hooft-Polyakov model in Tab. 2.1.

One can extend this result by promoting $\theta_{\rm H}$ to a dynamic field, say axion, and show that the electric charge of the monopole is similarly induced by the Witten effect [102]. The difference is that the electric charge spreads out in space, and the electric charge contained inside a sphere with a radius r is given by $Q_{\rm E}(r) = e_{\rm H}\theta(r)/(2\pi)$. Thus, the electric charge distribution depends on the profile of axion field around the monopole, which will be studied in the next chapter.

[1] Actually, there are excited states of monopoles which have non-zero electric charges ($Q_{\rm E} = ne_{\rm H}$) even without the Witten effect. These electric charges are nothing but the Noether charges under some gauge transformations, see appendix C for the discussion.

Table 2.1: The masses, electric and magnetic charges of the particles of the ′t Hooft-Polyakov model in the hidden sector, where $\alpha_{\rm H} = e_{\rm H}^2/(4\pi)$ is the hidden fine structure constant. Here we take the BPS limit for the hidden monopole mass for simplicity and its hidden electric charge is attributed to the Witten effect.

Particle	Mass	Hidden electric charge	Hidden magnetic charge
$\gamma_{\rm H}$	0	0	0
φ	$m_\varphi = \sqrt{2\lambda_\phi}\, v_{\rm H}$	0	0
$W_{\rm H}^{\pm}$	$m_{W_{\rm H}} = \sqrt{4\pi\alpha_{\rm H}}\, v_{\rm H}$	$Q_{\rm E} = \pm e_{\rm H}$	0
$\mathrm{M}(\overline{\mathrm{M}})$	$m_{\rm M} = \sqrt{4\pi/\alpha_{\rm H}}\, v_{\rm H}$	$Q_{\rm E} = \pm e_{\rm H}\theta_{\rm H}/(2\pi)$	$Q_{\rm M} = \pm 4\pi/e_{\rm H}$

2.2 Production Mechanism and Relic Abundance

In the ′t Hooft-Polyakov model, both massive gauge bosons and monopoles are stable because they carry (hidden) electric and/or magnetic charges under the unbroken $\mathrm{U}(1)_{\rm H}$ symmetry and there are no other lighter hidden charged particles. Therefore, they would contribute to the observed density of DM once produced. In this section, we will discuss and determine their production mechanisms and relic abundances, respectively.

2.2.1 Production of Hidden Massive Vector Bosons

The hidden sector is assumed to be in thermal equilibrium with the visible sector via some portal couplings at high temperatures. Therefore, the hidden massive vector bosons are in chemical equilibrium with the thermal bath and their abundances are fixed when the annihilation processes $W_{\rm H}^+ W_{\rm H}^- \longleftrightarrow \varphi\varphi, \gamma_{\rm H}\gamma_{\rm H}$ are decoupled as in the usual chemical freeze-out scenario. The Feynman diagrams of these annihilation processes are depicted in Fig. 2.2. The s-wave annihilation cross-section of the hidden massive vector bosons in the BPS limit is computed as (see appendix D for the computation)

$$\sigma_{\rm ann} v_{\rm rel} \;=\; \frac{107}{18}\frac{\pi\alpha_{\rm H}^2}{m_{W_{\rm H}}^2} \;+\; \mathcal{O}\!\left(\frac{\lambda_\phi}{\alpha_{\rm H}}\right) , \tag{2.47}$$

where $v_{\rm rel}$ is the relative velocity of the $W_{\rm H}^+ W_{\rm H}^-$ pair in their center-of-mass frame. In the non-relativistic regime $\left(v_{\rm rel} \ll 1\right)$, this annihilation cross-section is enhanced by the Sommerfeld effect resulting from (attractive) long-range force between the two incoming hidden massive vector bosons. Summing over all the t-channel ladder diagrams involving hidden photon exchange between $W_{\rm H}^+$ and $W_{\rm H}^-$ (see Fig. 2.3), one can obtain

$$\left(\sigma_{\rm ann} v_{\rm rel}\right)_{\rm S.E} \;=\; S(v_{\rm rel})\left(\sigma_{\rm ann} v_{\rm rel}\right) , \tag{2.48}$$

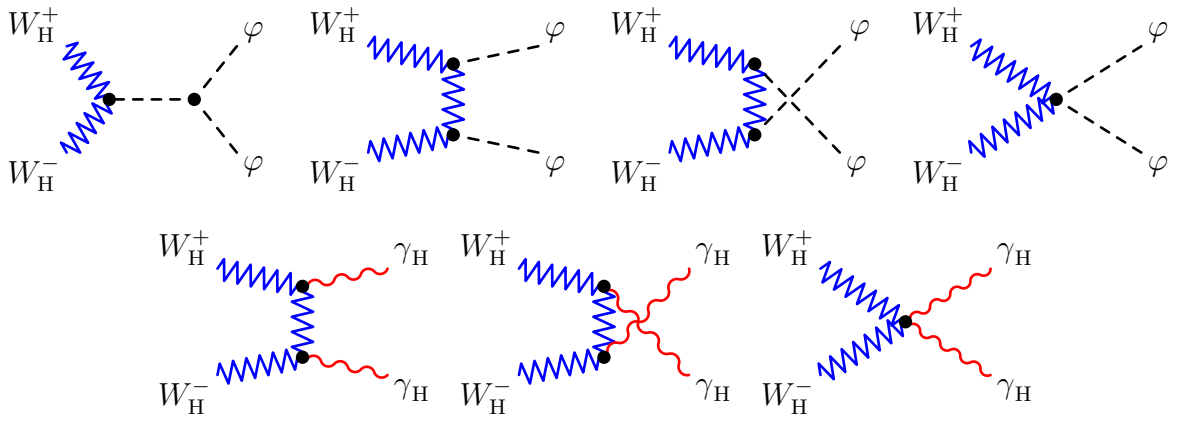

Figure 2.2: The Feynman diagrams of the annihilation processes $W_{\rm H}^+W_{\rm H}^- \longleftrightarrow \varphi\varphi, \gamma_{\rm H}\gamma_{\rm H}$.

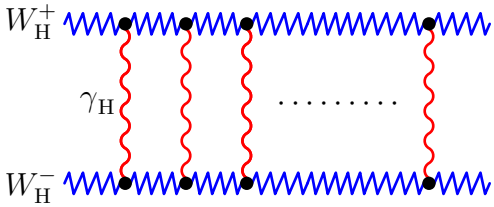

Figure 2.3: The Sommerfeld t-channel ladder diagram for the annihilation of the hidden massive vector bosons via the hidden photon exchange.

where the s-wave Sommerfeld factor reads

$$S(v_{\rm rel}) \;=\; \frac{2\pi\alpha_{\rm H}}{v_{\rm rel}}\frac{1}{1-e^{-2\pi\alpha_{\rm H}/v_{\rm rel}}}\;. \tag{2.49}$$

Then, the thermally-averaged Sommerfeld corrected s-wave cross-section is given by

$$\langle\sigma_{\rm ann}v_{\rm rel}\rangle_{\rm S.E} \;=\; \big\langle S(v_{\rm rel})\big\rangle\big(\sigma_{\rm ann}v_{\rm rel}\big)\;, \tag{2.50}$$

where

$$\big\langle S(v_{\rm rel})\big\rangle \;=\; \frac{x^{3/2}}{\sqrt{4\pi}}\int_0^\infty dv_{\rm rel}\,S(v_{\rm rel})\,v_{\rm rel}^2\,e^{-x\,v_{\rm rel}^2/4} \tag{2.51}$$

with $x \equiv m_{W_{\rm H}}/T$. Now, using the standard derivation for the Boltzmann equations (see (1.25)), the relic density of the hidden massive vector bosons is approximately given as

$$\Omega_{\rm W}h^2 \;\simeq\; \frac{1.07\times10^9\,x_f}{g_{*s,f}/\sqrt{g_{*\rho,f}}\;m_{\rm Pl}\,\langle\sigma_{\rm ann}v_{\rm rel}\rangle_{\rm eff}\,{\rm GeV}}\;, \tag{2.52}$$

$$x_f \;\simeq\; \ln\left(\frac{0.038\,g_W m_{\rm Pl} m_{W_{\rm H}}\,\langle\sigma_{\rm ann}v_{\rm rel}\rangle_{\rm eff}}{\sqrt{g_{*\rho,f}\,x_f}}\right)\;, \tag{2.53}$$

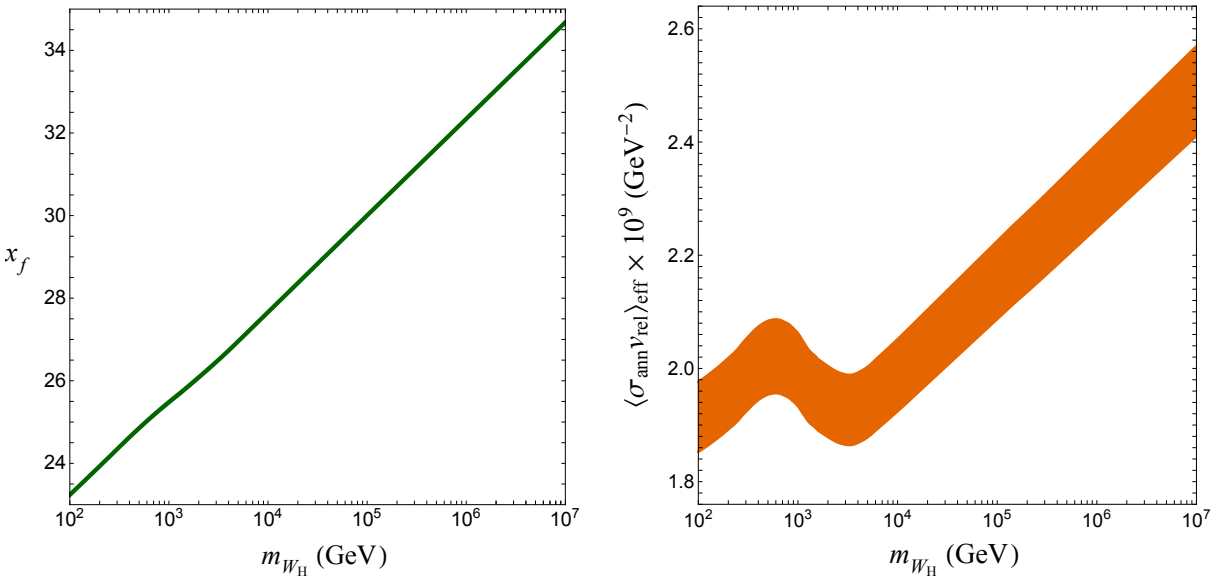

Figure 2.4: Ranges of x_f and $\langle\sigma_{\rm ann}v_{\rm rel}\rangle_{\rm eff}$ as functions of $m_{W_{\rm H}}$ corresponding to the 90% C.L. range of the DM relic density $0.1159 \leqslant \Omega_{\rm DM}\hat{h}^2 \leqslant 0.1233$.

where $x_f \equiv m_{W_{\rm H}}/T_f$ with T_f being the freeze-out temperature, $g_{*\rho,f}$ ($g_{*s,f}$) counts the effective relativistic energy (entropy) degrees of freedom with masses smaller than T_f, $g_W = 6$ is the number of $W_{\rm H}^{\pm}$ degrees of freedom, and the effective annihilation cross-section $\langle\sigma_{\rm ann}v_{\rm rel}\rangle_{\rm eff} \equiv \langle\sigma_{\rm ann}v_{\rm rel}\rangle_{\rm S.E}/2$ due to the two-component hidden massive vector bosons assuming equal amount of the number densities.

By solving (2.52) and (2.53) numerically, we present in Fig. 2.4 the allowed ranges of the freeze-out parameter and the effective annihilation cross-section as functions of the mass of DM without knowing the explicit form of $\langle\sigma_{\rm ann}v_{\rm rel}\rangle_{\rm eff}$. Then, by imposing these ranges on (2.47) to (2.51), we show the hidden fine structure constant as a function of the mass of the hidden massive vector boson in Fig. 2.5, where the results without the Sommerfeld effect are also displayed. The behavior of the color solid curves in this figure is easy to understand. At small values of $\alpha_{\rm H}$, the Sommerfeld effect plays no role since $S(v_{\rm rel}) \simeq 1$ in this region. Conversely, $S(v_{\rm rel}) \simeq 2\pi\alpha_{\rm H}/v_{\rm rel}$ at large values of $\alpha_{\rm H}$, and it is this enhancement factor that causes the solid curves deviate from the dashed ones.

2.2.2 Production of Hidden Monopoles

Throughout this thesis, we assume that the universe undergoes a second-order phase transition in the hidden sector at a critical temperature $T_{\rm c}$. Then, the abundance of the hidden monopole is determined by the Kibble-Zurek mechanism [95, 103], which predicts much larger number density of topological defects than the Kibble's original estimate. Here, we give a brief review of this mechanism in the following paragraphs.

During the second-order phase transition, the thermal system with temperature T

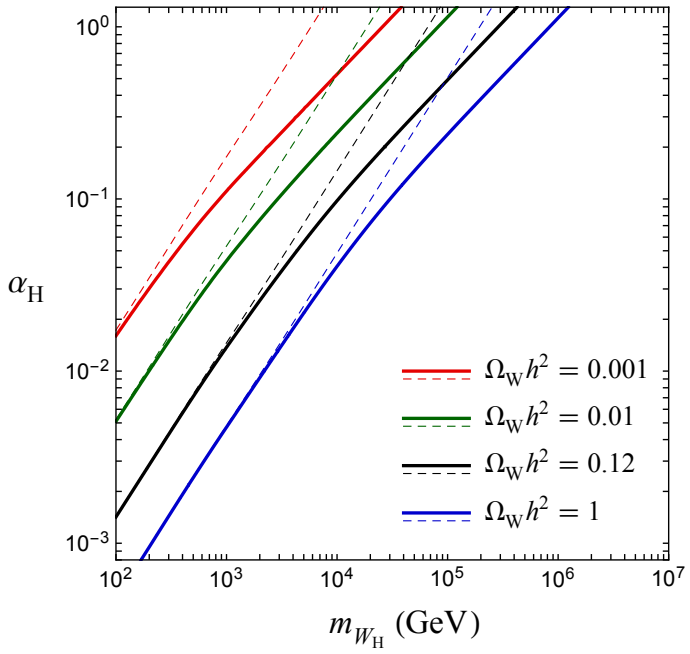

Figure 2.5: Values of $\alpha_{\rm H}$ as a function of $m_{W_{\rm H}}$ for different relic densities of the hidden massive vector boson, where the color solid (dashed) lines correspond to the case with (without) the Sommerfeld effect.

can be characterised by the correlation length $\xi(T)$ and the relaxation time $\tau(T)$ which diverge near the critical temperature. These physical quantities can be parameterized by using the critical exponents ν and μ respectively as

$$\xi(T) \,=\, \xi_0|\epsilon(T)|^{-\nu} \,, \quad \tau(T) \,=\, \tau_0|\epsilon(T)|^{-\mu} \,, \tag{2.54}$$

where $\epsilon(T) \,\equiv\, (T - T_{\rm c})/T_{\rm c}$ is the degree of proximity toward the critical temperature, and ξ_0 and τ_0 are temperature-independent parameters determined by the model. In the $'$t Hooft-Polyakov monopole model, these quantities can be computed from the following Landau-Ginzburg free energy of the form as

$$V(\phi, T) \,=\, \frac{1}{2}M(T)^2\phi^2 + \frac{1}{4}\lambda_\phi\phi^4 \,, \tag{2.55}$$

where $M(T)^2 \,\equiv\, 2m(T - T_{\rm c})$ is the effective mass of $\boldsymbol{\phi}$ with a mass parameter m. At high temperatures, $T \,\gg\, T_{\rm c}$, the $\mathrm{SU}(2)_{\rm H}$ gauge symmetry is unbroken, and the vacuum expectation value of the isovector scalar field vanishes throughout the universe. When $T \,\lesssim\, T_{\rm c} \,\simeq\, \sqrt{\lambda_\phi}v_{\rm H}$, the $\mathrm{SU}(2)_{\rm H}$ gauge symmetry is spontaneously broken as the value of $\langle\phi\rangle$ moves from 0 to $v_{\rm H}$. Then, a domain structure appears, where the direction of $\boldsymbol{\phi}$ in each domain is randomly chosen, and the size of them is characterised by $\xi(T)$. At low temperatures, $T \,\ll\, T_{\rm c}$, the free energy (2.55) in the true vacuum state reduces to

$$V(\phi) \,\simeq\, 2mT_{\rm c}\phi^2 + \frac{1}{4}\lambda_\phi\phi^4 \,. \tag{2.56}$$

Therefore, we have $m \simeq \frac{1}{2}m_\varphi^2/(2T_\mathrm{c}) \simeq \frac{1}{2}\lambda_\phi T_\mathrm{c}$. Now, the two-point correlation function in a scalar field theory tells us that

$$\big\langle\phi(x)\phi(y)\big\rangle \underset{|\boldsymbol{x}-\boldsymbol{y}|\to\infty}{\sim} e^{-M(T)|\boldsymbol{x}-\boldsymbol{y}|} \sim e^{-|\boldsymbol{x}-\boldsymbol{y}|/\xi(T)} \,. \tag{2.57}$$

It follows that

$$\xi(T) \sim \frac{1}{M(T)} \simeq \frac{1}{\sqrt{\lambda_\phi T_\mathrm{c}\big(T-T_\mathrm{c}\big)}} = \frac{1}{\sqrt{\lambda_\phi}\,T_\mathrm{c}}\frac{1}{\sqrt{|\epsilon(T)|}} \,, \tag{2.58}$$

namely $\nu = 1/2$ and $\xi_0 \simeq 1/\big(\sqrt{\lambda_\phi}\,T_\mathrm{c}\big)$. On the other hand, causality requires that $\xi \leqslant \tau$, and as we shall see soon that the Hubble friction for the isovector scalar field $\boldsymbol{\phi}$ can be neglected in the vicinity of the critical temperature. In such a case, one can approximate the relaxation time $\tau \approx \xi$, then we obtain $\mu = 1/2$ and $\tau_0 \simeq \xi_0$. Note that $\nu = \mu = 1/2$ are classical values, and their precise values are subject to the quantum effects.

To fix the correlation length around the critical temperature, let us first describe the behavior of a system during the second-order phase transition. At cosmic times far from t_c (the time at T_c), the relaxation time $\tau(t \ll t_\mathrm{c})$ is much smaller than $|t - t_\mathrm{c}|$. In other words, the system has sufficient time to follow the temperature evolution of the thermal plasma before the phase transition. When the universe approaches the phase transition, there exists a certain time point t_f at which the time left before the transition becomes equal to the relaxation time, $\tau(t_f) = |t_f - t_\mathrm{c}|$. Beyond this point, the correlation length $\xi(t > t_f)$ is frozen since the system can no longer change fast enough with the thermal plasma, and it is unfrozen after $t_\mathrm{c} + \tau(t_f)$ (see Fig. 2.6). Thus, the correlation length at the critical temperature is determined by $\xi(t_f)$ which can be evaluated as follows.

At freeze temperature T_f (the temperature at t_f), we have

$$\tau(t_f) \,=\, \tau_0|\epsilon(T_f)|^{-\mu} \,=\, |t_f - t_\mathrm{c}| \,\ll\, t_\mathrm{c} \,. \tag{2.59}$$

In the radiation-dominated epoch, the temperature $T \propto t^{-1/2}$ and the Hubble parameter $H = \dot{R}/R = 1/(2t)$, one can find

$$\frac{|t_f - t_\mathrm{c}|}{|\epsilon(T_f)|} \,=\, \frac{|t_f - t_\mathrm{c}|}{|(T_f - T_\mathrm{c})/T_\mathrm{c}|} \,\simeq\, 2t_\mathrm{c} \,=\, H(T_\mathrm{c})^{-1} \,\gg\, |t_f - t_\mathrm{c}| \,, \tag{2.60}$$

which implies that the Hubble expansion can be ignored when the system is close to the critical temperature during the phase transition as we expected. Plugging Eq. (2.60) into Eq. (2.59), we obtain

$$|\epsilon(T_f)| \,=\, \big[\tau_0 H(T_\mathrm{c})\big]^{1/(1+\mu)} \,, \quad H(T_\mathrm{c}) \,=\, \sqrt{\frac{4\pi^3 g_{*\rho}(T_\mathrm{c})}{45}}\,\frac{T_\mathrm{c}^2}{m_\mathrm{pl}} \,. \tag{2.61}$$

It follows that the correlation length at the critical temperature is given by

$$\xi(t_\mathrm{c}) \,=\, \xi(t_f) \,=\, \xi_0\big[\tau_0 H(T_\mathrm{c})\big]^{-\nu/(1+\mu)} \,. \tag{2.62}$$

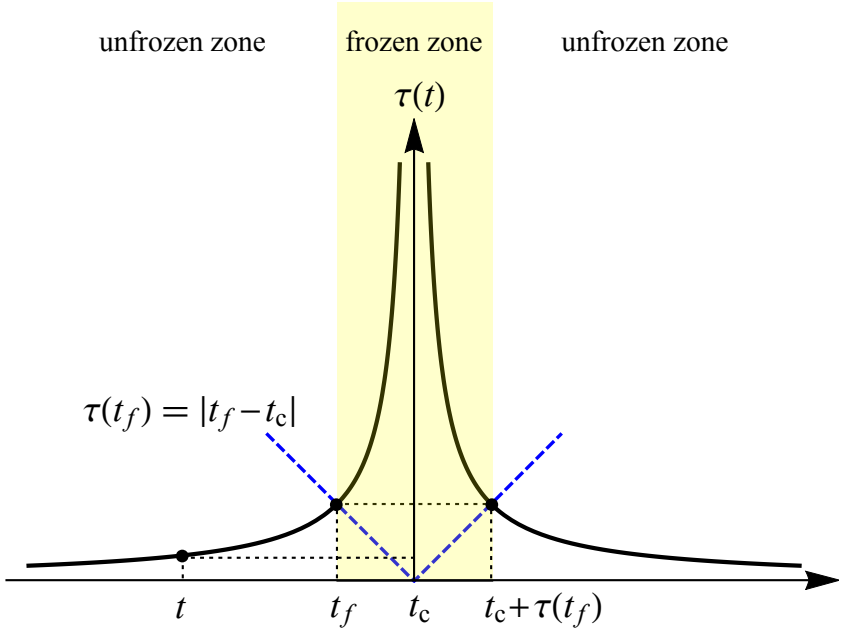

Figure 2.6: The illustration of a system during a second-order phase transition, where the yellow shaded region is the frozen zone during which the correlation length is unchanged.

Assuming at least one hidden monopole is produced in each volume of order $\xi(t_c)^3$, we yield the number density of the hidden monopole created at the critical temperature as $n_M(t_c) \sim \xi(t_c)^{-3}$. The current relic abundance of the hidden monopole from the Kibble-Zurek mechanism is estimated in Refs. [4, 104] as

$$\Omega_M h^2 \simeq 1.5 \times 10^9 \left(\frac{m_M}{1\,\text{TeV}}\right)\left(30\frac{T_c}{m_{Pl}}\right)^{3\nu/(1+\nu)}, \tag{2.63}$$

which has assumed that the M-$\overline{\text{M}}$ annihilation after the phase transition is negligible. Now, if one takes $m_M/T_c \simeq m_M/v_H = \sqrt{4\pi/\alpha_H} \simeq \mathcal{O}(1-10)$, then the mass of the hidden monopole should be around several hundred TeV to account for the observed DM density [104]. Moreover, if α_H is in the perturbative regime, then this relation also indicates that the hidden monopole DM is non-relativistic once produced. Using Eq.(2.63), we show the hidden fine structure constant as a function of the hidden monopole mass in Fig. 2.7.

2.2.3 The Combined Relic Abundance

With the predicted relic abundances (2.52) and (2.63), we present the combined relic density of the hidden massive vector bosons and the hidden monopoles in Fig. 2.8, where $\Omega_{DM}h^2 = \Omega_W h^2 + \Omega_M h^2$ is the total DM density, $r_M = \Omega_M/(\Omega_W + \Omega_M)$ is the fraction of the hidden monopole DM, and we have fixed the critical exponent $\nu = 0.5$ and 0.672.

From this figure, we select four benchmark points for our numerical study.[2] They are

[2]Some of the benchmark points may have strong annihilation effect in order to have a successful

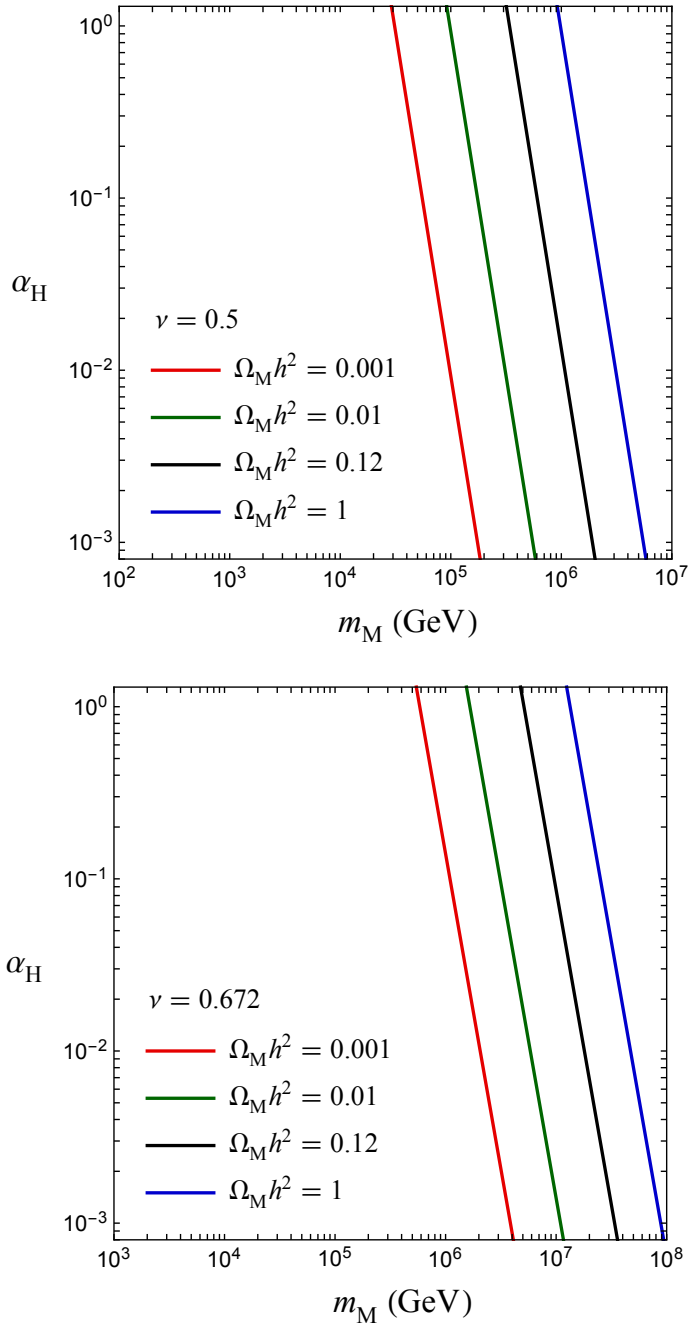

Figure 2.7: Values of $\alpha_{\rm H}$ as a function of $m_{\rm M}$ for different relic densities of the hidden monopole with the critical exponent $\nu = 0.5$ and 0.672 in the color solid lines.

summarized in Tab. 2.2, where the color bullets correspond to the color dots in Fig. 2.8, and the mass of the hidden massive vector bosons can be evaluated by the mass relation, $m_{W_{\rm H}} = \alpha_{\rm H} m_{\rm M}$, in the BPS limit. Notice that, although the precise fraction of the hidden monopole is subject to various uncertainties like the critical exponent and the presence of hidden fermions (that are necessary for the interaction of the axion to be introduced

second-order phase transition [3, 4].

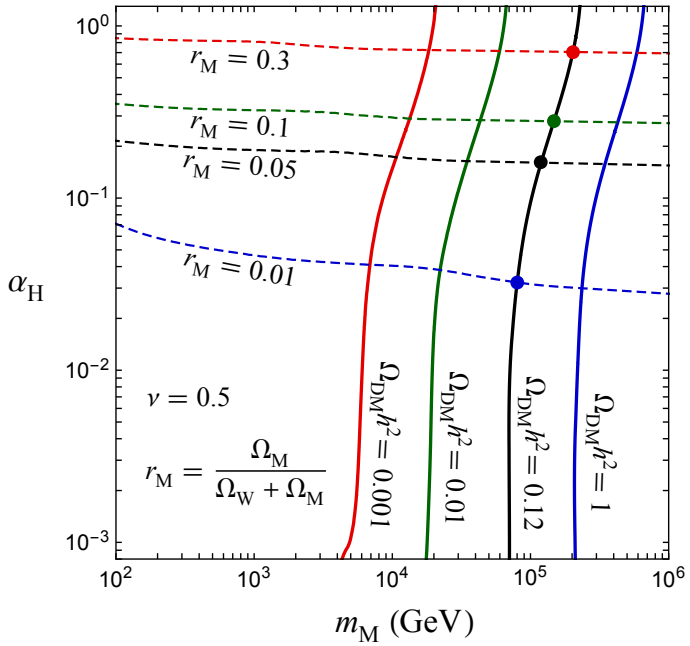

Figure 2.8: Values of $\alpha_{\rm H}$ as a function of $m_{\rm M}$ for different DM relic densities, which are indicated by the color solid curves, and the color dashed curves show the fraction of the hidden monopole. Here we have fixed the critical exponent $\nu = 0.5$.

Table 2.2: The benchmark points satisfied the current DM relic density, $\Omega_{\rm DM}h^2 \simeq 0.12$, in the ′t Hooft-Polyakov monopole model with the critical exponent $\nu = 0.5$.

Benchmark Points	$\alpha_{\rm H}$	$m_{\rm M}$ (TeV)	$m_{W_{\rm H}}$ (TeV)	$v_{\rm H}$ (TeV)	$r_{\rm M}$
• Benchmark Point 1	0.71	203	143	48	0.3
• Benchmark Point 2	0.28	148	41	22	0.1
• Benchmark Point 3	0.16	120	19	14	0.05
• Benchmark Point 4	0.03	80	3	4	0.01

in the next chapter), they do not change our results by more than an order of magnitude at least in the parameter region of our interest.

2.3 Other Aspects

2.3.1 Portal Couplings of Hidden Monopole DM

We have shown that the hidden monopole is a viable DM candidate for two reasons. First, it is an inevitable topological object if the universe undergoes a phase transition

in the hidden sector. Second, its stability is guaranteed by the topological nature. Then, the question is, can we detect them by the underground experiments? In the minimum form of the ′t Hooft-Polyakov model, the answer is No! One has to assume some portal couplings for the hidden sector to the visible sector. There are three possibilities which are discussed in the following.

• **Higgs portal** : It has been studied in Ref. [3] that the hidden monopole DM can interact with the SM particles through the Higgs portal interaction given by

$$\mathcal{L}_{\rm Higgs} \;=\; -\frac{1}{2}\lambda_{\phi H}\big(\boldsymbol{\phi}\cdot\boldsymbol{\phi}-v_{\rm H}^2\big)\left(H^\dagger H-\frac{1}{2}v^2\right)\,. \tag{2.64}$$

By which the differential monopole-proton scattering cross-section is calculated as

$$\frac{d\sigma_{{\rm M}+p\to{\rm M}+p}}{d\Omega} \;\simeq\; \frac{\lambda_{\phi H}^2 f_p^2}{256\pi^2}\frac{\mu_{\rm M}^2 m_p^2}{m_{\rm M}^2\big(m_h^2+2m_A E_{\rm r}\big)^2}\,, \tag{2.65}$$

where $f_p\simeq 0.468$ [105], $\mu_{\rm M}=m_{\rm M}m_p/(m_{\rm M}+m_p)$ is the reduced mass, $m_h\simeq 125.1\,{\rm GeV}$ is the mass of the Higgs boson, and m_A and $E_{\rm r}$ are the mass and the recoil energy of target atom, respectively. For elastic scattering, $2m_A E_{\rm r}\ll m_h^2$, they find

$$\sigma_{{\rm M}+p\to{\rm M}+p} \;\lesssim\; \frac{\lambda_{\phi H}^2 f_p^2}{64\pi m_{\rm M}^2}\frac{m_p^4}{m_h^4} \;\simeq\; 1.34\times 10^{-51}{\rm cm}^2\left(\frac{\lambda_{\phi H}}{0.1}\right)^2\left(\frac{m_{\rm M}}{100\,{\rm TeV}}\right)^{-2}\,. \tag{2.66}$$

It is far from the sensitivities of current or future direct detection searches, see Fig. 1.2.

• **Vector portal** : The hidden monopole DM can also couple to the visible sector via the vector portal interaction by introducing a kinetic mixing between the hidden sector ${\rm U}(1)_{\rm H}$ and the hypercharge ${\rm U}(1)_Y$. As discussed in Refs. [106, 107], one can write down the following dimensional-5 operator as

$$\frac{1}{M}\big(\boldsymbol{\phi}\cdot\boldsymbol{F}_{\rm H}^{\mu\nu}\big)B_{\mu\nu} \;\supset\; \frac{v_{\rm H}}{M}F_3^{\mu\nu}B_{\mu\nu}\,, \tag{2.67}$$

where $F_3^{\mu\nu}$ and $B_{\mu\nu}$ are the field strength tensors of ${\rm U}(1)_Y$ and ${\rm U}(1)_{\rm H}$, respectively, and M being a cut-off scale. This effective operator gives rise to the kinetic mixing of $v_{\rm H}/M$, which is of order 10^{-13} for $v_{\rm H}=10^5\,{\rm GeV}$ and $M=10^{18}\,{\rm GeV}$. Thus, both monopoles and $W_{\rm H}^\pm$ acquire a fractional electric charge of order $v_{\rm H}/M$ through the kinetic mixing. The current limit on such mini-charged DM is satisfied for the mass of $\mathcal{O}(100)\,{\rm TeV}$ and the kinetic mixing of $\mathcal{O}(10^{-13})$ [108, 109]. Again, such a small kinetic mixing makes the monopole-nucleon elastic scattering cross-section far below the sensitivities of present or prospective direct search experiments.

• **Axion portal** : The prototype of the axion portal interaction was first considered in Ref. [102]. By solving the equation of motion of a massless axion, they derive the field configuration of the axion around the GUTs monopole. However, the explicit calculation of the monopole-nucleon scattering cross-section by the axion portal has not been done

in the literature. Hence, it is worth exploring this possibility as the hope to probe the hidden monopole DM. We will discuss about it in more detail in the next chapter. Here let us show the result in advance. The monopole-proton elastic scattering cross-section via the axion portal coupling is estimated as

$$\sigma_{\mathrm{M}+p\to\mathrm{M}+p} \simeq 3.12\times10^{-40}\,\mathrm{cm}^2\left(\frac{\alpha_{\mathrm{H}}}{0.16}\right)^2\left(\frac{f_a}{10^5\,\mathrm{GeV}}\right)^{-2}\left(\frac{m_a}{10\,\mathrm{MeV}}\right)^{-4}, \tag{2.68}$$

where m_a and f_a are the mass and the decay constant of the axion, respectively. This cross-section can be sufficiently large to reach the sensitivities of current or future direct search experiments if the mass of the axion is light enough, see Fig. 1.2. In comparison with the Higgs portal, the corresponding cross-section is suppressed by the Higgs mass.

2.3.2 Self interaction between DM

The hidden massive vector bosons and the hidden monopoles both have long-ranged forces carried by the hidden photon due to the unbroken $\mathrm{U}(1)_{\mathrm{H}}$ symmetry. The DM with self-interaction may resolve some astrophysical issues such as the core-vs-cusp problem and the too-big-to-fail problem, see Ref. [3, 4] for more discussions.

Here let us comment on the bound state formation (BSF) of the DM with the self-interaction. The DM bound states can be formed via emission of a hidden photon. The corresponding cross-section times relative velocity can be written as [110]

$$\sigma_{\mathrm{BSF}}v_{\mathrm{rel}} = S_{\mathrm{BSF}}(v_{\mathrm{rel}})(\sigma_{\mathrm{ann}}v_{\mathrm{rel}})_0\,, \tag{2.69}$$

where

$$S_{\mathrm{BSF}}(v_{\mathrm{rel}}) = \frac{2^{10}\pi}{3}\frac{\zeta^5}{(1+\zeta^2)^2}\frac{e^{-4\zeta\,\mathrm{arccot}\,\zeta}}{1-e^{-2\pi\zeta}}\,, \quad (\sigma_{\mathrm{ann}}v_{\mathrm{rel}})_0 = \frac{\pi\alpha_{\mathrm{H}}^2}{m_{\mathrm{DM}}^2} \tag{2.70}$$

with $\zeta=\alpha_{\mathrm{H}}/v_{\mathrm{rel}}$. For $\zeta\gg1$, Eq. (2.69) can be approximated as

$$\sigma_{\mathrm{BSF}}v_{\mathrm{rel}} \simeq \frac{2^{10}\pi^2}{3e^4}\frac{\alpha_{\mathrm{H}}^3}{m_{\mathrm{DM}}^2 v_{\mathrm{rel}}}\,. \tag{2.71}$$

where $e\simeq2.718$. For the DM forming a bound state at the present time, one can require that $\Gamma_{\mathrm{BSF}}=n_{\mathrm{DM}}\sigma_{\mathrm{BSF}}v_{\mathrm{rel}}=\rho_{\mathrm{DM}}\sigma_{\mathrm{BSF}}v_{\mathrm{rel}}/m_{\mathrm{DM}}\gtrsim H_0$. From Eq. (2.71), it follows that

$$m_{\mathrm{DM}} \lesssim 7.3\,\mathrm{GeV}\left(\frac{\alpha_{\mathrm{H}}}{0.16}\right)\left(\frac{v_{\mathrm{rel}}}{10^{-3}}\right)^{-1/3}\left(\frac{\rho_{\mathrm{DM}}}{0.3\,\mathrm{GeV}\cdot\mathrm{cm}^{-3}}\right)^{1/3}. \tag{2.72}$$

Therefore, the hidden massive vector bosons and the hidden monopoles in this model are difficult to form the bound states due to their heavy masses.

Chapter 3

Monopole-Nucleon Interactions via Axion Portal Coupling

In this chapter, we will demonstrate how to compute the spin-dependent cross-section of the hidden monopole DM scattering off a nucleon via the axion portal coupling. Such calculation may look intractable since a monopole is a composite object and it is not clear how to express its interaction with the axion and the SM particles in the Lagrangian. In the following, we will show our derivation of the field configuration of the axion around the hidden monopole due to the Witten effect. In the case of the massless axion, it was first evaluated in Ref. [102]. Here we extend their result by introducing the axion mass term and apply the obtained axion configuration to estimate the cross-section. The inclusion of the axion mass is crucial because the tail of the axion profile gives the dominant contribution to the scattering cross-section. If the axion also has Yukawa-like interactions with the SM fermions, the hidden monopole surrounded by the axion can scatter off a nucleon. Then, its leading-order cross-section can be estimated by treating the axion configuration as an external classical field. This enables us to impose the current limits and future prospects from various DM direct detection experiments.

3.1 Axion Configuration around Monopole

To find out the axion profile around the hidden monopole, we consider the following Lagrangian density as

$$\mathcal{L}_a = -\frac{1}{4}F_{\rm H}^{\mu\nu}F_{{\rm H}\mu\nu} + \frac{1}{2}\partial^\mu a\partial_\mu a - \frac{1}{2}m_a^2 f_{\rm H}^2\left(\frac{a}{f_{\rm H}} - \theta_0\right)^2 + \frac{e_{\rm H}^2}{32\pi^2}\frac{a}{f_{\rm H}}F_{\rm H}^{\mu\nu}\widetilde{F}_{{\rm H}\mu\nu}\ , \tag{3.1}$$

where $a = a(r)$ is the axion field with $f_{\rm H}$ being the decay constant of the axion. If the shift symmetry of the axion is linearly realized as a global U(1) Peccei-Quinn symmetry in the UV completion, then it resides in the phase of a complex scalar, Φ. Thus, the decay

constant is considered to be an order of the vacuum expectation value of Φ in a simple setup. On the other hand, the axion coupling to the hidden photons can be induced if Φ has a coupling to hidden fermions charged under $\mathrm{SU}(2)_{\mathrm{H}}$. In Eq. (3.1), we have introduced the axion mass term, which may originate from another hidden $\mathrm{SU(N)}_{\mathrm{H}'}$ gauge theory. With gauge field strength $G_{\mathrm{H}'}$, θ_0 is the coefficient of the theta term, $\theta_0 G_{\mathrm{H}'}\widetilde{G}_{\mathrm{H}'}$, and the mass term is obtained by expanding the axion potential around θ_0. This expansion may break down when $\theta_0 \gtrsim 1$ as a/f_{H} changes its value more than $\mathcal{O}(1)$ around the monopole $\big[a(r \to 0) \approx 0\big]$. However, we neglect the possible deviation from the quadratic potential because the calculation of the scattering cross-section is essentially determined by the tail of the axion configuration, where the axion potential can be well approximated by the quadratic form. The axion also acquires a mass contribution from the $\mathrm{SU}(2)_{\mathrm{H}}$ instanton effect. To suppress this contribution, one has to require that $\alpha_{\mathrm{H}} \lesssim 0.2$ [111].

Now, let us place a monopole at the origin and derive the static field configuration of the axion around it. We suppose that, in the absence of the monopole, or at a sufficiently large distance from the monopole, the axion is stabilized at θ_0. Due to the Witten effect, the monopole is surrounded by electric charges with the total amount $e_{\mathrm{H}}\theta_0/2\pi$, which is independent of the axion decay constant. The electric field becomes much stronger as the axion approaches the monopole. As a result, the value of the axion field tends to zero to suppress the energy of the electric field. Thus, the axion configuration is determined by the balance between the gradient energy of the axion and the energy stored in the electric field around the monopole.

To derive the precise axion distribution around the monopole, one needs to minimize the Hamiltonian of the axion-monopole system given by

$$\begin{aligned} H_{a-\mathrm{M}} &= \int d^3x \left[\frac{1}{2}\dot{\theta}^2 + \frac{1}{2}f_{\mathrm{H}}^2\big(\nabla\theta\big)^2 + \frac{1}{2}m_a^2 f_{\mathrm{H}}^2\big(\theta-\theta_0\big)^2 + \frac{1}{2}|\boldsymbol{E}_{\mathrm{H}}|^2 + \frac{1}{2}|\boldsymbol{B}_{\mathrm{H}}|^2\right] \\ &\supset 2\pi f_{\mathrm{H}}^2 \int_{r_{\mathrm{c}}}^{\infty} dr \left[\left(r\frac{d\theta(r)}{dr}\right)^2 + m_a^2 r^2\big(\theta(r)-\theta_0\big)^2 + \frac{r_0^2}{r^2}\theta(r)^2\right], \end{aligned} \tag{3.2}$$

here we have defined a dimensionless axion field, $\theta \equiv a/f_{\mathrm{H}}$, and we have used Eqs. (2.46) and (3.1) and omitted the kinetic energy of the axion in the second line as we are only interested in the static field configuration. We have also dropped the energy density of the hidden magnetic field since it is not a function of the axion field. Notice that the theta term $\theta F\widetilde{F}$ in Eq. (2.42) does not contribute to the Hamiltonian density even if θ is spacetime dependent. The easiest way to prove this is to consider the following action

$$\mathcal{S}_\theta = \int d^4x\,\sqrt{-g}\,\theta(x)F^{\mu\nu}\widetilde{F}_{\mu\nu} = \frac{1}{2}\epsilon_{\mu\nu\alpha\beta}\int d^4x\,\theta(x)F^{\mu\nu}F^{\alpha\beta}\,, \tag{3.3}$$

where $\widetilde{F}_{\mu\nu} = \frac{1}{2}\epsilon_{\mu\nu\alpha\beta}F^{\alpha\beta}/\sqrt{-g}$. Therefore, the energy-momentum tensor of the θ term, $T_\theta^{\mu\nu} = \big(2/\sqrt{-g}\big)\delta\mathcal{S}_\theta/\delta g_{\mu\nu} = 0$. Furthermore, we have assumed spherically symmetrical

functions $\theta(r)$ in the second line and defined r_0 as

$$r_0 \equiv \frac{e_{\rm H}}{8\pi^2 f_{\rm H}} \ . \tag{3.4}$$

The physical meaning of r_0 will be clear later. The lower end of the integration is set by the core radius of the hidden monopole, $r_{\rm c}$. In the case of 't Hooft-Polyakov monopole, it is given by $r_{\rm c} \simeq m_{W_{\rm H}}^{-1}$, inside which the original $\mathrm{SU}(2)_{\rm H}$ gauge symmetry is restored. In the following analysis, we will assume that the core radius is negligible since the axion profile outside the core is considered to be insensitive to $r_{\rm c}$. This is because the electric field outside is simply determined by the Gauss's law, and it does not depend on the core radius. Thus, in practice, one may use only the $r > r_{\rm c}$ part of the axion profile obtained ignoring the core radius. Also, the typical momentum transfer in the monopole-nucleon scattering is much smaller than the mass of the hidden vector boson, and therefore, the scattering cross-section is sensitive to the axion profile far from the monopole.

What we want to know is the field configuration that minimizes the Hamiltonian. To this end, it is convenience to change the radial coordinate r to a dimensionless variable $z = r_0/r$. With this substitution, the Hamiltonian (3.2) becomes

$$H_{a-\rm M} = \frac{e_{\rm H} f_{\rm H}}{4\pi} \int_{r_{\rm c}/r_0}^{\infty} dz \left[\left(\frac{d\theta(z)}{dz} \right)^2 + \theta(z)^2 + \frac{m_a^2 r_0^2}{z^4} \big(\theta(z) - \theta_0 \big)^2 \right] . \tag{3.5}$$

Then, by minimizing Eq. (3.5), the equation of motion of the axion field to be solved is

$$\frac{d^2\theta(z)}{dz^2} = \theta(z) + \frac{m_a^2 r_0^2}{z^4} \big(\theta(z) - \theta_0 \big) \ . \tag{3.6}$$

In order for the energy density of the axion-monopole system to be finite, here we impose $\theta(z \to \infty) = 0$ and $\theta(z \to 0) = \theta_0$ as the boundary conditions of Eq. (3.6). Unfortunately, this differential equation cannot be solved analytically. Instead, we solve this differential equation with its asymptotic forms as

$$\frac{d^2\theta(z)}{dz^2} \simeq \begin{cases} \theta(z) & \text{for} \quad z > \sqrt{m_a r_0} \\ \dfrac{m_a^2 r_0^2}{z^4} \big(\theta(z) - \theta_0 \big) & \text{for} \quad z < \sqrt{m_a r_0} \end{cases} , \tag{3.7}$$

which has the analytical solutions given by

$$\theta(z) \simeq \begin{cases} \theta_>(z) \equiv \theta_0 \left(\dfrac{1 + \sqrt{m_a r_0}}{1 + 2\sqrt{m_a r_0}} \right) e^{-z + \sqrt{m_a r_0}} & \text{for} \quad z > \sqrt{m_a r_0} \\ \theta_<(z) \equiv \theta_0 \left(1 - \dfrac{z}{1 + 2\sqrt{m_a r_0}} \, e^{-m_a r_0/z + \sqrt{m_a r_0}} \right) & \text{for} \quad z < \sqrt{m_a r_0} \end{cases} . \tag{3.8}$$

Note that this solution is smooth at $z = \sqrt{m_a r_0}$, and we have checked that the asymptotic solutions given by (3.8) agree with the numerical solutions of (3.6) to very high accuracy.

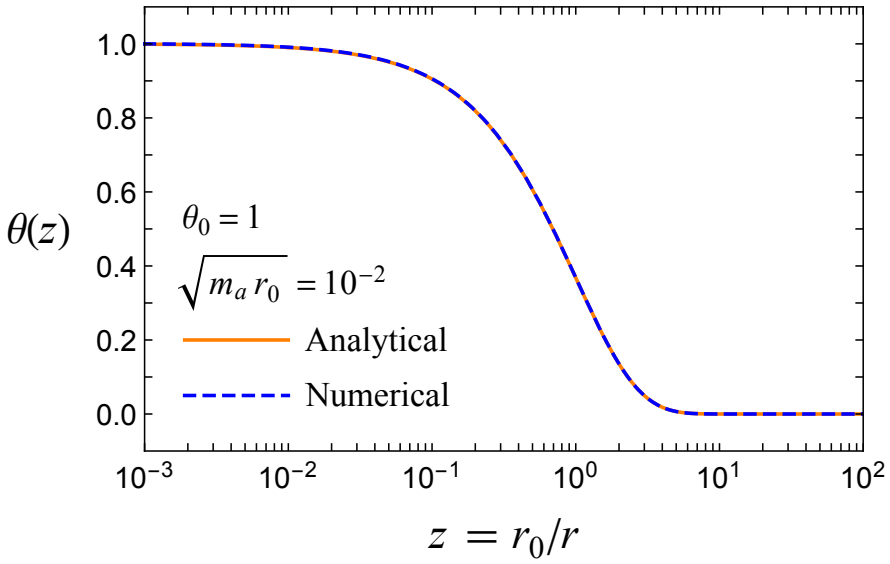

Figure 3.1: The configuration of the axion field around the monopole as a function of $z = r_0/r$ for $\theta_0 = 1$ and $\sqrt{m_a r_0} = 10^{-2}$. The monopole is located at $z \to \infty$ (i.e. $r = 0$), and the axion field takes the vacuum value θ_0 at $z \to 0$ (i.e. $r \to \infty$). The core radius is assumed to be negligibly small for simplicity. The obtained profile is valid for $r > r_c$.

See Fig. 3.1 as an example, where we take $\theta_0 = 1$ and $\sqrt{m_a r_0} = 10^{-2}$, and we make a comparison between the analytical and numerical solutions. One can see that the two lines agree very well with each other. In this figure, the hidden monopole is located at $z \to \infty$ (i.e. $r = 0$), and the axion field takes the vacuum value θ_0 at $z \to 0$ (i.e. $r \to \infty$). The axion field value starts to decrease around $z \simeq 1$ (i.e. $r \simeq r_0$), and this is due to the fact that a nonzero axion field costs large energy stored in the hidden electric field near the origin because of $E_{\rm H}(r)^2 \propto \theta(r)^2/r^4$.

So far we have not specified the relationship between m_a and $1/r_0$. For our purpose, we are interested in relatively light axion masses between 10 MeV and 10 GeV (the mass region of scalar particles searched by the beam-dump experiments such as CHARM and SHiP), while the axion decay constant $f_{\rm H}$ is constrained to be much larger than m_a in this mass range. From Eq. (3.4), on can readily show that

$$\sqrt{m_a r_0} = \sqrt{\frac{e_{\rm H}}{8\pi^2}\frac{m_a}{f_{\rm H}}} \simeq 0.13\left(\frac{\alpha_{\rm H}}{0.16}\right)^{1/4}\left(\frac{m_a}{f_{\rm H}}\right)^{1/2} \ll 1 \,. \tag{3.9}$$

Hence, in the following calculation, we assume that $m_a r_0 \ll 1$, for which the axion mass is relevant only in the tail of the axion field configuration around the monopole. As we shall see, those outer parts contribute most to the scattering cross-section, and this is because the typical momentum transfer between the monopole and the nucleon is much smaller than m_a. It is also clear that the precise size of the monopole core radius does not affect the calculation of the cross-section.

3.2 Spin-Dependent Elastic Scattering Cross-Section of Monopole and Nucleon

With the obtained axion field profile (3.8), we can now calculate the amplitude of the monopole-nucleon scattering by introducing the following axion-nucleon interaction as

$$H_{a-\mathrm{N}} = \int d^3x\, \mathcal{H}_{a-\mathrm{N}} = \frac{C_{\mathrm{N}} m_{\mathrm{N}}}{f_a} \int d^3x \left[a(x) \overline{\psi}_{\mathrm{N}}(x) i\gamma^5 \psi_{\mathrm{N}}(x) \right] , \tag{3.10}$$

where N presents the nucleon (proton p or neutron n), C_{N} is a constant of order unity, $m_{\mathrm{N}} \simeq 1\,\mathrm{GeV}$ is the nucleon mass, and f_a is an energy scale characterizing the strength of the axion-nucleon coupling. In the following calculation, we will assume $f_a = f_{\mathrm{H}}$ for simplicity, but f_a can be much larger or smaller than f_{H} in a slightly contrived setup, e.g. clockwork axion [112]. The values of C_p and C_n are actually model-dependent. In our numerical computation, we choose $|C_p| \simeq 0.4$ and $|C_n| \simeq 0.05$, which are typical values in the DFSZ axion model [44].

In our setup, the monopole is much heavier than nucleons, and so, we can treat $a(x)$ as a classical static scalar field around the monopole while we treat $\psi_{\mathrm{N}}(x)$ as the usual quantized Dirac field in the same manner of the Rutherford scattering. Then, the amplitude of the monopole-nucleon scattering mediated by the axion to the lowest order is calculated as below [113]

$$\begin{aligned}
& i\mathcal{M}_{\mathrm{M+N\to M+N}} \times (2\pi)\delta\big(E'_{\mathrm{N}} - E_{\mathrm{N}}\big) \\
&= -i \int d^4x \left\langle p'_{\mathrm{N}}, s'_{\mathrm{N}} \middle| \mathcal{H}_{a-\mathrm{N}} \middle| p_{\mathrm{N}}, s_{\mathrm{N}} \right\rangle = \frac{C_{\mathrm{N}} m_{\mathrm{N}}}{f_a} \int d^4x\, a(x) \left\langle p'_{\mathrm{N}}, \overline{s'_{\mathrm{N}} \middle| \overline{\psi}_{\mathrm{N}}}(x) \gamma^5 \overline{\psi_{\mathrm{N}}(x) \middle| p_{\mathrm{N}}}, s_{\mathrm{N}} \right\rangle \\
&= \frac{C_{\mathrm{N}} m_{\mathrm{N}}}{f_a} \int d^3x\, a(\boldsymbol{x})\, e^{-i(\boldsymbol{p}'_{\mathrm{N}} - \boldsymbol{p}_{\mathrm{N}})\cdot \boldsymbol{x}} \int dt\, e^{i(E'_{\mathrm{N}} - E_{\mathrm{N}})\cdot t} \times \left[\overline{u}(p'_{\mathrm{N}}, s'_{\mathrm{N}}) \gamma^5 u(p_{\mathrm{N}}, s_{\mathrm{N}}) \right] \\
&= C_{\mathrm{N}} m_{\mathrm{N}} \int d^3x\, \theta(\boldsymbol{x})\, e^{-i\boldsymbol{q}\cdot\boldsymbol{x}} \times (2\pi)\delta\big(E'_{\mathrm{N}} - E_{\mathrm{N}}\big) \times \left[\overline{u}(p'_{\mathrm{N}}, s'_{\mathrm{N}}) \gamma^5 u(p_{\mathrm{N}}, s_{\mathrm{N}}) \right] ,
\end{aligned} \tag{3.11}$$

it follows that

$$i\mathcal{M}_{\mathrm{M+N\to M+N}} = C_{\mathrm{N}} m_{\mathrm{N}} \widetilde{\theta}(\boldsymbol{q}) \left[\overline{u}(p'_{\mathrm{N}}, s'_{\mathrm{N}}) \gamma^5 u(p_{\mathrm{N}}, s_{\mathrm{N}}) \right] , \tag{3.12}$$

where $u_{\mathrm{N}}(p)$ is the Dirac spinor, $\boldsymbol{q} = \boldsymbol{p}'_{\mathrm{N}} - \boldsymbol{p}_{\mathrm{N}}$ is the transferred 3-momentum, and $\widetilde{\theta}(\boldsymbol{q})$ is the 3-dimensional Fourier transform of $\theta(\boldsymbol{x})$ given by

$$\widetilde{\theta}(\boldsymbol{q}) \equiv \int d^3x\, \theta(\boldsymbol{x})\, e^{-i\boldsymbol{q}\cdot\boldsymbol{x}} = \frac{4\pi r_0^2}{|\boldsymbol{q}|} \int_0^{r_0/r_{\mathrm{c}}} dz\, \frac{\theta(z)}{z^3} \sin\left(\frac{|\boldsymbol{q}| r_0}{z} \right) . \tag{3.13}$$

Here we have introduced the cut-off in the integration corresponding to the core radius because the axion configuration derived before is valid only for $r > r_{\mathrm{c}}$. Plugging Eq. (3.8)

into Eq. (3.13), we have

$$\widetilde{\theta}(\boldsymbol{q}) = \frac{4\pi r_0^2}{|\boldsymbol{q}|}\left[\int_0^{\sqrt{m_a r_0}} dz\,\frac{\theta_<(z)}{z^3}\sin\left(\frac{|\boldsymbol{q}|r_0}{z}\right) + \int_{\sqrt{m_a r_0}}^{r_0/r_\mathrm{c}} dz\,\frac{\theta_>(z)}{z^3}\sin\left(\frac{|\boldsymbol{q}|r_0}{z}\right)\right] \tag{3.14}$$

for $\sqrt{m_a r_0} < r_0/r_\mathrm{c}$, and

$$\widetilde{\theta}(\boldsymbol{q}) = \frac{4\pi r_0^2}{|\boldsymbol{q}|}\int_0^{r_0/r_\mathrm{c}} dz\,\frac{\theta_<(z)}{z^3}\sin\left(\frac{|\boldsymbol{q}|r_0}{z}\right) \tag{3.15}$$

for $\sqrt{m_a r_0} > r_0/r_\mathrm{c}$. The integral of (3.14) and (3.15) involves an IR divergence at small z, which can be removed by inserting the regulator, $\lim_{\delta\to 0} e^{-\delta/z}$. Then, both integrations give approximately the same result (see appendix E.1 for the more detailed derivations),

$$\widetilde{\theta}(\boldsymbol{q}) \simeq -4\pi\theta_0\left(\frac{r_0}{m_a^2} + \frac{r_\mathrm{c}^3}{3}\right) + \mathcal{O}(\epsilon_q^2) \tag{3.16}$$

for $\sqrt{m_a r_0} \ll 1$. Here we have defined $\epsilon_q = |\boldsymbol{q}|/m_a \simeq m_\mathrm{N} v_\mathrm{DM}/m_a \ll 1$, where $v_\mathrm{DM} \simeq 10^{-3}$ is the typical speed of DM with respect to the reference frame of the nucleon at the solar radius in our Galaxy. Notice that if $m_a \lesssim 10^{-3}\,\mathrm{GeV}$, then one has to do the integrations numerically, because ϵ_q is no longer smaller than unity. However, for the interesting range of the axion decay constant, such a light axion is tightly constrained by astrophysics [5], and we do not consider it in this thesis. Also, we have numerically checked that Eq. (3.16) gives a good approximation to Eqs. (3.14) and (3.15) as long as $\sqrt{m_a r_0} \ll 1$ no matter the size of r_0/r_c. This is because the DM-nucleon scattering is a low-energy process and therefore the integral is dominated by small z (i.e. large r).

From Eqs. (3.12) and (3.16), we can now calculate the squared matrix element of the monopole-nucleon scattering with averaging (summing) over the initial (final) spins as

$$\begin{aligned}
&\overline{\left|\mathcal{M}_{\mathrm{M+N}\to\mathrm{M+N}}\right|^2} \\
&= \left[C_\mathrm{N} m_\mathrm{N}\widetilde{\theta}(\boldsymbol{q})\right]^2\left[-\frac{1}{2}\sum_{s_\mathrm{N},\,s'_\mathrm{N}}\overline{u}(p'_\mathrm{N},s'_\mathrm{N})\gamma^5 u(p_\mathrm{N},s_\mathrm{N})\,\overline{u}(p_\mathrm{N},s_\mathrm{N})\gamma^5 u(p'_\mathrm{N},s'_\mathrm{N})\right] \\
&= -\frac{1}{2}\left[C_\mathrm{N} m_\mathrm{N}\widetilde{\theta}(\boldsymbol{q})\right]^2 \mathrm{tr}\left[\left(\not{p}'_\mathrm{N} + m_\mathrm{N}\right)\gamma^5\left(\not{p}_\mathrm{N} + m_\mathrm{N}\right)\gamma^5\right] \\
&= -\frac{1}{2}\left[C_\mathrm{N} m_\mathrm{N}\widetilde{\theta}(\boldsymbol{q})\right]^2 \times 4\left(m_\mathrm{N}^2 - p'_\mathrm{N}\cdot p_\mathrm{N}\right) = -\left[C_\mathrm{N} m_\mathrm{N}\widetilde{\theta}(\boldsymbol{q})\right]^2 q^2 \\
&= 16\pi^2\theta_0^2 C_\mathrm{N}^2 m_\mathrm{N}^2\left(\frac{r_0}{m_a^2} + \frac{r_\mathrm{c}^3}{3}\right)^2|\boldsymbol{q}|^2\,,
\end{aligned} \tag{3.17}$$

where $q = p'_\mathrm{N} - p_\mathrm{N}$ is the transferred four-momentum, and $q^2 = -|\boldsymbol{q}|^2$ for an elastic scattering. For our benchmark point, the second term in the bracket of the last line of (3.17) is negligible since $r_\mathrm{c} \simeq m_{W_\mathrm{H}}^{-1} \propto m_\mathrm{M}^{-1}$ and we consider very heavy monopole mass,

namely the effect of the hidden monopole core can be neglected. Then, the resulting differential spin-dependent cross-section of the hidden monopole DM elastic scattering off a nucleon is evaluated as [113]

$$\frac{d\sigma_{\mathrm{M+N\to M+N}}}{d\Omega} = \frac{\overline{\left|\mathcal{M}_{\mathrm{M+N\to M+N}}\right|^2}}{16\pi^2} \simeq \frac{\alpha_{\mathrm{H}}\theta_0^2 C_{\mathrm{N}}^2}{16\pi^3}\frac{m_{\mathrm{N}}^2}{m_a^4 f_a^2}|\boldsymbol{q}|^2 \ , \tag{3.18}$$

where Eq. (3.4) has been used. We will use this result to constraint the axion decay constant by DM direct detection experiments in the next section.

Before ending this section, let us briefly discuss the hidden vector boson DM in our model setup since it can also interact with nucleus through the axion exchange. The elastic scattering of the hidden vector boson DM and a nucleon can be described by the following dimensional-7 effective operator as

$$\mathcal{O}_{\mathrm{N}W}^{(7)} = \frac{\alpha_{\mathrm{H}}}{8\pi}\frac{m_{\mathrm{N}}}{m_a^2 f_a^2}\overline{\psi}_{\mathrm{N}} i\gamma_5 \psi_{\mathrm{N}} W_{\mathrm{H}}^{\pm\mu\nu}\widetilde{W}_{\mathrm{H}\mu\nu}^{\mp} \ , \tag{3.19}$$

and from which the differential cross-section of the hidden gauge boson scattering off a nucleon is computed as (see appendix E.2 for the computation)

$$\frac{d\sigma_{W+\mathrm{N}\to W+\mathrm{N}}}{d\Omega} \simeq \frac{\alpha_{\mathrm{H}}^2}{1536\pi^4}\frac{m_{\mathrm{N}}^2}{m_a^4 f_a^4}|\boldsymbol{q}|^4 \ . \tag{3.20}$$

Comparing Eq. (3.20) with Eq. (3.18), we find that

$$\frac{d\sigma_{W+\mathrm{N}\to W+\mathrm{N}}/d\Omega}{d\sigma_{\mathrm{M+N}\to\mathrm{M+N}}/d\Omega} \simeq \frac{\alpha_{\mathrm{H}}}{96\pi\theta_0^2 C_{\mathrm{N}}^2}\frac{|\boldsymbol{q}|^2}{f_a^2} \ll 1 \ . \tag{3.21}$$

and therefore, the hidden gauge boson-nucleon scattering is negligible. This motivates us to focus on the hidden monopole-nucleon scattering via the axion portal.

Lastly, with the results of (3.18) and (3.20) one may wonder why the hidden monopole-nucleon scattering cross-section is suppressed only by the decay constant squared rather than fourth power of it. If one goes back to the calculation, one can see that the peculiar dependence on f_a comes from the axion configuration around the monopole, and that the dominant contribution to the scattering cross-section comes from $r \sim \sqrt{r_0/m_a}$, where the axion mass becomes relevant.

3.3 Limits from DM Direct Detection Experiments

Now let us estimate the present limits on the predicted scattering cross-section (3.18) from the DM direct detection experiments. To this end, usually one has to evaluate the differential recoil rate of DM on nuclei. Here we adopt another approach by considering the following dimensional-6 pseudo-scalar operator given in Ref. [114] since it gives the same dependence of the scattering cross section on the transferred momentum $\boldsymbol{q}$,

$$\mathcal{O}^{(6)}_{\chi\mathrm{N}} = \frac{g_{\chi\mathrm{N}}}{\Lambda^2}\left(\overline{\psi}_\chi\psi_\chi\right)\left(\overline{\psi}_\mathrm{N} i\gamma^5\psi_\mathrm{N}\right) , \tag{3.22}$$

where χ is a fermionic DM with $g_{\chi\mathrm{N}}$ being the coupling strength to the nucleon, and Λ is the cut-off scale of the theory. The tree-level matrix element of the χ-N scattering in the non-relativistic limit is given by

$$\begin{aligned}\mathcal{M}_{\chi+\mathrm{N}\to\chi+\mathrm{N}} &= \frac{g_{\chi\mathrm{N}}}{\Lambda^2}\langle p'_\chi, s'_\chi|\overline{\psi}_\chi\psi_\chi|p_\chi, s_\chi\rangle\langle p'_\mathrm{N}, s'_\mathrm{N}|\overline{\psi}_\mathrm{N}\gamma^5\psi_\mathrm{N}|p_\mathrm{N}, s_\mathrm{N}\rangle \\ &\simeq \frac{2g_{\chi\mathrm{N}}m_\chi}{\Lambda^2}\left[\xi^\dagger(s'_\chi)\xi(s_\chi)\right]\left[\xi^\dagger(s'_\mathrm{N})(\boldsymbol{q}\cdot\boldsymbol{\sigma})\xi(s_\mathrm{N})\right] ,\end{aligned} \tag{3.23}$$

where m_χ is the mass of χ, $\xi(s)$ is the two-component spinor with s being the state of spin, $\boldsymbol{\sigma} = (\sigma_1, \sigma_2, \sigma_3)$ is the Pauli spin matrix vector, and the bilinear matrix elements in the non-relativistic limit behave as

$$\langle p'_\chi, s'_\chi|\overline{\psi}_\chi\psi_\chi|p_\chi, s_\chi\rangle \simeq 2m_\chi\xi^\dagger(s'_\chi)\xi(s_\chi) , \tag{3.24}$$

$$\langle p'_\mathrm{N}, s'_\mathrm{N}|\overline{\psi}_\mathrm{N}\gamma^5\psi_\mathrm{N}|p_\mathrm{N}, s_\mathrm{N}\rangle \simeq \xi^\dagger(s'_\mathrm{N})(\boldsymbol{q}\cdot\boldsymbol{\sigma})\xi(s_\mathrm{N}) . \tag{3.25}$$

Then, the squared matrix element of the χ-N scattering with averaging (summing) over the initial (final) spins is calculated as

$$\begin{aligned}\overline{|\mathcal{M}_{\chi+\mathrm{N}\to\chi+\mathrm{N}}|^2} &= \frac{4g^2_{\chi\mathrm{N}}m^2_\chi}{\Lambda^4}\times\frac{1}{2}\sum_{s_\chi, s'_\chi}\left[\xi^\dagger(s'_\chi)\xi(s_\chi)\right]\left[\xi^\dagger(s_\chi)\xi(s'_\chi)\right] \\ &\qquad\times\frac{1}{2}\sum_{s_\mathrm{N}, s'_\mathrm{N}}\left[\xi^\dagger(s'_\mathrm{N})(\boldsymbol{q}\cdot\boldsymbol{\sigma})\xi(s_\mathrm{N})\right]\left[\xi^\dagger(s_\mathrm{N})(\boldsymbol{q}\cdot\boldsymbol{\sigma})\xi(s'_\mathrm{N})\right] \\ &= \frac{g^2_{\chi\mathrm{N}}m^2_\chi}{\Lambda^4}\sum_{s'_\chi}\left[\xi^\dagger(s'_\chi)\xi(s'_\chi)\right]\sum_{s'_\mathrm{N}}\left[\xi^\dagger(s'_\mathrm{N})(\boldsymbol{q}\cdot\boldsymbol{\sigma})^2\xi(s'_\mathrm{N})\right] \\ &= \frac{g^2_{\chi\mathrm{N}}m^2_\chi}{\Lambda^4}\times 2\times 2|\boldsymbol{q}|^2 = \frac{4g^2_{\chi\mathrm{N}}m^2_\chi}{\Lambda^4}|\boldsymbol{q}|^2 .\end{aligned} \tag{3.26}$$

It follows that the differential cross-section of χ-N scattering is estimated as

$$\frac{d\sigma_{\chi+\mathrm{N}\to\chi+\mathrm{N}}}{d\Omega} \simeq \frac{\overline{|\mathcal{M}_{\chi+\mathrm{N}\to\chi+\mathrm{N}}|^2}}{64\pi^2\left(m_\chi + m_\mathrm{N}\right)^2} \simeq \frac{g^2_{\chi\mathrm{N}}}{16\pi^2\Lambda^4}|\boldsymbol{q}|^2 , \tag{3.27}$$

where we have assumed that $m_\chi \gg m_\mathrm{N}$ in the last equality. Thus, one can see that this has the same momentum dependence as (3.18). Note also that the operator (3.22) violates CP corresponding to the fact that the axion profile around the monopole breaks CP.

Since (3.18) and (3.27) we have derived are spin-dependent cross-sections, therefore, we have to consider the DM search experiments that use target nuclei with spin carried mostly by the unpaired proton or neutron. In the following, we will focus on the COUPP and PICO experiments because they adopt ^{19}F which has unpaired proton and they

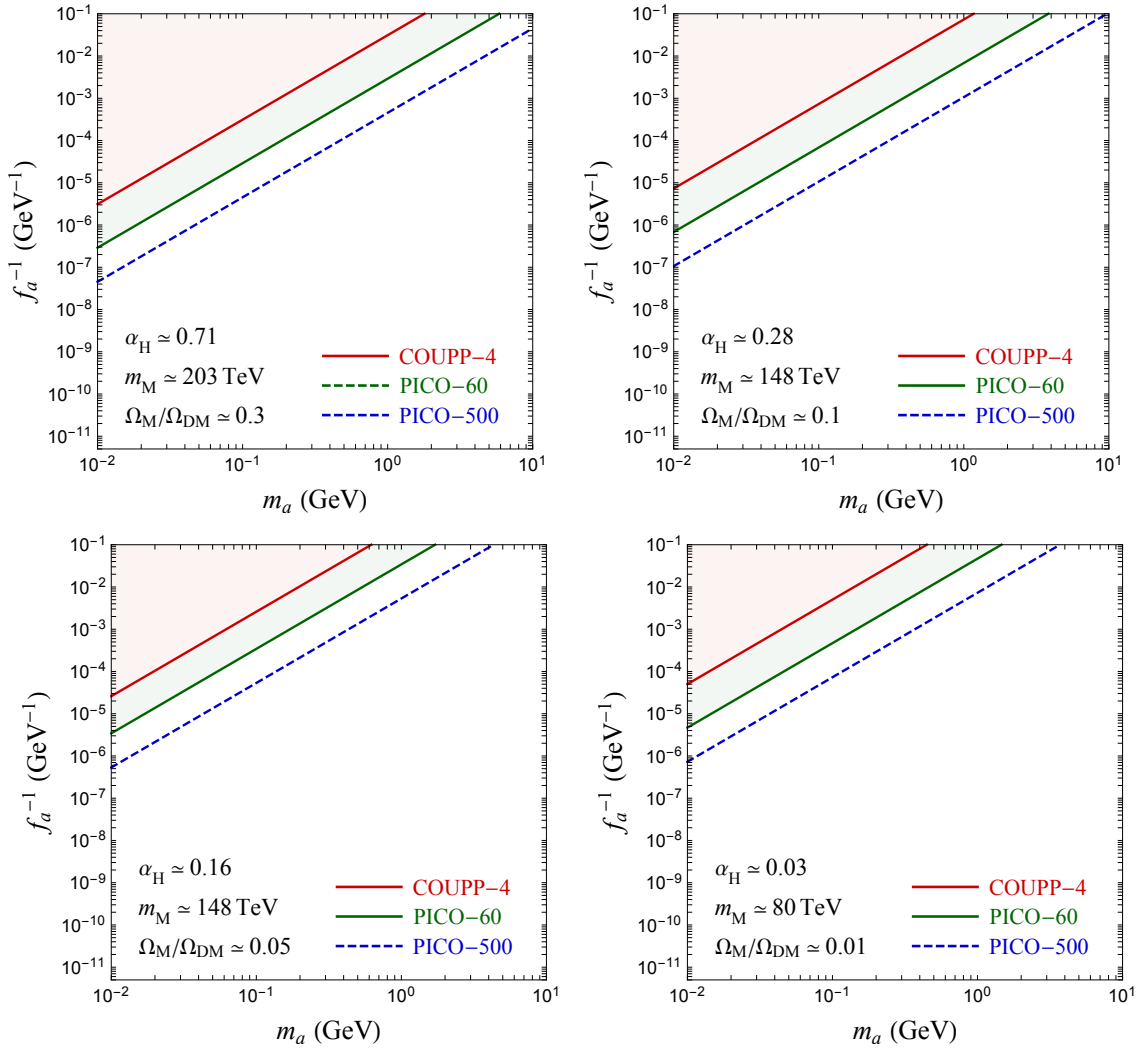

Figure 3.2: The lower bound of the decay constant as a function of the axion mass by imposing the constraints from the DM direct detection experiments with our benchmark points, where the red and green shaded regions are excluded by the current experiments COUPP-4 and PICO-60, respectively, and the blue dashed line is the future sensitivity by PICO-500. The percentage of DM interacting with the nucleon is considered, which is indicated by the ratio Ω_M/Ω_{DM} in these plots. Here we have concentrated on the case of proton and fixed $\theta_0 = 3$.

are sensitive to the spin-dependent cross-section. Making a comparison of (3.18) with (3.27) and referring the results analyzed in Ref. [114], we present the limits on the axion decay constant from the DM direct search experiments as a function of the axion mass with our benchmark points in Fig. 3.2, where the amount of DM interacting with the nucleon is taken into account as explained in the previous subsection. In these plots, the red and green shaded areas are ruled out by the current experiments COUPP-4 (4.0 kg CF_3I) [115] and PICO-60 (52 kg C_3F_8) [36], respectively, and the blue dashed line is the future prospect by PICO-500 (C_3F_8) [116].

Chapter 4

Implications for Axion Search Experiments & Others

In the previous chapter, we introduce an axion as a mediator connecting the hidden sector and the visible sector, and we consider the mass range of the axion from 10 MeV to 10 GeV. Such a long-lived light axion can be captured by beam-dump experiments using the proton beams (e.g. CHARM and SHiP, etc.). In particular, the exotic scalars or pseudo-scalars with couplings to the SM fermions and photons are sensitive to these experiments. On the other hand, the presence of the axion may change the predictions for some B-meson rare decays such as $B \to K + \text{invisible}$ and $B \to K\mu^+\mu^-$. We will discuss the impacts of the light axion decay on these subjects in this chapter.

4.1 The Beam-Dump Experiments

4.1.1 Experimental Setup

A sketch of the setup for a beam-dump experiment is shown in Fig. 4.1. In this figure, a proton beam with high intensity impinges onto a dense block of heavy material (beam-dump), at which the hadronic states are produced and subsequently decay into other lighter hadrons and a new particle, which eventually decays into the SM particles such as electrons, muons, and photons. These visible particles can be probed in the detector. The expected number of events N_{det} in the case of the axion is then given by

$$N_{\text{det}} \approx N_a \left[\exp\left(-\frac{\ell}{\gamma_a \beta_a c \tau_a} \right) - \exp\left(-\frac{\ell + \Delta\ell}{\gamma_a \beta_a c \tau_a} \right) \right] \sum_{X = e,\, \mu,\, \gamma} \mathcal{B}\left(a \to X\bar{X}\right) , \tag{4.1}$$

where N_a is the number of the axion produced at the target, which is ℓ away from the detector with the length $\Delta\ell$, $\gamma_a = \left(1 - \beta_a^2\right)^{-1/2}$ is the boost factor of the axion, c is the speed of light, τ_a is the lifetime of the axion, and $\mathcal{B}\left(a \to X\bar{X}\right)$ is the branching fraction

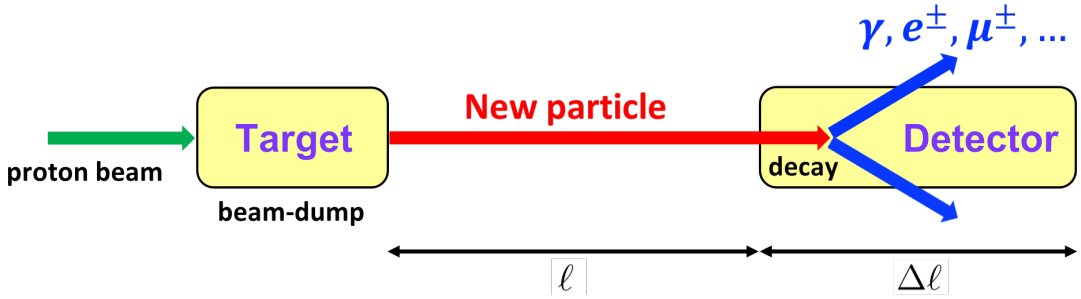

Figure 4.1: The schematic design of a beam-dump experiment.

Table 4.1: The parameter settings and the bounds of the beam-dump facilities.

Bump-Dump Facility	ℓ (m)	$\Delta\ell$ (m)	$\gamma_a = E_a/m_a$	Bound of $N_{\rm det}$
CHARM [117]	480	35	$10\,\text{GeV}/m_a$	< 2.3 (90% C.L.)
SHiP [118]	70	55	$25\,\text{GeV}/m_a$	< 3

of the axion decay into visible particle X. The understanding of (4.1) is intuitive, where the subtraction of the exponential factors is the probability of the axion decay within the detector region and $\sum_{X=e,\mu,\gamma}\mathcal{B}(a\to X\bar{X})$ is the probability of the axion decay into the visible particles.

In this thesis, we will impose the constraints from CHARM (current limit) and SHiP (future prospect) to our model. We summarize their parameter settings and the experimental bounds in Tab. 4.1, where the bound of $N_{\rm det}$ for CHARM is due to the observing null events, and for SHiP is by assuming that no background events will be detected. The explicit forms of N_a for CHARM and SHiP can be found in [119] and [118], respectively.

4.1.2 The Axion Decay Channels

The predicted number of events $N_{\rm det}$ depends crucially on the lifetime of the axion τ_a. Any additional decay mode of the axion would change various experimental bounds on the axion decay constant f_a. In this section, we will discuss the axion decay channels in our model and show the constraints on f_a from CHARM and SHiP at the end of section.

In our setup (3.1), the axion is coupled to the hidden photons and then can decay into a hidden photon pair with the decay rate given by

$$\Gamma\left(a\to\gamma_{\rm H}\gamma_{\rm H}\right) = \frac{\alpha_{\rm H}^2 m_a^3}{256\pi^3 f_{\rm H}^2}\,. \tag{4.2}$$

On the other hand, the axion can interact with the SM particles through the Yukawa-like coupling, where the couplings between the axion and the SM fermions are proportional

to the SM Yukawa couplings, the Lagrangian density is given by

$$\mathcal{L}_Y = \frac{\partial_\mu a}{2f_a}\sum_f C_f \overline{\psi}_f \gamma^\mu \gamma^5 \psi_f = -\frac{a}{f_a}\sum_f C_f m_f \overline{\psi}_f i\gamma^5 \psi_f \,, \tag{4.3}$$

where C_f is the model-dependent parameter, m_f is the mass of the fermion, and we have used the integration by part and the equation of motion of the fermion field in the second equality of (4.3). This interaction may be induced in a setup like the DFSZ axion model [80, 81]. From Eq. (4.3), the rates of the axion decaying into the SM fermions and photons are calculated as

$$\Gamma\big(a \to f\bar{f}\big) = C_f^2 \frac{N_f^{\rm c} m_f^2 m_a}{8\pi f_a^2}\sqrt{1-\frac{4m_f^2}{m_a^2}} \,, \tag{4.4}$$

$$\Gamma\big(a \to \gamma\gamma\big) = C_f^2 \frac{\alpha^2 m_a^3}{256\pi^3 f_a^2}\left|\sum_f N_f^{\rm c} Q_f^2 \mathcal{F}_\gamma\!\left(\frac{m_a^2}{4m_f^2}\right)\right|^2 \,, \tag{4.5}$$

where $\alpha = e^2/(4\pi)$ is the fine structure constant, $N_f^{\rm c}\,(Q_f)$ is the color (charge) of the fermion, and $\mathcal{F}_\gamma$ is the loop function which can be found in [120]. With the decay channels (4.2), (4.4), and (4.5), the lifetime of the axion is given by

$$\tau_a = \frac{1}{\Gamma_a} = \frac{1}{\Gamma\big(a \to \gamma_{\rm H}\gamma_{\rm H}\big) + \Gamma\big(a \to \text{vis.}\big)} \,, \tag{4.6}$$

where Γ_a is the total decay width of the axion, and $\Gamma\big(a \to \gamma_{\rm H}\gamma_{\rm H}\big)$ and $\Gamma\big(a \to \text{vis.}\big)$ are the rates of the axion decay into the hidden photons and the visible particles $(e^\pm, \mu^\pm, \gamma, \cdots)$, respectively. It follows that the branching ratio of the axion decay into particle X is

$$\mathcal{B}\big(a \to X\bar{X}\big) = \tau_a \Gamma\big(a \to X\bar{X}\big) = \frac{\Gamma\big(a \to X\bar{X}\big)}{\Gamma\big(a \to \gamma_{\rm H}\gamma_{\rm H}\big) + \Gamma\big(a \to \text{vis.}\big)} \,. \tag{4.7}$$

We show in Fig. 4.2, the branching ratios of the axion in the case with and without the hidden photon for comparison. One can see that the branching fractions of the axion with the masses above $2m_\mu$ in these two cases are almost the same. However, in the mass region just below $2m_\mu$, the axion mainly decays into the hidden photons in the latter case assuming $\alpha_{\rm H} \gg \alpha$. Then, one can expect that the constraints of the decay constant from the beam-dump experiments would change in this mass range even if the detectors are unable to measure the hidden photons.

Applying Eqs. (4.1) and (4.7), and the parameter inputs in Tab. 4.1, we present how the hidden photon decay channel affects the limits on f_a from CHARM and SHiP with different values of $\alpha_{\rm H}$ in Fig. 4.3. In these plots, the parameter region of f_a^{-1} above the color lines corresponds to the case where the axion decays before arriving at the detector. Due to the hidden photon decay mode of the axion, the upper parts of these color lines

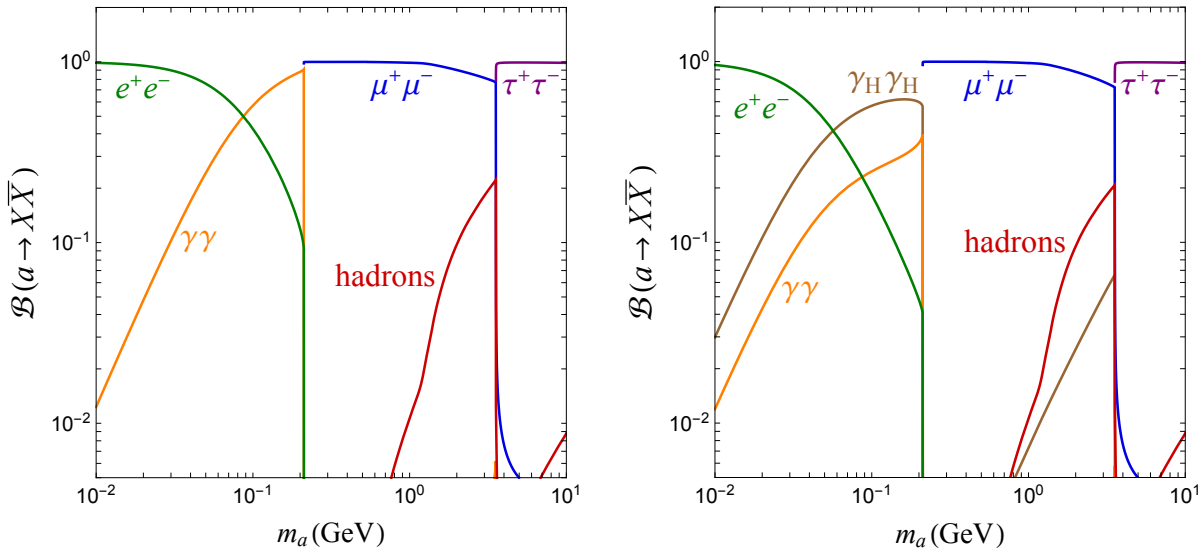

Figure 4.2: The axion decay branching ratios in the case without the hidden photon (left panel figure) and in the case with the hidden photon (right panel figure), here we have fixed $\alpha_{\rm H} = 0.16$, and assumed $f_a = f_{\rm H}$ and $C_f = 1$ for simplicity. Note that in this mass region, the axion decays into hadrons rather than quark-antiquark pairs due to the QCD confinement. The decay width of the axion into the hadrons can be found in [119].

shrink as one has to reduce the coupling strength ($\propto f_a^{-1}$) between the axion and the SM particles in order to reach the same predicted event numbers. On the other hand, the parameter region of f_a^{-1} below the color lines corresponds to the case where the axion decays after leaving from the detector. In this region, the axion is sufficiently long-lived such that the predicted event numbers is $N_a \Delta\ell \sum_{X=e,\mu,\gamma} \Gamma\big(a \to X\bar{X}\big)/\big(\gamma_a \beta_a c\big)$, which explains why the lower parts of the color lines are insensitive to $\alpha_{\rm H}$.

4.2 The Rare B Meson Decays

In this section, we will show the bounds on the axion decay constant from B-meson rare decays in the presence of the hidden photon. It turns out that $B \to K + \text{inv}$ provides the most stringent constraint on the axion decay constant. The experimental bound for the branching ratio of $B \to K + \text{inv}$ is given by [121]

$$\mathcal{B}\big(B \to K + \text{inv}\big)_{\rm exp} \;<\; 5.3 \times 10^{-5}\;. \tag{4.8}$$

On the other hand, the theoretical prediction of $B \to K + \text{inv}$ can be written as [119]

$$\mathcal{B}\big(B \to K + \text{inv}\big) \;=\; \mathcal{B}\big(B \to Ka\big) P_{\rm esc}(\boldsymbol{p}_a)\;, \tag{4.9}$$

where $P_{\rm esc}(\boldsymbol{p}_a)$ is the probability of the axion with momentum $\boldsymbol{p}_a$ for it to escape from the detector. Now, let us evalutate $P_{\rm esc}(\boldsymbol{p}_a)$ with the hidden photon in the following. The

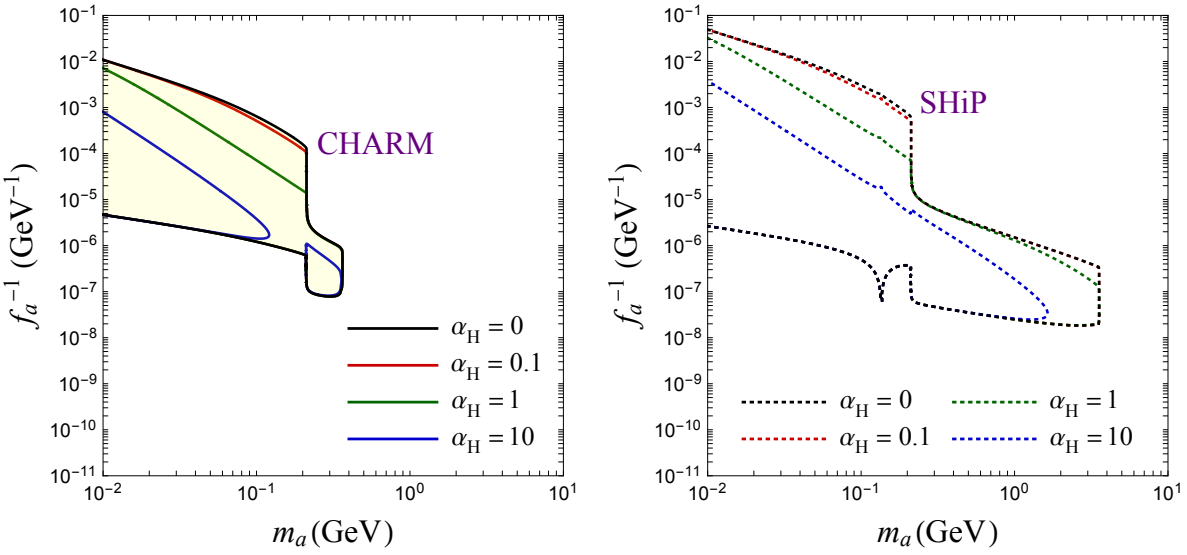

Figure 4.3: The effects of the decay channel $a \to \gamma_H \gamma_H$ on CHARM (left panel) and SHiP (right panel) with different choices of α_H, assuming the Yukawa-like coupling for the axion, where the yellow shaded regions are excluded by current experiments. Again, we have set $f_a = f_H$ and $C_f = 1$ (in the later plots also) for simplicity

definition of the escape probability is given by

$$P_{\rm esc}(\boldsymbol{p}_a) \;=\; 1 - \frac{N_{\rm vis}(t)}{N_a(0)} \;, \tag{4.10}$$

where $N_a(0)$ is the original number of the axion produced from B-meson decay at $t = 0$, and $N_{\rm vis}(t)$ being the event numbers of the axion decaying into the visible particles at time t. The decay numbers of the axion and the production event numbers of the visible particles between t and $t + dt$ are given by

$$dN_a(t) \;=\; -\frac{\Gamma_a}{\gamma_a} N_a(t)\, dt \;, \quad dN_{\rm vis}(t) \;=\; \frac{\Gamma\big(a \to \text{vis.}\big)}{\gamma_a} N_a(t)\, dt \;, \tag{4.11}$$

and by the integration, we have

$$\frac{N_a(t)}{N_a(0)} \;=\; \exp\!\left(-\frac{\Gamma_a}{\gamma_a} t\right) \;, \quad \frac{N_{\rm vis}(t)}{N_a(0)} \;=\; \frac{\Gamma\big(a \to \text{vis.}\big)}{\Gamma_a} \left[1 - \exp\!\left(-\frac{\Gamma_a}{\gamma_a} t\right)\right] \;. \tag{4.12}$$

Plugging Eq. (4.12) into Eq. (4.10), and use $t = \ell / v_a = \gamma_a m_a \ell / |\boldsymbol{p}_a|$ in the laboratory frame, we then arrive at

$$P_{\rm esc}(\boldsymbol{p}_a) \;=\; \mathcal{B}\big(a \to \gamma_H \gamma_H\big) + \mathcal{B}\big(a \to \text{vis.}\big) \exp\!\left(-\frac{m_a \Gamma_a \ell}{|\boldsymbol{p}_a|}\right) \;, \tag{4.13}$$

where

$$|\boldsymbol{p}_a| \;=\; \frac{1}{2 m_B} \sqrt{\Big[m_B^2 - \big(m_K + m_a\big)^2\Big] \Big[m_B^2 - \big(m_K - m_a\big)^2\Big]} \tag{4.14}$$

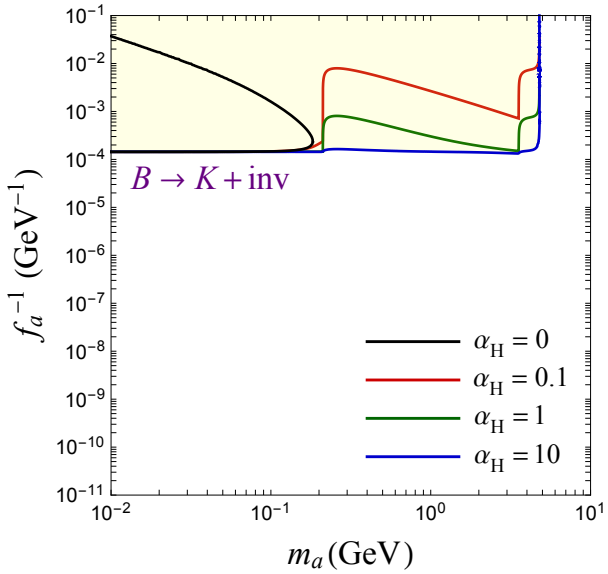

Figure 4.4: The effects of the decay channel $a \to \gamma_H \gamma_H$ on B^0 decaying into K_S^0 plus missing energy, where the yellow shaded regions is excluded by the current bound.

with m_B and m_K are the masses for B-meson and K-meson, respectively. The result of (4.13) makes sense since the first term corresponds to the case where the axion decays into missing energy and the second term is the case where the axion decays into the visible particles outside the detector region. Both cases are identified with escaped events.

Imposing (4.8) on (4.9) with (4.13), we present the constraint from B^0 decaying into K_S^0 with missing energy for the axion decay constant with the different values of α_H in Fig. 4.4, where we have used the formulas of $\mathcal{B}(B \to Ka)$ in Ref. [119], and adopted $\ell = 4\,\text{m}$. One can see that the excluding region of f_a^{-1} is enlarged to above $2m_\mu$ in the presence of the hidden photon and this is because $\mathcal{B}\big(B \to K + \text{inv}\big) \approx \mathcal{B}\big(a \to \gamma_H \gamma_H\big)$ in this mass region, which has a non-negligible contribution even if it is a sub-dominant decay mode at $m_a > 2m_\mu$ (see right panel of Fig. 4.2). The constraints from $B \to K\mu^+\mu^-$ and $B \to \mu^+\mu^-$ are not shown here since we have checked that the modifications from them are weaker than the others.

4.3 The Combined Result

Combining the results from Fig. 3.2, Fig. 4.3, and Fig. 4.4 with benchmark point 3, we present the upshot of this thesis in Fig. 4.5, where the bounds from B-meson decays $B \to K\mu^+\mu^-$ and $B_s \to \mu^+\mu^-$, and BBN are also shown. One can see that the hidden monopole DM and the axion can be found by the future experiments such as PICO-500 and SHiP in the parameter regions around (i) $m_a = \mathcal{O}(10)\,\text{MeV}$ and $f_a = \mathcal{O}(10^5)\,\text{GeV}$, and (ii) $m_a = \mathcal{O}(100)\,\text{MeV}$ and $f_a = \mathcal{O}(10^4)\,\text{GeV}$. The latter is opened compared to the

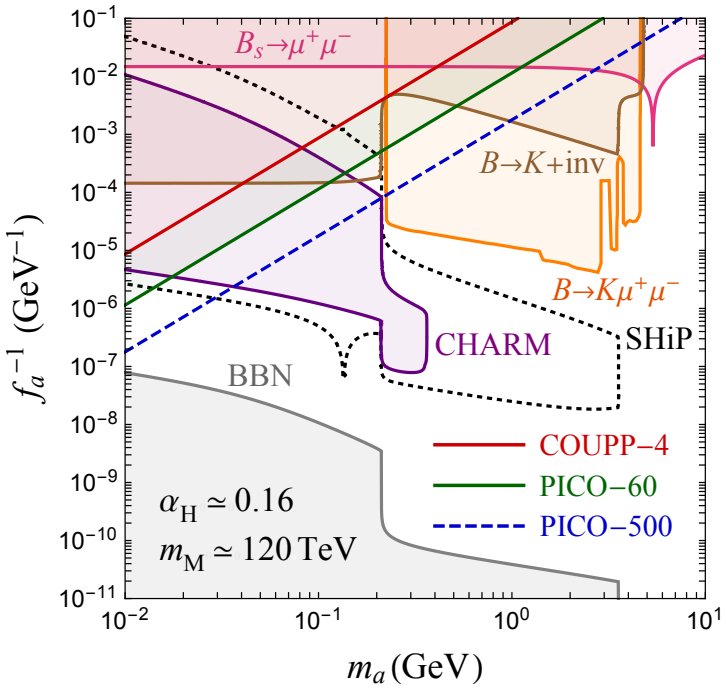

Figure 4.5: The axion decay constant versus the axion mass, where the shaded regions are excluded by the current experiments such as COUPP-4, PICO-60, CHARM, and some B-meson rare decays and by the cosmological constraints like BBN. On the other hand, the dashed line and the dotted curve indicate the future sensitivities by PICO-500 and SHiP experiments, respectively. For the BBN constraint, we simply require that the lifetime of the axion should be less than one second, a time when the BBN starts to occur after the Big Bang. In this plot, we have fixed $\theta_0 = 3$.

previous analysis [119], and this is due to the decay channel of the axion into the hidden photons. The combined results for other benchmark points are shown in appendix F.

Lastly, let us comment on the SN1987A supernova bound for the parameter space we found. The QCD axions (and other light particles with feeble interactions) are considered to be produced in the proto-neutron star (see Refs. [122, 123] andr eferences therein). If the QCD axion carries away too much energy from it, the neutrino burst duration would be shorter than ~ 10 sec. in contradiction with the observation.[1] Compared to the QCD axion, the axion in our scenario has a much heavier mass, and it decays into the hidden photons with a sizable branching fraction. The temperature of the proto-neutron star can be as high as a few tens MeV, and so, the parameter region (i) may be subject to the SN1987A bound. A more detailed analysis is necessary to estimate the bound. In any case, the SN1987A supernova bound is not included in our analysis partly due to the incomplete understanding of the supernova explosion mechanism.

[1] It was recently pointed out in Ref. [124] that the accretion disk formed around the proto-neutron star (or black hole) may explain the late-time neutrino emission ($t \gtrsim 5$ sec.).

4.4 Dark Radiation and $\Delta N_{\rm eff}$

In the $'$t Hooft-Polyakov monopole model, the massless hidden photon $\gamma_{\rm H}$ contributes to dark radiation which can be quantified in terms of the number of the extra neutrino species, $\Delta N_{\rm eff}$ (see Eq. (1.18) for the definition). In the minimal construction without the axion portal coupling, it was estimated in Ref. [4], where the entropy stored in the $W_{\rm H}^{\pm}$ is transferred to the hidden photons after the temperature falls below the mass of $W_{\rm H}^{\pm}$. Let us see how this is changed in our model setup. To be concrete, we fix the axion mass and decay constant around the region of $m_a = \mathcal{O}(10)\,\text{MeV}$ and $f_a = \mathcal{O}(10^5)\,\text{GeV}$, where both the hidden monopole DM and the axion are within the experimental reach. In this parameter region, the axion keeps the hidden photons in equilibrium with the SM sector at temperatures well below the mass of $W_{\rm H}^{\pm}$ or the PQ fermions, and the hidden photon is considered to decouple from the SM plasma at a temperature around the electroweak scale. Thus, we do not need to take into account the entropy stored in the heavy hidden particles. For the reference parameter region, the axion remains in thermal equilibrium and abundant until the temperature becomes comparable to the mass of the axion. In particular, the axion mainly decays into the hidden photons as the axion becomes non-relativistic and its abundance gets Boltzmann suppressed. This production of the hidden photons dominates over the contribution at the decoupling of the hidden photons.

Now, let us estimate $\Delta N_{\rm eff}$ contributed by the hidden photons from these sources in our model setup. First, the hidden photons decoupled from the SM thermal bath gives

$$\Delta N_{\rm eff,dec} \;=\; \frac{8}{7}\left[\frac{g_{*s,\rm SM}(T_{\nu,\rm dec})}{g_{*s,\rm SM}(T_{\rm H,dec})}\right]^{4/3} \;\simeq\; 0.05\;, \tag{4.15}$$

where we have used Eq. (1.21), and $g_{*s,\rm SM}(T_{\nu,\rm dec}) = 10.75$ and $g_{*s,\rm SM}(T_{\rm H,dec}) = 106.75$. One the other hand, the contribution of the hidden photon from the decay of the axion ($a \to \gamma_{\rm H}\gamma_{\rm H}$) can be calculated by using energy conservation. Assuming all the energy of the axion transfers to the energy of the hidden photon, we have $\rho_{\gamma_{\rm H},\rm d} = \rho_{a,\rm d} = \pi^2 T_{\rm d}^4/30$, where $T_{\rm d} \simeq \mathcal{O}(10\,\text{MeV})$, then, $\rho_{\gamma_{\rm H},\rm BBN} = \rho_{\gamma_{\rm H},\rm d}(R_{\rm d}/R_{\rm BBN})^4$. By using entropy conservation $\left[g_{*s}(T)R(T)^3T^3 = \text{constant}\right]$, we obtain

$$\Delta N_{\rm eff,d} \;=\; \frac{4}{7}\left[\frac{g_{*s,\rm SM}(T_{\rm BBN})}{g_{*s,\rm SM}(T_{\rm d})}\right]^{4/3} \;\simeq\; \frac{4}{7}\;. \tag{4.16}$$

Hence, we have $\Delta N_{\rm eff} \simeq 4/7 + 0.05 \sim 0.6$, which is consistent with the estimation given in Ref. [125] assuming the presence of the axion coupling to leptons. In the other viable parameter region, $m_a = \mathcal{O}(100)\,\text{MeV}$, $f_a = \mathcal{O}(10^4)\,\text{GeV}$, the contribution to dark radiation will be smaller since the axion disappears from the plasma at higher temperatures. The dark radiation with $\Delta N_{\rm eff} \gtrsim 0.5$ can relax the H_0 tension significantly [126].[2]

[2] See Ref. [127] for the anthropic bound on $\Delta N_{\rm eff}$.

Chapter 5

Conclusions

In this thesis, we have studied the possibility that the hidden monopoles which contribute to a sizable fraction of the observed DM density are coupled to the SM sector via the axion portal interaction. We have determined the axion configuration around the monopole so that it minimizes the energy of the system, and then estimated the elastic scattering cross-section of the monopole with a nucleon via the axion portal coupling. Using the fact that the dependence of the cross-section on the transferred momentum is the same as that for a CP-violating pseudo-scalar coupling between quarks and a Dirac DM particle, we have translated the experimental bounds on the spin-dependent scattering cross-section with a nucleon to limit the model parameters. The axion itself can also be searched for at the beam-dump experiment. Combining the current limits and future prospects for the search of DM and axions, we have found two viable parameter regions around $(m_a/\mathrm{MeV}, f_a/\mathrm{GeV}) = \mathcal{O}(10, 10^5)$ and $\mathcal{O}(100, 10^4)$ where the monopole DM and the axion are respectively within the reach of the future experiments such as PICO-500 and SHiP.

Appendix A

Some Derivations in Chapter 2

A.1 The Derivation of the Equations of Motion

Let us start with Eq. (2.7) to derive the equations of motion in the ′t Hooft-Polyakov model. First, the Lagrangian density Eq. (2.1) can be expanded as

$$\begin{aligned}
\mathcal{L}_{\mathrm{H}} &= -\frac{1}{4}\boldsymbol{F}_{\mathrm{H}}^{\mu\nu}\cdot\boldsymbol{F}_{\mathrm{H}\mu\nu}+\frac{1}{2}\mathcal{D}^{\mu}\boldsymbol{\phi}\cdot\mathcal{D}_{\mu}\boldsymbol{\phi}-\mathcal{V}(\phi)\\
&= -\frac{1}{4}\big(\partial^{\mu}\boldsymbol{A}_{\mathrm{H}}^{\nu}-\partial^{\nu}\boldsymbol{A}_{\mathrm{H}}^{\mu}+e_{\mathrm{H}}\boldsymbol{A}_{\mathrm{H}}^{\mu}\times\boldsymbol{A}_{\mathrm{H}}^{\nu}\big)\cdot\big(\partial_{\mu}\boldsymbol{A}_{\mathrm{H}\nu}-\partial_{\nu}\boldsymbol{A}_{\mathrm{H}\mu}+e_{\mathrm{H}}\boldsymbol{A}_{\mathrm{H}\mu}\times\boldsymbol{A}_{\mathrm{H}\nu}\big)\\
&\quad+\frac{1}{2}\big(\partial^{\mu}\boldsymbol{\phi}+e_{\mathrm{H}}\boldsymbol{A}_{\mathrm{H}}^{\mu}\times\boldsymbol{\phi}\big)\cdot\big(\partial_{\mu}\boldsymbol{\phi}+e_{\mathrm{H}}\boldsymbol{A}_{\mathrm{H}\mu}\times\boldsymbol{\phi}\big)-\frac{1}{4}\lambda_{\phi}\big(\boldsymbol{\phi}\cdot\boldsymbol{\phi}-\upsilon_{\mathrm{H}}^{2}\big)^{2}\,,\\
&= -\frac{1}{2}\big(\partial^{\mu}\boldsymbol{A}_{\mathrm{H}}^{\nu}\cdot\partial_{\mu}\boldsymbol{A}_{\mathrm{H}\nu}-\partial^{\mu}\boldsymbol{A}_{\mathrm{H}}^{\nu}\cdot\partial_{\nu}\boldsymbol{A}_{\mathrm{H}\mu}\big)-e_{\mathrm{H}}\big[\partial^{\mu}\boldsymbol{A}_{\mathrm{H}}^{\nu}\cdot\big(\boldsymbol{A}_{\mathrm{H}\mu}\times\boldsymbol{A}_{\mathrm{H}\nu}\big)\big]\\
&\quad-\frac{1}{4}e_{\mathrm{H}}^{2}\big(\boldsymbol{A}_{\mathrm{H}}^{\mu}\times\boldsymbol{A}_{\mathrm{H}}^{\nu}\big)\cdot\big(\boldsymbol{A}_{\mathrm{H}\mu}\times\boldsymbol{A}_{\mathrm{H}\nu}\big)+\frac{1}{2}\partial^{\mu}\boldsymbol{\phi}\cdot\partial_{\mu}\boldsymbol{\phi}+e_{\mathrm{H}}\partial^{\mu}\boldsymbol{\phi}\cdot\big(\boldsymbol{A}_{\mathrm{H}\mu}\times\boldsymbol{\phi}\big)\\
&\quad+\frac{1}{2}e_{\mathrm{H}}^{2}\big(\boldsymbol{A}_{\mathrm{H}}^{\mu}\times\boldsymbol{\phi}\big)\cdot\big(\boldsymbol{A}_{\mathrm{H}\mu}\times\boldsymbol{\phi}\big)-\frac{1}{4}\lambda_{\phi}\big(\boldsymbol{\phi}\cdot\boldsymbol{\phi}-\upsilon_{\mathrm{H}}^{2}\big)^{2}\,,
\end{aligned}\tag{A.1}$$

where

$$\begin{aligned}
&\big(\boldsymbol{A}_{\mathrm{H}}^{\mu}\times\boldsymbol{A}_{\mathrm{H}}^{\nu}\big)\cdot\big(\boldsymbol{A}_{\mathrm{H}\mu}\times\boldsymbol{A}_{\mathrm{H}\nu}\big)\\
&= \big(\boldsymbol{A}_{\mathrm{H}}^{\mu}\cdot\boldsymbol{A}_{\mathrm{H}\mu}\big)\big(\boldsymbol{A}_{\mathrm{H}}^{\nu}\cdot\boldsymbol{A}_{\mathrm{H}\nu}\big)-\big(\boldsymbol{A}_{\mathrm{H}}^{\mu}\cdot\boldsymbol{A}_{\mathrm{H}\nu}\big)\big(\boldsymbol{A}_{\mathrm{H}}^{\nu}\cdot\boldsymbol{A}_{\mathrm{H}\mu}\big)\,,
\end{aligned}\tag{A.2}$$

$$\big(\boldsymbol{A}_{\mathrm{H}}^{\mu}\times\boldsymbol{\phi}\big)\cdot\big(\boldsymbol{A}_{\mathrm{H}\mu}\times\boldsymbol{\phi}\big) = \big(\boldsymbol{A}_{\mathrm{H}}^{\mu}\cdot\boldsymbol{A}_{\mathrm{H}\mu}\big)\big(\boldsymbol{\phi}\cdot\boldsymbol{\phi}\big)-\big(\boldsymbol{A}_{\mathrm{H}}^{\mu}\cdot\boldsymbol{\phi}\big)\big(\boldsymbol{A}_{\mathrm{H}\mu}\cdot\boldsymbol{\phi}\big)\,.\tag{A.3}$$

Then, one can show that

$$\partial_{\mu}\left(\frac{\partial\mathcal{L}_{\mathrm{H}}}{\partial\big(\partial_{\mu}\boldsymbol{A}_{\mathrm{H}\nu}\big)}\right)=-\partial_{\mu}\boldsymbol{F}_{\mathrm{H}}^{\mu\nu}\,,\quad\partial_{\mu}\left(\frac{\partial\mathcal{L}_{\mathrm{H}}}{\partial\big(\partial_{\mu}\boldsymbol{\phi}\big)}\right)=\partial_{\mu}\partial^{\mu}\boldsymbol{\phi}+e_{\mathrm{H}}\partial_{\mu}\big(\boldsymbol{A}_{\mathrm{H}}^{\mu}\times\boldsymbol{\phi}\big)\,,\tag{A.4}$$

and

$$\begin{aligned}
\frac{\partial \mathcal{L}_{\rm H}}{\partial \boldsymbol{A}_{{\rm H}\nu}} &= e_{\rm H}\boldsymbol{A}_{{\rm H}\mu}\times\big(\partial^\mu \boldsymbol{A}^\nu_{\rm H}-\partial^\nu \boldsymbol{A}^\mu_{\rm H}\big)+e^2_{\rm H}\Big[\boldsymbol{A}^\mu_{\rm H}\big(\boldsymbol{A}_{{\rm H}\mu}\cdot\boldsymbol{A}^\nu_{\rm H}\big)-\boldsymbol{A}^\nu_{\rm H}\big(\boldsymbol{A}_{{\rm H}\mu}\cdot\boldsymbol{A}^\mu_{\rm H}\big)\Big]\\
&\quad+e_{\rm H}\boldsymbol{\phi}\times\partial^\nu\boldsymbol{\phi}+e^2_{\rm H}\Big[\boldsymbol{A}^\nu_{\rm H}\big(\boldsymbol{\phi}\cdot\boldsymbol{\phi}\big)-\boldsymbol{\phi}\big(\boldsymbol{\phi}\cdot\boldsymbol{A}^\nu_{\rm H}\big)\Big]\\
&= e_{\rm H}\boldsymbol{A}_{{\rm H}\mu}\times\big(\partial^\mu \boldsymbol{A}^\nu_{\rm H}-\partial^\nu \boldsymbol{A}^\mu_{\rm H}\big)+e^2_{\rm H}\Big[\boldsymbol{A}_{{\rm H}\mu}\times\big(\boldsymbol{A}^\mu_{\rm H}\times\boldsymbol{A}^\nu_{\rm H}\big)\Big]\\
&\quad+e_{\rm H}\boldsymbol{\phi}\times\partial^\nu\boldsymbol{\phi}+e^2_{\rm H}\Big[\boldsymbol{\phi}\times\big(\boldsymbol{A}^\nu_{\rm H}\times\boldsymbol{\phi}\big)\Big]\\
&= e_{\rm H}\boldsymbol{A}_{{\rm H}\mu}\times\boldsymbol{F}^{\mu\nu}_{\rm H}+e_{\rm H}\boldsymbol{\phi}\times\mathcal{D}^\nu\boldsymbol{\phi}\ ,
\end{aligned}$$

$$\begin{aligned}
\frac{\partial \mathcal{L}_{\rm H}}{\partial \boldsymbol{\phi}} &= e_{\rm H}\partial^\mu\boldsymbol{\phi}\times\boldsymbol{A}_{{\rm H}\mu}-e^2_{\rm H}\Big[\boldsymbol{A}^\mu_{\rm H}\big(\boldsymbol{A}_{{\rm H}\mu}\cdot\boldsymbol{\phi}\big)-\boldsymbol{\phi}\big(\boldsymbol{A}_{{\rm H}\mu}\cdot\boldsymbol{A}^\mu_{\rm H}\big)\Big]-\lambda_\phi\big(\boldsymbol{\phi}\cdot\boldsymbol{\phi}-\upsilon^2_{\rm H}\big)\boldsymbol{\phi}\\
&= -e_{\rm H}\boldsymbol{A}_{{\rm H}\mu}\times\partial^\mu\boldsymbol{\phi}-e^2_{\rm H}\Big[\boldsymbol{A}_{{\rm H}\mu}\times\big(\boldsymbol{A}^\mu_{\rm H}\times\boldsymbol{\phi}\big)\Big]-\lambda_\phi\big(\boldsymbol{\phi}\cdot\boldsymbol{\phi}-\upsilon^2_{\rm H}\big)\boldsymbol{\phi}\\
&= -\big(\partial_\mu+e_{\rm H}\boldsymbol{A}_{{\rm H}\mu}\times\big)\big(\partial^\mu\boldsymbol{\phi}+e_{\rm H}\boldsymbol{A}^\mu_{\rm H}\times\boldsymbol{\phi}\big)+\partial_\mu\partial^\mu\boldsymbol{\phi}+e_{\rm H}\partial_\mu\big(\boldsymbol{A}^\mu_{\rm H}\times\boldsymbol{\phi}\big)\\
&\quad-\lambda_\phi\big(\boldsymbol{\phi}\cdot\boldsymbol{\phi}-\upsilon^2_{\rm H}\big)\boldsymbol{\phi}\\
&= -\mathcal{D}_\mu\mathcal{D}^\mu\boldsymbol{\phi}+\partial_\mu\partial^\mu\boldsymbol{\phi}+e_{\rm H}\partial_\mu\big(\boldsymbol{A}^\mu_{\rm H}\times\boldsymbol{\phi}\big)-\lambda_\phi\big(\boldsymbol{\phi}\cdot\boldsymbol{\phi}-\upsilon^2_{\rm H}\big)\boldsymbol{\phi}\ .
\end{aligned}\tag{A.5}$$

From Eq. (2.6), if follows that

$$\mathcal{D}_\mu\boldsymbol{F}^{\mu\nu}_{\rm H}+e_{\rm H}\boldsymbol{\phi}\times\mathcal{D}^\nu\boldsymbol{\phi}=0\ ,\quad \mathcal{D}_\mu\mathcal{D}^\mu\boldsymbol{\phi}+\lambda_\phi\big(\boldsymbol{\phi}\cdot\boldsymbol{\phi}-\upsilon^2_{\rm H}\big)\boldsymbol{\phi}=0\ .\tag{A.6}$$

Actually, one can easily derive the equation of motion of $\boldsymbol{\phi}$ by using the gauge invariant Euler-Lagrange equation, which given by

$$\mathcal{D}_\mu\left(\frac{\partial\mathcal{L}_{\rm H}}{\partial(\mathcal{D}_\mu\boldsymbol{\phi})}\right)=\frac{\partial\mathcal{L}_{\rm H}}{\partial\boldsymbol{\phi}}\ .\tag{A.7}$$

In the chapter 2, we have checked that the asymptotic solutions (2.12) satisfies the secend equation of motion in Eq. (A.6). Let us check it satisfies the first one as well. At first, we have

$$\begin{aligned}
F^{ij}_{{\rm H}a} &= \partial^i A^j_{{\rm H}a}-\partial^j A^i_{{\rm H}a}+e_{\rm H}\epsilon_{abc}A^i_{{\rm H}b}A^j_{{\rm H}c}\\
&= -\epsilon_{ajk}\partial^i\left(\frac{r^k}{e_{\rm H}r^2}\right)+\epsilon_{aik}\partial^j\left(\frac{r^k}{e_{\rm H}r^2}\right)+e_{\rm H}\epsilon_{abc}\left(\epsilon_{bik}\frac{r^k}{e_{\rm H}r^2}\right)\left(\epsilon_{cjl}\frac{r^l}{e_{\rm H}r^2}\right)\\
&= -\frac{1}{e_{\rm H}}\epsilon_{ajk}\left(\frac{\delta_i{}^k r^2-2r_i r^k}{r^4}\right)+\frac{1}{e_{\rm H}}\epsilon_{aik}\left(\frac{\delta_j{}^k r^2-2r_j r^k}{r^4}\right)+\frac{1}{e_{\rm H}}\big(\delta_{ak}\delta_{ci}-\delta_{ai}\delta_{ck}\big)\epsilon_{cjl}\frac{r^k r^l}{r^4}\\
&= -2\epsilon_{aij}\frac{1}{e_{\rm H}r^2}+2\big(\epsilon_{aik}r^j-\epsilon_{ajk}r^i\big)\frac{r^k}{e_{\rm H}r^4}+\epsilon_{ijk}\frac{r^a r^k}{e_{\rm H}r^4}\ ,
\end{aligned}\tag{A.8}$$

Then,

$$\begin{aligned}
\partial_i F^{ij}_{\mathrm{H}a} \;=\; & -\frac{2}{e_{\mathrm{H}}}\epsilon_{aij}\partial_i\left(\frac{1}{r^2}\right)+\frac{2}{e_{\mathrm{H}}}\epsilon_{aik}\partial_i\left(\frac{r^j r^k}{r^4}\right)\\
& -\frac{2}{e_{\mathrm{H}}}\epsilon_{ajk}\partial_i\left(\frac{r^i r^k}{r^4}\right)+\frac{1}{e_{\mathrm{H}}}\epsilon_{ijk}\partial_i\left(\frac{r^a r^k}{r^4}\right)\\
=\; & -\frac{2}{e_{\mathrm{H}}}\epsilon_{aij}\left(-\frac{2r^i}{r^4}\right)+\frac{2}{e_{\mathrm{H}}}\epsilon_{aik}\left[\frac{\big(\delta^{ij}r^k+\delta^{ik}r^j\big)r^4-4r^i r^j r^k r^2}{r^8}\right]\\
& -\frac{2}{e_{\mathrm{H}}}\epsilon_{ajk}\left[\frac{\big(\delta^{ii}r^k+\delta^{ik}r^i\big)r^4-4r^i r^i r^k r^2}{r^8}\right]\\
& +\frac{1}{e_{\mathrm{H}}}\epsilon_{ijk}\left[\frac{\big(\delta^{ia}r^k+\delta^{ik}r^a\big)r^4-4r^i r^a r^k r^2}{r^8}\right]\\
=\; & -\epsilon_{ajk}\frac{r^k}{e_{\mathrm{H}}r^4}\;,
\end{aligned}\tag{A.9}$$

and

$$\begin{aligned}
e_{\mathrm{H}}\epsilon_{abc}A_{\mathrm{H}ib}F^{ij}_{\mathrm{H}c} \;=\; & e_{\mathrm{H}}\epsilon_{abc}\left(\epsilon_{bik}\frac{r^k}{e_{\mathrm{H}}r^2}\right)F^{ij}_{\mathrm{H}c}\\
=\; & \big(\delta_{ak}\delta_{ci}-\delta_{ai}\delta_{ck}\big)\frac{r^k}{r^2}\left[-2\epsilon_{cij}\frac{1}{e_{\mathrm{H}}r^2}+2\big(\epsilon_{cil}r^j-\epsilon_{cjl}r^i\big)\frac{r^l}{e_{\mathrm{H}}r^4}+\epsilon_{ijl}\frac{r^c r^l}{e_{\mathrm{H}}r^4}\right]\\
=\; & +\epsilon_{ajk}\frac{r^k}{e_{\mathrm{H}}r^4}\;.
\end{aligned}\tag{A.10}$$

Therefore,

$$\mathcal{D}_i F^{ij}_{\mathrm{H}a} \;=\; \partial_i F^{ij}_{\mathrm{H}a}+e_{\mathrm{H}}\epsilon_{abc}A_{\mathrm{H}ib}F^{ij}_{\mathrm{H}c} \;=\; 0\;.\tag{A.11}$$

With $\mathcal{D}_i F^{i0}_{\mathrm{H}a}=\mathcal{D}_0 F^{i0}_{\mathrm{H}a}=0$, we obtain the expected result

$$\mathcal{D}_\mu \boldsymbol{F}^{\mu\nu}_{\mathrm{H}}+e_{\mathrm{H}}\boldsymbol{\phi}\times\mathcal{D}^\nu\boldsymbol{\phi} \;=\; 0\;.\tag{A.12}$$

A.2 The Derivation of $\boldsymbol{F}_{\mathrm{H}}^{\mu\nu}$ in the Scalar Vacuum

The gauge field strength tensor is given by

$$\boldsymbol{F}_{\mathrm{H}}^{\mu\nu} = \partial^{\mu}\boldsymbol{A}_{\mathrm{H}}^{\nu} - \partial^{\nu}\boldsymbol{A}_{\mathrm{H}}^{\mu} + e_{\mathrm{H}}\boldsymbol{A}_{\mathrm{H}}^{\mu} \times \boldsymbol{A}_{\mathrm{H}}^{\nu} \,. \tag{A.13}$$

Plugging Eq. (2.16) into Eq. (A.14), we have

$$\begin{aligned}
\boldsymbol{F}_{\mathrm{H}}^{\mu\nu} &= \partial^{\mu}\left[\frac{1}{\upsilon_{\mathrm{H}}}A_{\mathrm{H}}^{\nu}\boldsymbol{\phi} - \frac{1}{e_{\mathrm{H}}\upsilon_{\mathrm{H}}^{2}}\big(\boldsymbol{\phi}\times\partial^{\nu}\boldsymbol{\phi}\big)\right] - \partial^{\nu}\left[\frac{1}{\upsilon_{\mathrm{H}}}A_{\mathrm{H}}^{\mu}\boldsymbol{\phi} - \frac{1}{e_{\mathrm{H}}\upsilon_{\mathrm{H}}^{2}}\big(\boldsymbol{\phi}\times\partial^{\mu}\boldsymbol{\phi}\big)\right] \\
&\quad + e_{\mathrm{H}}\left[\frac{1}{\upsilon_{\mathrm{H}}}A_{\mathrm{H}}^{\mu}\boldsymbol{\phi} - \frac{1}{e_{\mathrm{H}}\upsilon_{\mathrm{H}}^{2}}\big(\boldsymbol{\phi}\times\partial^{\mu}\boldsymbol{\phi}\big)\right] \times \left[\frac{1}{\upsilon_{\mathrm{H}}}A_{\mathrm{H}}^{\nu}\boldsymbol{\phi} - \frac{1}{e_{\mathrm{H}}\upsilon_{\mathrm{H}}^{2}}\big(\boldsymbol{\phi}\times\partial^{\nu}\boldsymbol{\phi}\big)\right] \\
&= \frac{1}{\upsilon_{\mathrm{H}}}\boldsymbol{\phi}\,\partial^{\mu}A_{\mathrm{H}}^{\nu} + \frac{1}{\upsilon_{\mathrm{H}}}A_{\mathrm{H}}^{\nu}\partial^{\mu}\boldsymbol{\phi} - \frac{1}{e_{\mathrm{H}}\upsilon_{\mathrm{H}}^{2}}\partial^{\mu}\boldsymbol{\phi}\times\partial^{\nu}\boldsymbol{\phi} - \frac{1}{e_{\mathrm{H}}\upsilon_{\mathrm{H}}^{2}}\boldsymbol{\phi}\times\partial^{\mu}\partial^{\nu}\boldsymbol{\phi} \\
&\quad - \frac{1}{\upsilon_{\mathrm{H}}}\boldsymbol{\phi}\,\partial^{\nu}A_{\mathrm{H}}^{\mu} - \frac{1}{\upsilon_{\mathrm{H}}}A_{\mathrm{H}}^{\mu}\partial^{\nu}\boldsymbol{\phi} + \frac{1}{e_{\mathrm{H}}\upsilon_{\mathrm{H}}^{2}}\partial^{\nu}\boldsymbol{\phi}\times\partial^{\mu}\boldsymbol{\phi} + \frac{1}{e_{\mathrm{H}}\upsilon_{\mathrm{H}}^{2}}\boldsymbol{\phi}\times\partial^{\nu}\partial^{\mu}\boldsymbol{\phi} \\
&\quad - \frac{1}{\upsilon_{\mathrm{H}}^{3}}A_{\mathrm{H}}^{\mu}\big[\boldsymbol{\phi}\big(\boldsymbol{\phi}\cdot\partial^{\nu}\boldsymbol{\phi}\big) - \partial^{\nu}\boldsymbol{\phi}\big(\boldsymbol{\phi}\cdot\boldsymbol{\phi}\big)\big] + \frac{1}{\upsilon_{\mathrm{H}}^{3}}A_{\mathrm{H}}^{\nu}\big[\boldsymbol{\phi}\big(\boldsymbol{\phi}\cdot\partial^{\mu}\boldsymbol{\phi}\big) - \partial^{\mu}\boldsymbol{\phi}\big(\boldsymbol{\phi}\cdot\boldsymbol{\phi}\big)\big] \\
&\quad + \frac{1}{e_{\mathrm{H}}\upsilon_{\mathrm{H}}^{4}}\boldsymbol{\phi}\big[\boldsymbol{\phi}\cdot\big(\partial^{\mu}\boldsymbol{\phi}\times\partial^{\nu}\boldsymbol{\phi}\big)\big] \\
&= \frac{1}{\upsilon_{\mathrm{H}}}\boldsymbol{\phi}\big(\partial^{\mu}A_{\mathrm{H}}^{\nu} - \partial^{\nu}A_{\mathrm{H}}^{\mu}\big) - \frac{2}{e_{\mathrm{H}}\upsilon_{\mathrm{H}}^{2}}\partial^{\mu}\boldsymbol{\phi}\times\partial^{\nu}\boldsymbol{\phi} + \frac{1}{e_{\mathrm{H}}\upsilon_{\mathrm{H}}^{4}}\boldsymbol{\phi}\big[\boldsymbol{\phi}\cdot\big(\partial^{\mu}\boldsymbol{\phi}\times\partial^{\nu}\boldsymbol{\phi}\big)\big] \,,
\end{aligned} \tag{A.14}$$

where we have utilized $\boldsymbol{\phi}\cdot\boldsymbol{\phi} = \upsilon_{\mathrm{H}}^{2}$ and $\boldsymbol{\phi}\cdot\partial^{\mu}\boldsymbol{\phi} = 0$ in the scalar vacuum, and using $\mathcal{D}^{\mu}\boldsymbol{\phi} = \partial^{\mu}\boldsymbol{\phi} + e_{\mathrm{H}}\boldsymbol{A}_{\mathrm{H}}^{\mu}\times\boldsymbol{\phi} = 0$, we have

$$\begin{aligned}
\partial^{\mu}\boldsymbol{\phi}\times\partial^{\nu}\boldsymbol{\phi} &= e_{\mathrm{H}}^{2}\big[\big(\boldsymbol{A}_{\mathrm{H}}^{\mu}\times\boldsymbol{\phi}\big)\cdot\big(\boldsymbol{A}_{\mathrm{H}}^{\nu}\times\boldsymbol{\phi}\big)\big] \\
&= e_{\mathrm{H}}^{2}\boldsymbol{A}_{\mathrm{H}}^{\nu}\big[\big(\boldsymbol{A}_{\mathrm{H}}^{\mu}\times\boldsymbol{\phi}\big)\cdot\boldsymbol{\phi}\big] - e_{\mathrm{H}}^{2}\boldsymbol{\phi}\big[\big(\boldsymbol{A}_{\mathrm{H}}^{\mu}\times\boldsymbol{\phi}\big)\cdot\boldsymbol{A}_{\mathrm{H}}^{\nu}\big] \\
&= -e_{\mathrm{H}}^{2}\boldsymbol{\phi}\left[-\frac{1}{e_{\mathrm{H}}\upsilon_{\mathrm{H}}^{2}}\big(\boldsymbol{\phi}\times\partial^{\mu}\boldsymbol{\phi}\big)\times\boldsymbol{\phi}\right]\cdot\boldsymbol{A}_{\mathrm{H}}^{\nu} \\
&= -\frac{e_{\mathrm{H}}}{\upsilon_{\mathrm{H}}^{2}}\boldsymbol{\phi}\big[\boldsymbol{\phi}\big(\boldsymbol{\phi}\cdot\partial^{\mu}\boldsymbol{\phi}\big) - \partial^{\mu}\boldsymbol{\phi}\big(\boldsymbol{\phi}\cdot\boldsymbol{\phi}\big)\big]\cdot\boldsymbol{A}_{\mathrm{H}}^{\nu} \\
&= e_{\mathrm{H}}\boldsymbol{\phi}\,\partial^{\mu}\boldsymbol{\phi}\cdot\left[-\frac{1}{e_{\mathrm{H}}\upsilon_{\mathrm{H}}^{2}}\big(\boldsymbol{\phi}\times\partial^{\nu}\boldsymbol{\phi}\big)\right] \\
&= \frac{1}{\upsilon_{\mathrm{H}}^{2}}\boldsymbol{\phi}\big[\boldsymbol{\phi}\cdot\big(\partial^{\mu}\boldsymbol{\phi}\times\partial^{\nu}\boldsymbol{\phi}\big)\big] \,.
\end{aligned} \tag{A.15}$$

Therefore,

$$\boldsymbol{F}_{\mathrm{H}}^{\mu\nu} = \frac{1}{\upsilon_{\mathrm{H}}}\boldsymbol{\phi}\big(\partial^{\mu}A_{\mathrm{H}}^{\nu} - \partial^{\nu}A_{\mathrm{H}}^{\mu}\big) - \frac{1}{e_{\mathrm{H}}\upsilon_{\mathrm{H}}^{4}}\boldsymbol{\phi}\big[\boldsymbol{\phi}\cdot\big(\partial^{\mu}\boldsymbol{\phi}\times\partial^{\nu}\boldsymbol{\phi}\big)\big] \,. \tag{A.16}$$

Appendix B

The Mass of the Hidden Monopole with Non-zero λ_ϕ

To estimate the hidden monopole with the non-zero quartic coupling λ_ϕ. We have to consider the general 't Hooft-Polyakov Ansatz given by

$$\phi_a(r) \;=\; \frac{r^a}{e_{\rm H} r^2}\mathcal{H}\big(e_{\rm H}\upsilon_{\rm H} r\big)\;, \tag{B.1}$$

$$A^j_{{\rm H}a}(r) \;=\; -\epsilon_{ajk}\frac{r^k}{e_{\rm H} r^2}\Big[1-\mathcal{K}\big(e_{\rm H}\upsilon_{\rm H} r\big)\Big]\;,\quad A^0_{{\rm H}a}(r) \;=\; 0\;, \tag{B.2}$$

where $\mathcal{H}(e_{\rm H}\upsilon_{\rm H} r)$ and $\mathcal{K}(e_{\rm H}\upsilon_{\rm H} r)$ are arbitrary functions. Let us introduce a dimensionless variable $\xi \equiv e_{\rm H}\upsilon_{\rm H} r$, then (B.1) and (B.2) becomes

$$\phi_a(\xi) \;=\; \upsilon_{\rm H}\frac{\xi^a}{\xi^2}\mathcal{H}(\xi)\;,\quad A^j_{{\rm H}a}(\xi) \;=\; -\upsilon_{\rm H}\epsilon_{ajk}\frac{\xi^k}{\xi^2}\Big[1-\mathcal{K}(\xi)\Big]\;,\quad A^0_{{\rm H}a}(\xi) \;=\; 0\;. \tag{B.3}$$

In this static solution, only the energies of the hidden magnetic field and the isovector scalar field contribute to the mass of the hidden monopole. First, one can show that

$$\begin{aligned}
F^{ij}_{{\rm H}a} \;&=\; e_{\rm H}\upsilon_{\rm H}\left[\frac{\partial}{\partial\xi_i}A^j_{{\rm H}a}(\xi)-\frac{\partial}{\partial\xi_j}A^i_{{\rm H}a}(\xi)\right]+\epsilon_{abc}e_{\rm H}A^i_{{\rm H}b}(\xi)A^j_{{\rm H}c}(\xi)\\
&=\; -e_{\rm H}\upsilon^2_{\rm H}\epsilon_{ajk}\frac{\partial}{\partial\xi_i}\left\{\frac{\xi^k}{\xi^2}\Big[1-\mathcal{K}(\xi)\Big]\right\}+e_{\rm H}\upsilon^2_{\rm H}\epsilon_{aik}\frac{\partial}{\partial\xi_j}\left\{\frac{\xi^k}{\xi^2}\Big[1-\mathcal{K}(\xi)\Big]\right\}\\
&\quad +e_{\rm H}\upsilon^2_{\rm H}\epsilon_{abc}\epsilon_{bik}\epsilon_{cjl}\frac{\xi^k\xi^l}{\xi^4}\Big[1-\mathcal{K}(\xi)\Big]^2\\
&=\; -e_{\rm H}\upsilon^2_{\rm H}\epsilon_{ajk}\left\{\left(\frac{\delta_i{}^k\xi^2-2\xi_i\xi^k}{\xi^4}\right)\Big[1-\mathcal{K}(\xi)\Big]-\frac{\xi^k}{\xi^2}\frac{\partial}{\partial\xi_i}\mathcal{K}(\xi)\right\}\\
&\quad +e_{\rm H}\upsilon^2_{\rm H}\epsilon_{aik}\left\{\left(\frac{\delta_j{}^k\xi^2-2\xi_j\xi^k}{\xi^4}\right)\Big[1-\mathcal{K}(\xi)\Big]-\frac{\xi^k}{\xi^2}\frac{\partial}{\partial\xi_j}\mathcal{K}(\xi)\right\}\\
&\quad +e_{\rm H}\upsilon^2_{\rm H}\big(\delta_{ak}\delta_{ci}-\delta_{ai}\delta_{ck}\big)\epsilon_{cjl}\frac{\xi^k\xi^l}{\xi^4}\Big[1-\mathcal{K}(\xi)\Big]^2\;,
\end{aligned} \tag{B.4}$$

where

$$\frac{\partial}{\partial \xi_{i,j}}\mathcal{K}(\xi) \;=\; \frac{\partial \xi}{\partial \xi_{i,j}}\frac{\partial}{\partial \xi}\mathcal{K}(\xi) \;=\; -\frac{\xi^{i,j}}{\xi}\frac{\partial}{\partial \xi}\mathcal{K}(\xi)\;. \tag{B.5}$$

It follows that

$$\begin{aligned} F^{ij}_{\mathrm{H}a} \;=\; e_{\mathrm{H}}\upsilon_{\mathrm{H}}^2\Bigg[-2\epsilon_{aij}\frac{1-\mathcal{K}}{\xi^2} + \big(\epsilon_{aik}\xi^j - \epsilon_{ajk}\xi^i\big)\frac{\xi^k}{\xi^3}\left(2\frac{1-\mathcal{K}}{\xi} + \frac{\partial \mathcal{K}}{\partial \xi}\right) \\ + \epsilon_{ijk}\frac{\xi^a\xi^k}{\xi^4}\big(1-\mathcal{K}\big)^2\Bigg]\;, \end{aligned} \tag{B.6}$$

where $\mathcal{K} = \mathcal{K}(\xi)$. Then, using Eqs. (2.10) and (B.6), one can find

$$\boldsymbol{B}^j_{\mathrm{H}}\cdot\boldsymbol{B}^j_{\mathrm{H}} \;=\; \frac{1}{2}F^{kl}_{\mathrm{H}a}F^{kl}_{\mathrm{H}a} \;=\; \frac{e_{\mathrm{H}}^2\upsilon_{\mathrm{H}}^4}{\xi^4}\left[\big(\mathcal{K}^2-1\big)^2 + 2\xi^2\left(\frac{\partial \mathcal{K}}{\partial \xi}\right)^2\right]\;. \tag{B.7}$$

On the other hand, we have

$$\begin{aligned} \mathcal{D}^j\phi_a \;&=\; e_{\mathrm{H}}\upsilon_{\mathrm{H}}\frac{\partial}{\partial \xi_j}\phi_a(\xi) + e_{\mathrm{H}}\epsilon_{abc}A^j_{\mathrm{H}b}(\xi)\phi_c(\xi) \\ &=\; e_{\mathrm{H}}\upsilon_{\mathrm{H}}^2\frac{\partial}{\partial \xi_j}\left[\frac{\xi^a}{\xi^2}\mathcal{H}(\xi)\right] - e_{\mathrm{H}}\upsilon_{\mathrm{H}}^2\epsilon_{abc}\epsilon_{bjk}\frac{\xi^k\xi^c}{\xi^4}\big[1-\mathcal{K}(\xi)\big]\mathcal{H}(\xi) \\ &=\; e_{\mathrm{H}}\upsilon_{\mathrm{H}}^2\left[\left(\frac{\delta_j{}^a\xi^2 - 2\xi_j\xi^a}{\xi^4}\right)\mathcal{H}(\xi) - \frac{\xi^j\xi^a}{\xi^3}\frac{\partial}{\partial \xi}\mathcal{H}(\xi)\right] \\ &\quad + e_{\mathrm{H}}\upsilon_{\mathrm{H}}^2\big(\delta_{aj}\delta_{ck} - \delta_{ak}\delta_{cj}\big)\frac{\xi^k\xi^c}{\xi^4}\big[1-\mathcal{K}(\xi)\big]\mathcal{H}(\xi) \\ &=\; e_{\mathrm{H}}\upsilon_{\mathrm{H}}^2\left\{\frac{\xi^j\xi^a}{\xi^4}\left[\mathcal{H}(\xi) - \xi\frac{\partial}{\partial \xi}\mathcal{H}(\xi)\right] + \big(\xi^j\xi^a - \delta^{ja}\xi^2\big)\frac{\mathcal{K}(\xi)\mathcal{H}(\xi)}{\xi^4}\right\}\;. \end{aligned} \tag{B.8}$$

Then,

$$\mathcal{D}^j\boldsymbol{\phi}\cdot\mathcal{D}^j\boldsymbol{\phi} \;=\; \frac{e_{\mathrm{H}}^2\upsilon_{\mathrm{H}}^4}{\xi^4}\left[\left(\mathcal{H} - \xi\frac{\partial \mathcal{H}}{\partial \xi}\right)^2 + 2\mathcal{K}\mathcal{H}\right]\;, \tag{B.9}$$

where $\mathcal{H} = \mathcal{H}(\xi)$. Finally, we have

$$\mathcal{V}(\phi) \;=\; \frac{1}{4}\lambda_\phi\big(\phi_a\phi_a - \upsilon_{\mathrm{H}}^2\big)^2 \;=\; \frac{\lambda_\phi\upsilon_{\mathrm{H}}^4}{4\xi^4}\big(\mathcal{H}^2-\xi^2\big)^2\;. \tag{B.10}$$

Plugging Eqs. (B.7), (B.9), and (B.10) into (2.30), we obtain

$$\begin{aligned} m_{\mathrm{M}} \;=\; \frac{4\pi\upsilon_{\mathrm{H}}}{e_{\mathrm{H}}}\int_0^\infty \frac{d\xi}{\xi^2}\Bigg[\xi^2\left(\frac{\partial \mathcal{K}}{\partial \xi}\right)^2 + \frac{1}{2}\left(\mathcal{H} - \xi\frac{\partial \mathcal{H}}{\partial \xi}\right)^2 + \frac{1}{2}\big(\mathcal{K}^2-1\big)^2 \\ + \mathcal{K}^2\mathcal{H}^2 + \frac{\lambda_\phi}{4e_{\mathrm{H}}^2}\big(\mathcal{H}^2-\xi^2\big)^2\Bigg]\;. \end{aligned} \tag{B.11}$$

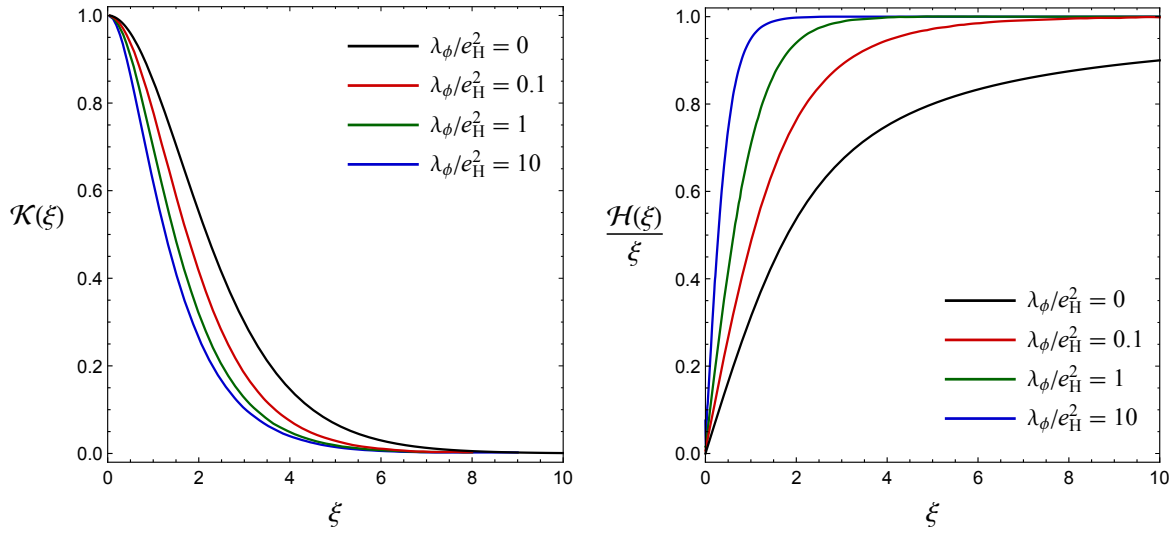

Figure B.1: The numerical solutions of $\mathcal{H}(\xi)$ and $\mathcal{K}(\xi)$ satisfied the boundary conditions.

This integration is finite provided that the following boundary conditions are satisfied

$$\begin{cases} \mathcal{H}(\xi) \to \xi\,, \quad \mathcal{K}(\xi) \to 0 \quad \text{as} \quad \xi \to \infty \\ \mathcal{H}(\xi) \to 0\,, \quad \mathcal{K}(\xi) \to 1 \quad \text{as} \quad \xi \to 0 \end{cases} . \tag{B.12}$$

Note that the first boundary condition leads to the asymptotic forms at spatial infinity and the second one ensures the fields are nonsingular at the origin. Now, by minimizing the total energy density in (B.11), we yield a coupled nonlinear equations of motion as

$$\xi^2 \frac{\partial^2 \mathcal{K}}{\partial \xi^2} = \mathcal{K}\mathcal{H}^2 + \mathcal{K}\left(\mathcal{K}^2 - 1\right)\,, \quad \xi^2 \frac{\partial^2 \mathcal{H}}{\partial \xi^2} = 2\mathcal{K}^2\mathcal{H} + \frac{\lambda_\phi}{e_{\rm H}^2}\mathcal{H}\left(\mathcal{H}^2 - \xi^2\right)\,. \tag{B.13}$$

This ordinary differential equation has no analytic solution. However, for $\lambda_\phi = 0$, Prasad and Sommerfield find a closed form with the correct boundary conditions as [100]

$$\mathcal{H}(\xi) = \frac{\xi}{\tanh \xi} - 1\,, \quad \mathcal{K}(\xi) = \frac{\xi}{\sinh \xi}\,. \tag{B.14}$$

Plugging the solution (B.14) into (B.11) and performing the integration, we obtain

$$m_{\rm M} = \frac{4\pi \upsilon_{\rm H}}{e_{\rm H}}\,. \tag{B.15}$$

Particularly, we call the monopole with $\lambda_\phi/e_{\rm H}^2 = 0$ the BPS monopole. For non-zero value of λ_ϕ, one has to solve (B.13) numerically, we present the results with different choices of $\lambda_\phi/e_{\rm H}^2$ in Fig. B.1. With this numerical solution, we can then evaluate the monopole mass depending on λ_ϕ, the result can be seen in Fig. B.2, where we define $m_{\rm M} = 4\pi\upsilon_{\rm H}\mathcal{F}(\beta)/e_{\rm H}$ with $\beta \equiv \lambda_\phi/e_{\rm H}^2$, and $\mathcal{F}(\beta)$ is a monotonically increasing function with $\mathcal{F}(0) = 1$ and $\mathcal{F}(\infty) \simeq 1.787$ [128].

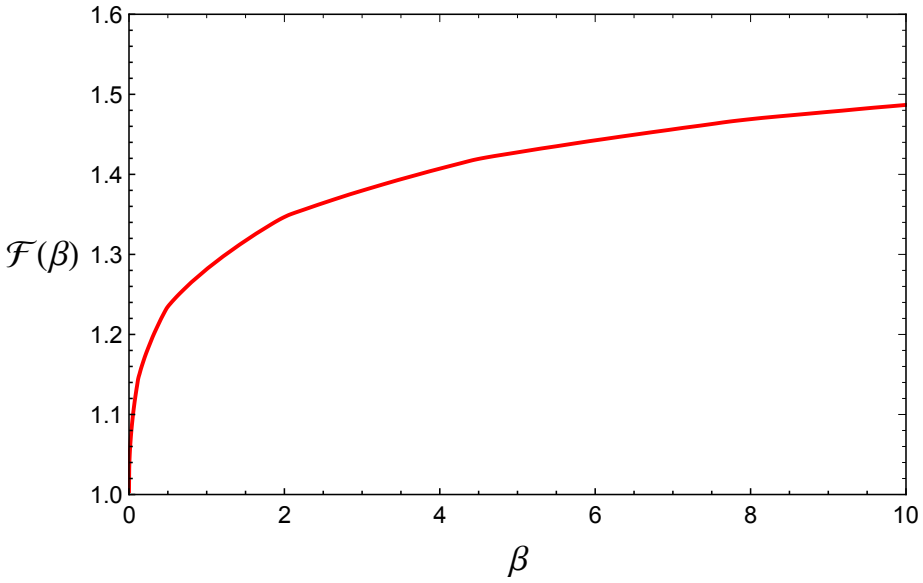

Figure B.2: The values of f as a function β, where $\beta \equiv \lambda_\phi / e_{\rm H}^2$.

With the configurations of the gauge field and the isocalar field in whole region, one can estimate the core radius $r_{\rm c}$ of the monopole. In the core region, the values of all the fields tend to zero, thereby, the energy density inside the core region is

$$\rho(r < r_{\rm c}) \sim \mathcal{V}(0) \sim \frac{1}{4}\lambda_\phi \upsilon_{\rm H}^4 \sim \frac{1}{4} e_{\rm H}^2 \upsilon_{\rm H}^4 \,, \tag{B.16}$$

here we have assumed $\lambda_\phi / e_{\rm H}^2$ is of order unity. On the other hand, the field configuration outside the core region is approximately given by the asymptotic forms, thus, the energy density is mainly contributed by the magnetic field as

$$\rho(r > r_{\rm c}) \sim \frac{1}{2} \boldsymbol{B}_{\rm H}^j \cdot \boldsymbol{B}_{\rm H}^j = \frac{1}{2 e_{\rm H}^2 r^4} \,. \tag{B.17}$$

The monopole mass is then estimated as

$$m_{\rm M} = \int_0^{r_{\rm c}} d^3 r \, \rho(r < r_{\rm c}) + \int_{r_{\rm c}}^{\infty} d^3 r \, \rho(r > r_{\rm c}) = \frac{1}{3} \pi r_{\rm c}^3 e_{\rm H}^2 \upsilon_{\rm H}^4 + \frac{2\pi}{e_{\rm H}^2 r_{\rm c}} \,. \tag{B.18}$$

Finding $r_{\rm c}$ to minimize the monopole mass gives

$$r_{\rm c} = \frac{2^{1/4}}{e_{\rm H} \upsilon_{\rm H}} \simeq \frac{1}{m_{W_{\rm H}}} \,, \tag{B.19}$$

and

$$m_{\rm M} \simeq \frac{2.2 \pi \upsilon_{\rm H}}{e_{\rm H}} \,, \tag{B.20}$$

which is consistent with the calculation in Eq. (B.15) up to some error.

Appendix C

The General Electric Charge of Dyon

Under particular gauge transformations, the monopoles can have the corresponding Noether charges, which can be identified with the electric charges. To derive the form of the Noether charges, let us first rewrite the covariant derivative as

$$\mathcal{D}^\mu \boldsymbol{\phi} \,=\, \partial^\mu \boldsymbol{\phi} + e_{\rm H} \boldsymbol{A}^\mu_{\rm H} \times \boldsymbol{\phi} \,=\, \partial^\mu \boldsymbol{\phi} + e_{\rm H} \big(\boldsymbol{J} \cdot \boldsymbol{A}^\mu_{\rm H} \big) \boldsymbol{\phi} \ , \tag{C.1}$$

where $\boldsymbol{J} = (J_1, J_2, J_3)$ is the generator vector with

$$J_1 \,=\, \begin{pmatrix} 0 & 0 & 0 \\ 0 & 0 & -1 \\ 0 & 1 & 0 \end{pmatrix} \ , \quad J_2 \,=\, \begin{pmatrix} 0 & 0 & 1 \\ 0 & 0 & 0 \\ -1 & 0 & 0 \end{pmatrix} \ , \quad J_3 \,=\, \begin{pmatrix} 0 & -1 & 0 \\ 1 & 0 & 0 \\ 0 & 0 & 0 \end{pmatrix} \ , \tag{C.2}$$

which satisfy the commutation relation, $[J_a, J_b] = \epsilon_{abc} J_c$. In this convention, the gauge transformarions left the Lagrangian invariant are given by

$$\boldsymbol{\phi} \,\to\, O \boldsymbol{\phi} \ , \quad \boldsymbol{J} \cdot \boldsymbol{A}^\mu_{\rm H} \,\to\, O \big(\boldsymbol{J} \cdot \boldsymbol{A}^\mu_{\rm H} \big) O^{\rm T} - \frac{1}{e_{\rm H}} \big(\partial^\mu O \big) O^{\rm T} \ , \tag{C.3}$$

where $O = \exp\big(\boldsymbol{J} \cdot \boldsymbol{\theta} \big)$ and $O^{\rm T} = O^{-1} = \exp\big(-\boldsymbol{J} \cdot \boldsymbol{\theta} \big)$ with $\boldsymbol{\theta}$ being an arbitrary rotation angle. By taking an infinitesimal rotation about the $\boldsymbol{\theta}$-axis, (C.3) becomes

$$\boldsymbol{\phi} \,\to\, \big(1 + \boldsymbol{J} \cdot \boldsymbol{\theta} \big) \boldsymbol{\phi} + \mathcal{O}(\boldsymbol{\theta}^2) \ , \quad \boldsymbol{A}^\mu_{\rm H} \,\to\, \boldsymbol{A}^\mu_{\rm H} - \frac{1}{e_{\rm H}} \mathcal{D}^\mu \boldsymbol{\theta} + \mathcal{O}(\boldsymbol{\theta}^2) \ . \tag{C.4}$$

Now, let us consider an operator $\hat{N}$ which generates gauge transformations about the direction of $\boldsymbol{\phi}$ in the scalar vacuum. By setting $\boldsymbol{\theta} = \boldsymbol{\phi} / \upsilon_{\rm H}$, we obtain

$$\boldsymbol{\phi} \,\to\, \boldsymbol{\phi} + \mathcal{O}(\boldsymbol{\theta}^2) \ , \quad \boldsymbol{A}^\mu_{\rm H} \,\to\, \boldsymbol{A}^\mu_{\rm H} - \frac{1}{e_{\rm H} \upsilon_{\rm H}} \mathcal{D}^\mu \boldsymbol{\phi} + \mathcal{O}(\boldsymbol{\theta}^2) \ . \tag{C.5}$$

Therefore, up to the first order of $\boldsymbol{\theta}$, we have

$$\delta \boldsymbol{\phi} \,=\, 0 \ , \quad \delta \boldsymbol{A}^\mu_{\rm H} \,=\, - \frac{1}{e_{\rm H} \upsilon_{\rm H}} \mathcal{D}^\mu \boldsymbol{\phi} \ . \tag{C.6}$$

With (C.6), the Noether charge $Q_{\rm N}$ as the eigenvalue of the operator $\hat{N}$ is calculated as

$$\begin{aligned} Q_{\rm N} &= \int d^3x \left[\frac{\partial \mathcal{L}_{\rm H}}{\partial(\partial_0 \boldsymbol{A}_{{\rm H}\mu})} \cdot \delta \boldsymbol{A}_{{\rm H}\mu} + \frac{\partial \mathcal{L}_{\rm H}}{\partial(\partial_0 \boldsymbol{\phi})} \cdot \delta \boldsymbol{\phi} \right] \\ &= \int d^3x \left[\frac{\partial \mathcal{L}_{\rm H}}{\partial(\partial_0 \boldsymbol{A}_{{\rm H}j})} \cdot \delta \boldsymbol{A}_{{\rm H}j} \right] \\ &= \frac{1}{e_{\rm H} v_{\rm H}} \int d^3x \, \boldsymbol{E}^j_{\rm H} \cdot \mathcal{D}^j \boldsymbol{\phi} \, = \, \frac{Q_{\rm E}}{e_{\rm H}} \, , \end{aligned} \tag{C.7}$$

where we have used Eq. (2.37) for the last equality. Because $e^{2\pi i \hat{N}}|0\rangle = e^{2\pi i Q_{\rm N}}|0\rangle = |0\rangle$, then the Noether charge is an integer. Thus, we have $Q_{\rm E} = n e_{\rm H}$ for some $n \in \mathbb{Z}$. In the presence of the CP-violating term (2.42), the Noether charge is modified as

$$\begin{aligned} Q_{\rm N} &= \frac{Q_{\rm E}}{e_{\rm H}} + \int d^3x \left[\frac{\partial \mathcal{L}_\theta}{\partial(\partial_0 \boldsymbol{A}_{{\rm H}j})} \cdot \delta \boldsymbol{A}_{{\rm H}j} \right] \\ &= \frac{Q_{\rm E}}{e_{\rm H}} + \frac{1}{e_{\rm H} v_{\rm H}} \frac{\theta_{\rm H} e_{\rm H}^2}{16\pi^2} \int d^3x \, \epsilon^{0jkl} \boldsymbol{F}^{kl}_{\rm H} \cdot \mathcal{D}^j \boldsymbol{\phi} \\ &= \frac{Q_{\rm E}}{e_{\rm H}} - \frac{1}{v_{\rm H}} \frac{\theta_{\rm H} e_{\rm H}}{8\pi^2} \int d^3x \, \boldsymbol{B}^j_{\rm H} \cdot \mathcal{D}^j \boldsymbol{\phi} \\ &= \frac{Q_{\rm E}}{e_{\rm H}} - \frac{\theta_{\rm H} e_{\rm H} Q_{\rm M}}{8\pi^2} \, = \, \frac{Q_{\rm E}}{e_{\rm H}} - \frac{\theta_{\rm H}}{2\pi} \, , \end{aligned} \tag{C.8}$$

where we have used Eq. (2.36). Then, the general electric charge of dyon is given by

$$Q_{\rm E} \, = \, \left(n + \frac{\theta_{\rm H}}{2\pi} \right) e_{\rm H} \, . \tag{C.9}$$

If CP is not violated, the dyons satisfy the Dirac quantisation

$$Q_{\rm E}({\rm M}) Q_{\rm M}({\rm M}) \, = \, 4\pi n \, . \tag{C.10}$$

On the other hand, in the ′t Hooft-Polyakov model with CP violation, the massive vector bosons and the monopoles satisfiy the Zwanziger-Schwinger quantisation condition as

$$Q_{\rm E}(W^\pm) Q_{\rm M}({\rm M}) - Q_{\rm E}({\rm M}) Q_{\rm M}(W^\pm) \, = \, \pm 4\pi \, . \tag{C.11}$$

Lastly, let us comment on the excited states of monopoles. The charge conservation allows the process ${\rm M}^* \to n W^\pm_{\rm H} + {\rm M}$ to occur if it is not kinematic forbidden, where ${\rm M}^*$ is the excited state of the monopole with the electric charge $Q_{\rm E} = n e_{\rm H}$. However, since $m_{{\rm M}^*} < n m_{W_{\rm H}} + m_{\rm M}$, thus ${\rm M}^*$ is stable, and then contribute to DM. Nevertheless, the masses of the excited monopoles are not very different from the ground state monopole. Therefore, they do not change our results too much.

Appendix D

Annihilation Cross-Section of the Hidden Massive Vector Bosons

The Lagrangian density relevant to annihilation of the hidden massive gauge bosons can be extracted from (2.1) with the field definitions (2.4) as

$$\begin{aligned}\mathcal{L}_{\mathrm{H}} \supset & -\frac{m_{\varphi}^2}{2v_{\mathrm{H}}}\varphi^3 + \frac{2m_{W_{\mathrm{H}}}^2}{v_{\mathrm{H}}}\varphi W_{\mathrm{H}}^{+\mu}W_{\mathrm{H}\mu}^{-} + \frac{m_{W_{\mathrm{H}}}^2}{v_{\mathrm{H}}^2}\varphi^2 W_{\mathrm{H}}^{+\mu}W_{\mathrm{H}\mu}^{-} \\ & + ie_{\mathrm{H}}\left(F_{\mathrm{H}\mu\nu}W_{\mathrm{H}}^{+\mu}W_{\mathrm{H}}^{-\nu} + W_{\mathrm{H}\mu\nu}^{+}W_{\mathrm{H}}^{-\mu}A_{\mathrm{H}}^{\nu} - W_{\mathrm{H}\mu\nu}^{-}W_{\mathrm{H}}^{+\mu}A_{\mathrm{H}}^{\nu}\right) \\ & - e_{\mathrm{H}}^2\left(W_{\mathrm{H}}^{+\mu}W_{\mathrm{H}\mu}^{-}A_{\mathrm{H}}^{\nu}A_{\mathrm{H}\nu} - W_{\mathrm{H}}^{+\mu}A_{\mathrm{H}\mu}W_{\mathrm{H}}^{-\nu}A_{\mathrm{H}\nu}\right) , \end{aligned} \tag{D.1}$$

where $F_{\mathrm{H}\mu\nu} = \partial_\mu A_{\mathrm{H}\nu} - \partial_\nu A_{\mathrm{H}\mu}$ and $W_{\mathrm{H}\mu\nu}^{\pm} = \partial_\mu W_{\mathrm{H}\nu}^{\pm} - \partial_\nu W_{\mathrm{H}\mu}^{\pm}$. The Feynman rule of each interaction vertex and propagators are shown in Fig. D.1. Then, the amplitudes of $W_{\mathrm{H}}^{+}W_{\mathrm{H}}^{-} \to \varphi\varphi$ and $W_{\mathrm{H}}^{+}W_{\mathrm{H}}^{-} \to \gamma_{\mathrm{H}}\gamma_{\mathrm{H}}$ are given by

$i\mathcal{M}_{W_{\mathrm{H}}^{+}W_{\mathrm{H}}^{-}\to\varphi\varphi} =$

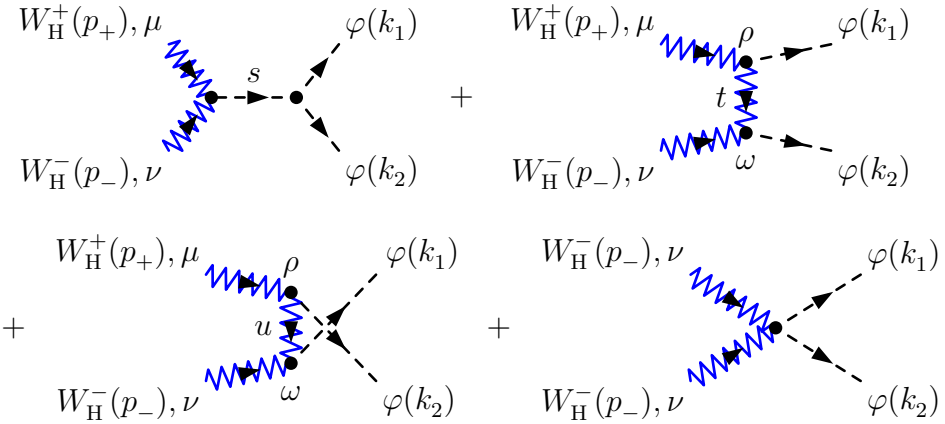

$$\begin{aligned} = & \; 2i\frac{m_{W_{\mathrm{H}}}^2}{v_{\mathrm{H}}^2}\left\{\left(1 + \frac{3m_{\varphi}^2}{s - m_{\varphi}^2}\right)g_{\mu\nu} + \frac{2m_{W_{\mathrm{H}}}^2}{t - m_{W_{\mathrm{H}}}^2}\left[g_{\mu\nu} - \frac{(p_+ - k_1)_\mu (p_+ - k_1)_\nu}{m_{W_{\mathrm{H}}}^2}\right]\right. \\ & \left. + \frac{2m_{W_{\mathrm{H}}}^2}{u - m_{W_{\mathrm{H}}}^2}\left[g_{\mu\nu} - \frac{(p_+ - k_2)_\mu (p_+ - k_2)_\nu}{m_{W_{\mathrm{H}}}^2}\right]\right\}\varepsilon^{\mu}(p_+, \lambda_+)\varepsilon^{\nu}(p_-, \lambda_-) , \end{aligned} \tag{D.2}$$

$$
i\mathcal{M}_{W_{\rm H}^+W_{\rm H}^-\to\gamma_{\rm H}\gamma_{\rm H}} =
$$

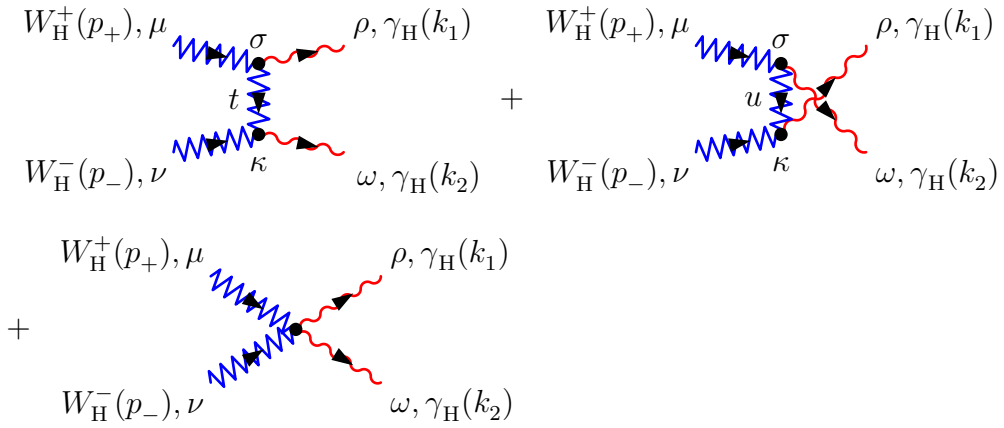

$$
\begin{aligned}
&= ie_{\rm H}^2 \Bigg\{ \Big[g_{\mu\sigma}(2p_+ - k_1)_\rho + g_{\sigma\rho}(2k_1 - p_+)_\mu - g_{\rho\mu}(p_+ + k_1)_\sigma \Big] \\
&\qquad \times \frac{1}{t - m_{W_{\rm H}}^2} \left[g^{\sigma\kappa} - \frac{(p_+ - k_1)^\sigma (p_+ - k_1)^\kappa}{m_{W_{\rm H}}^2} \right] \\
&\qquad \times \Big[g_{\kappa\nu}(k_2 - 2p_-)_\omega + g_{\nu\omega}(p_- + k_2)_\kappa + g_{\omega\kappa}(p_- - 2k_2)_\nu \Big] \\
&\qquad + \Big[g_{\mu\sigma}(2p_+ - k_2)_\omega + g_{\sigma\omega}(2k_2 - p_+)_\mu - g_{\omega\mu}(p_+ + k_2)_\sigma \Big] \\
&\qquad\quad \times \frac{1}{u - m_{W_{\rm H}}^2} \left[g^{\sigma\kappa} - \frac{(p_+ - k_2)^\sigma (p_+ - k_2)^\kappa}{m_{W_{\rm H}}^2} \right] \\
&\qquad\quad \times \Big[g_{\kappa\nu}(k_1 - 2p_-)_\rho + g_{\nu\rho}(p_- + k_1)_\kappa + g_{\rho\kappa}(p_- - 2k_1)_\nu \Big] \\
&\qquad - \big(2g_{\mu\nu}g_{\rho\omega} - g_{\mu\rho}g_{\nu\omega} - g_{\mu\omega}g_{\nu\rho} \big) \Bigg\} \\
&\qquad \times \varepsilon^\mu(p_+,\lambda_+)\varepsilon^\nu(p_-,\lambda_-)\varepsilon^{\rho*}(k_1,\lambda_1)\varepsilon^{\omega*}(k_2,\lambda_2) \ , \qquad \text{(D.3)}
\end{aligned}
$$

where $s = (p_+ + p_-)^2$, $t = (p_+ - k_1)^2$ and $u = (p_+ - k_2)^2$. One can check that (D.3) satisfies the Ward identity. The squared amplitudes with averaging (summing) over initial (final) polarizations in the nonrelativistic limit $\big($e.g. $s \approx 4m_{W_{\rm H}}^2$, $t \approx u \approx m_\varphi^2 - m_{W_{\rm H}}^2\big)$ are

$$
\begin{aligned}
\overline{\left|\mathcal{M}_{W_{\rm H}^+W_{\rm H}^-\to\varphi\varphi}\right|^2} &= \frac{1}{3}\cdot\frac{1}{3}\sum_{\lambda_+,\lambda_-}\left|\mathcal{M}_{W_{\rm H}^+W_{\rm H}^-\to\varphi\varphi}\right|^2 \\
&= \frac{16\big(11r^4 - 80r^3 + 240r^2 - 320r + 176\big)}{9(r-2)^2(r-4)^2} e_{\rm H}^4 \ , \qquad \text{(D.4)}
\end{aligned}
$$

$$
\overline{\left|\mathcal{M}_{W_{\rm H}^+W_{\rm H}^-\to\gamma_{\rm H}\gamma_{\rm H}}\right|^2} = \frac{1}{3}\cdot\frac{1}{3}\sum_{\lambda_+,\lambda_-}\sum_{\lambda_1,\lambda_2}\left|\mathcal{M}_{W_{\rm H}^+W_{\rm H}^-\to\gamma_{\rm H}\gamma_{\rm H}}\right|^2 = \frac{170}{9} e_{\rm H}^4 \ , \qquad \text{(D.5)}
$$

where $r \equiv m_\varphi^2/m_{W_{\rm H}}^2 = \lambda_\phi/(2\pi\alpha_{\rm H})$. Notice that the Lorenz condition $p_\mu\varepsilon^\mu(p) = 0$ for the gauge bosons $\big(W_{\rm H}^\pm,\ \gamma_{\rm H}\big)$ has been used in deriving (D.4) and (D.5).

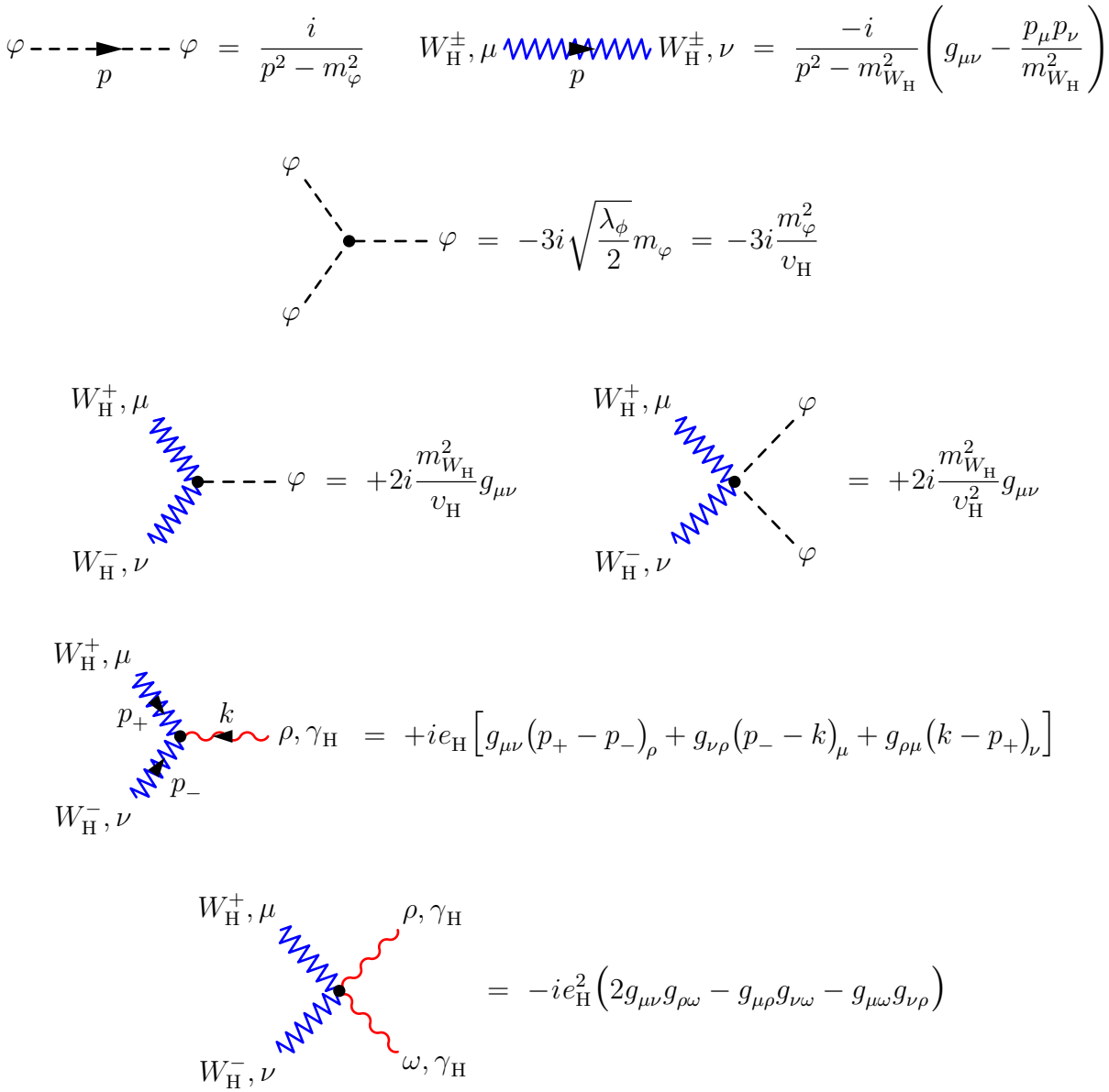

Figure D.1: The Feynman rules of the interaction vertices between $W_{\rm H}^\pm$ and $\varphi/\gamma_{\rm H}$.

It follows that the s-wave annihilation cross-section of the hidden massive gauge bosons up to order r^2 is

$$\begin{aligned}
\sigma_{\rm ann} v_{\rm rel} &= \sigma_{W_{\rm H}^+ W_{\rm H}^- \to \varphi\varphi} v_{\rm rel} + \sigma_{W_{\rm H}^+ W_{\rm H}^- \to \gamma_{\rm H}\gamma_{\rm H}} v_{\rm rel} \\
&= \frac{\pi\alpha_{\rm H}^2}{144 m_{W_{\rm H}}^2}\left(856 - 144r + 19r^2\right) + \mathcal{O}(r^3) \\
&= \frac{856 e_{\rm H}^4}{2304\pi m_{W_{\rm H}}^2} - \frac{24 e_{\rm H}^2 \lambda_\phi}{192\pi m_{W_{\rm H}}^2} + \frac{(19/9)\lambda_\phi^2}{64\pi m_{W_{\rm H}}^2} + \mathcal{O}(\lambda_\phi^3) \ , \qquad \text{(D.6)}
\end{aligned}$$

where the factor of $1/2$ is taken into account for identical particles in the final states. Our result slightly disagrees with Ref. [4].

Appendix E

Some Derivations in Chapter 3

E.1 The Derivation of $\widetilde{\theta}(\boldsymbol{q})$

The equation of motion of the axion field as a function of $z \equiv r_0/r$ is given by

$$\frac{d^2\theta(z)}{dz^2} = \theta(z) + \frac{z_m^4}{z^4}\big(\theta(z) - \theta_0\big) \,, \tag{E.1}$$

where $z_m \equiv \sqrt{m_a r_0} \ll 1$. With these definitions, the differential equation (E.1) takes the asymptotic form as

$$\frac{d^2\theta(z)}{dz^2} \simeq \begin{cases} \theta(z) & \text{for} \quad z > z_m \\ \\ \dfrac{z_m^4}{z^4}\big(\theta(z) - \theta_0\big) & \text{for} \quad z > z_m \end{cases} \,, \tag{E.2}$$

which has the analytical solution satisfied the boundary conditions $\theta(z \to \infty) = 0$ and $\theta(z \to 0) = \theta_0$ as

$$\theta(z) \simeq \begin{cases} \theta_0 \dfrac{(1+z_m)e^{z_m - z}}{1+2z_m} & \text{for} \quad z > z_m \\ \\ \theta_0\left(1 - \dfrac{e^{z_m}}{1+2z_m} z e^{-z_m^2/z}\right) & \text{for} \quad z < z_m \end{cases} \,. \tag{E.3}$$

From Eq. (3.13), the 3-dimensional Fourier transform of $\theta(\boldsymbol{x})$ can be expressed as

$$\widetilde{\theta}(\boldsymbol{q}) = \frac{4\pi r_0^3}{z_m^2 \epsilon_q} \int_0^{z_c} dz \, \frac{\theta(z)}{z^3} \sin\left(\frac{z_m^2 \epsilon_q}{z}\right) \,, \tag{E.4}$$

here we have defined $z_c \equiv r_0/r_c$, and

$$\epsilon_q \equiv \frac{|\boldsymbol{q}| r_0}{z_m^2} = \frac{|\boldsymbol{q}|}{m_a} = \left(\frac{m_N m_M}{m_N + m_M}\right)\frac{v_{DM}}{m_a} \simeq \frac{m_N}{m_a} v_{DM} \ll 1 \,. \tag{E.5}$$

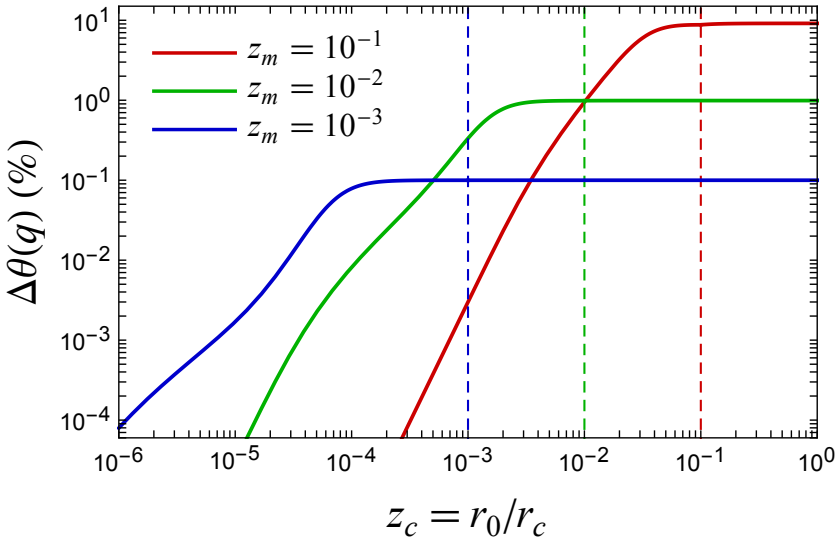

Figure E.1: $\Delta\theta(\boldsymbol{q})$ versus z_c with different values of z_m (color dashed lines).

Now, plugging Eq. (E.3) into Eq. (E.4) and taking a Taylor expansion in ϵ_q, we have

$$\begin{aligned}\widetilde{\theta}(\boldsymbol{q}) &= \frac{4\pi\theta_0 r_0^3}{z_m^2\epsilon_q}\lim_{\delta\to 0}\int_0^{z_c} dz\left(\frac{e^{-\delta/z}}{z^3}-\frac{e^{z_m}}{1+2z_m}\frac{e^{-z_m^2/z}}{z^2}\right)\sin\left(\frac{z_m^2\epsilon_q}{z}\right)\\ &\simeq -4\pi\theta_0 r_0^3\left[\frac{1}{3z_c^3}+\frac{z_c+z_m^2}{z_c z_m^4(1+2z_m)}e^{z_m(1-z_m/z_c)}\right]+\mathcal{O}(\epsilon_q^2)\ ,\end{aligned} \tag{E.6}$$

for $0 < z_c < z_m$, and

$$\begin{aligned}\widetilde{\theta}(\boldsymbol{q}) &= \frac{4\pi\theta_0 r_0^3}{z_m^2\epsilon_q}\left[\frac{(1+z_m)e^{z_m}}{1+2z_m}\int_{z_m}^{z_c} dz\,\frac{e^{-z}}{z^3}\sin\left(\frac{z_m^2\epsilon_q}{z}\right)\right.\\ &\qquad\left.+\lim_{\delta\to 0}\int_0^{z_m} dz\left(\frac{e^{-\delta/z}}{z^3}-\frac{e^{z_m}}{1+2z_m}\frac{e^{-z_m^2/z}}{z^2}\right)\sin\left(\frac{z_m^2\epsilon_q}{z}\right)\right]\\ &\simeq -4\pi\theta_0 r_0^3\left[\frac{e^{z_m}(1+z_m)}{3(1+2z_m)}\left(\frac{1}{z_c^3}-\frac{1}{z_m^3}\right)+\frac{2z_m^2+4z_m+3}{3z_m^4(1+2z_m)}\right]+\mathcal{O}(\epsilon_q^2)\ ,\end{aligned} \tag{E.7}$$

for $0 < z_m < z_c$. In the both integrations, we have inserted the regulator $\lim_{\delta\to 0} e^{-\delta/z}$ to absorb IR divergence at $z \to 0$. Next, let us take the Taylar expansion in z_m for Eqs. (E.6) and (E.7), we arrive at the same result

$$\widetilde{\theta}(\boldsymbol{q}) \simeq -4\pi\theta_0 r_0^3\left(\frac{1}{z_m^4}+\frac{1}{3z_c^3}\right)+\mathcal{O}(z_m^{-3}) \simeq -4\pi\theta_0\left(\frac{r_0}{m_a^2}+\frac{r_c^3}{3}\right)\ . \tag{E.8}$$

In Fig. E.1, we compare Eq. (E.8) with Eqs. (E.6) and (E.7) for $z_m < 1$, where $\Delta\theta(\boldsymbol{q})$ is the relative errors of Eqs. (E.6) and (E.7) to Eq. (E.8). One can see that $\Delta\theta(\boldsymbol{q})$ is very small as long as $z_m \ll 1$ regardless of the size of z_c.

E.2 The Derivation of $d\sigma_{W+\mathrm{N}\to W+\mathrm{N}}/d\Omega$

The effective Lagrangian describing the elastic scattering of the hidden gauge boson and a nucleon is given by

$$\mathcal{L}_{\mathrm{N}W} \;=\; \frac{\alpha_{\mathrm{H}}}{8\pi}\frac{m_{\mathrm{N}}}{m_a^2 f_a^2}\,\overline{\psi}_{\mathrm{N}} i\gamma_5 \psi_{\mathrm{N}} W_{\mathrm{H}}^{\pm\mu\nu}\widetilde{W}^{\mp}_{\mathrm{H}\mu\nu}\;, \tag{E.9}$$

from which the scattering amplitude of the hidden gauge boson to a nucleon is written as

$$\begin{aligned}\mathcal{M}_{W+\mathrm{N}\to W+\mathrm{N}} \;=\; &\frac{\alpha_{\mathrm{H}}}{4\pi}\frac{m_{\mathrm{N}}}{m_a^2 f_a^2}\,\overline{u}_{\mathrm{N}}(p'_{\mathrm{N}},s'_{\mathrm{N}})\gamma^5 u_{\mathrm{N}}(p_{\mathrm{N}},s_{\mathrm{N}})\\ &\times\,\epsilon_{\mu\nu\rho\sigma}p_W^{\mu}p_W'^{\rho}\varepsilon^{\nu}\big(p_W,\lambda_W\big)\varepsilon^{\sigma *}\big(p'_W,\lambda'_W\big)\;.\end{aligned} \tag{E.10}$$

The squared matrix element of the $W^{\pm}$-N scattering with averaging (summing) over the initial (final) spins and polarizations is calculated as follows

$$\begin{aligned}\overline{\big|\mathcal{M}_{W+\mathrm{N}\to W+\mathrm{N}}\big|^2} \;&=\; \frac{\alpha_{\mathrm{H}}^2}{16\pi^2}\frac{m_{\mathrm{N}}^2}{m_a^4 f_a^4}\left[-\frac{1}{2}\sum_{s_{\mathrm{N}},\,s'_{\mathrm{N}}}\overline{u}(p'_{\mathrm{N}},s'_{\mathrm{N}})\gamma^5 u(p_{\mathrm{N}},s_{\mathrm{N}})\,\overline{u}(p_{\mathrm{N}},s_{\mathrm{N}})\gamma^5 u(p'_{\mathrm{N}},s'_{\mathrm{N}})\right]\\ &\quad\times\Big(\epsilon_{\mu\nu\rho\sigma}\epsilon_{\bar{\mu}\bar{\nu}\bar{\rho}\bar{\sigma}}p_W^{\mu}p_W^{\bar{\mu}}p_W'^{\rho}p_W'^{\bar{\rho}}\Big)\\ &\quad\times\left[\frac{1}{3}\sum_{\lambda_W,\,\lambda'_W}\varepsilon^{\nu}\big(p_W,\lambda_W\big)\varepsilon^{\bar{\nu}*}\big(p_W,\lambda_W\big)\varepsilon^{\sigma *}\big(p'_W,\lambda'_W\big)\varepsilon^{\bar{\sigma}}\big(p'_W,\lambda'_W\big)\right]\\ &=\; -\frac{\alpha_{\mathrm{H}}^2}{96\pi^2}\frac{m_{\mathrm{N}}^2}{m_a^4 f_a^4}\,\mathrm{tr}\Big[\big(\not{p}'_{\mathrm{N}}+m_{\mathrm{N}}\big)\gamma^5\big(\not{p}_{\mathrm{N}}+m_{\mathrm{N}}\big)\gamma^5\Big]\\ &\quad\times\Big(\epsilon_{\mu\nu\rho\sigma}\epsilon_{\bar{\mu}\bar{\nu}\bar{\rho}\bar{\sigma}}p_W^{\mu}p_W^{\bar{\mu}}p_W'^{\rho}p_W'^{\bar{\rho}}\Big)\left(g^{\nu\bar{\nu}}-\frac{p_W^{\nu}p_W^{\bar{\nu}}}{m_{W_{\mathrm{H}}}^2}\right)\left(g^{\sigma\bar{\sigma}}-\frac{p_W'^{\sigma}p_W'^{\bar{\sigma}}}{m_{W_{\mathrm{H}}}^2}\right)\\ &=\; -\frac{\alpha_{\mathrm{H}}^2}{96\pi^2}\frac{m_{\mathrm{N}}^2}{m_a^4 f_a^4}\times 4\big(m_{\mathrm{N}}^2-p'_{\mathrm{N}}\cdot p_{\mathrm{N}}\big)\times 2\Big[\big(p_W\cdot p'_W\big)^2-p_W^2 p_W'^2\Big]\\ &=\; -\frac{\alpha_{\mathrm{H}}^2}{96\pi^2}\frac{m_{\mathrm{N}}^2}{m_a^4 f_a^4}\times 2q^2\times 2\left[\frac{1}{4}\big(q^2\big)^2-m_{W_{\mathrm{H}}}^2 q^2\right]\\ &=\; \frac{\alpha_{\mathrm{H}}^2}{24\pi^2}\frac{m_{\mathrm{N}}^2 m_{W_{\mathrm{H}}}^2}{m_a^4 f_a^4}\big(q^2\big)^2+\mathcal{O}\Big[\big(q^2\big)^3\Big]\;\simeq\;\frac{\alpha_{\mathrm{H}}^2}{24\pi^2}\frac{m_{\mathrm{N}}^2 m_{W_{\mathrm{H}}}^2}{m_a^4 f_a^4}|\boldsymbol{q}|^4\;.\end{aligned} \tag{E.11}$$

Then, the differential cross section of the hidden gauge boson scattering off a nucleon is

$$\frac{d\sigma_{W+\mathrm{N}\to W+\mathrm{N}}}{d\Omega}\;\simeq\;\frac{\overline{\big|\mathcal{M}_{W+\mathrm{N}\to W+\mathrm{N}}\big|^2}}{64\pi^2\big(m_{W_{\mathrm{H}}}+m_{\mathrm{N}}\big)^2}\;\simeq\;\frac{\alpha_{\mathrm{H}}^2}{1536\pi^4}\frac{m_{\mathrm{N}}^2}{m_a^4 f_a^4}|\boldsymbol{q}|^4\;, \tag{E.12}$$

which is suppressed in the fourth powers of the transferred momentum, and this is easy to undenstand since the Lagrangion (E.9) includes γ^5 and $\epsilon_{\mu\nu\rho\sigma}$, each giving out one $|\boldsymbol{q}|^2$.

Appendix F

The Combined Results for Other Benchmark Points

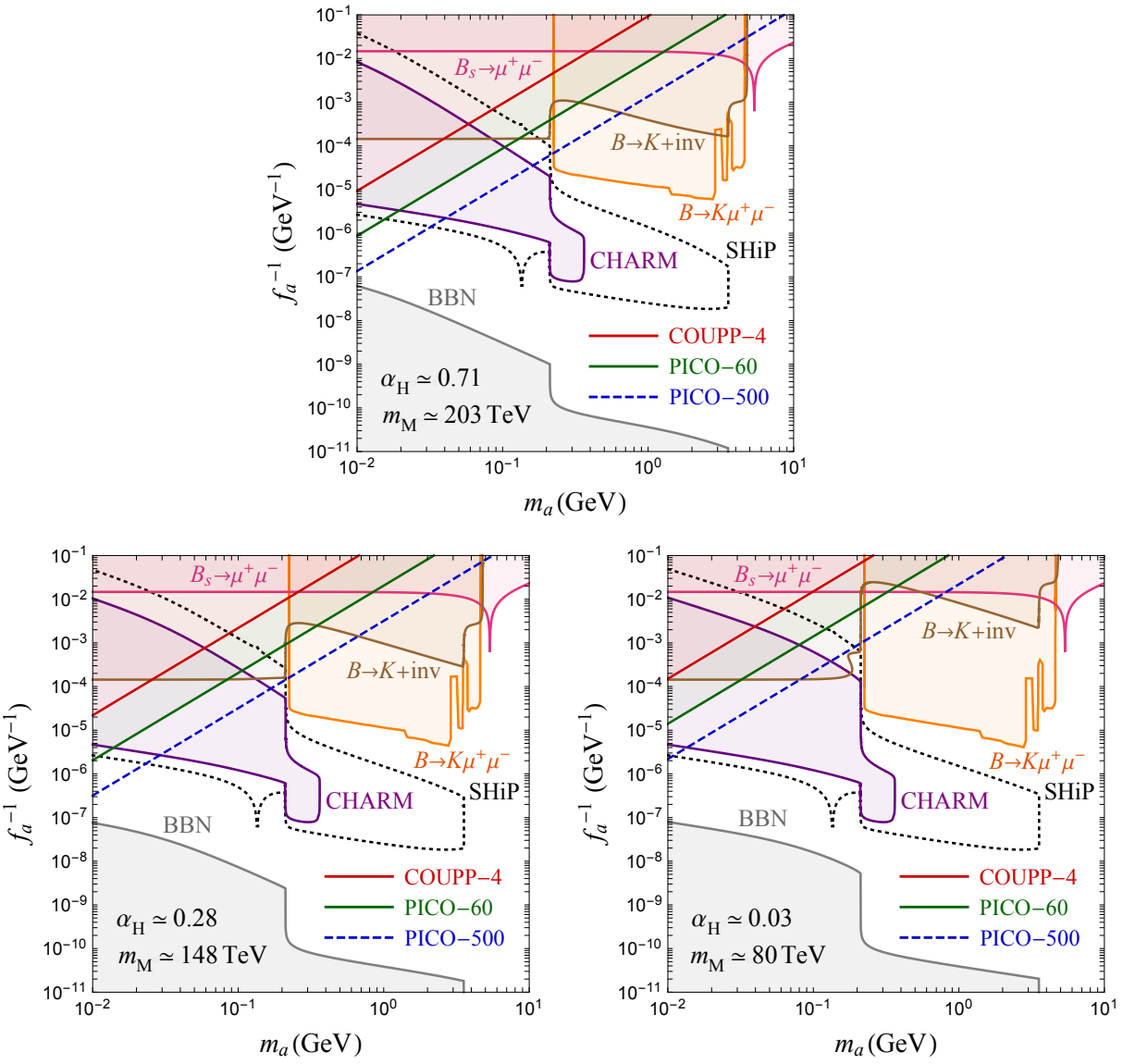

Figure F.1: The combined results for benchmark point 1, 2 and 4 with $\theta_0 = 1$.

Bibliography

[1] G. 't Hooft, Nucl. Phys. B **79**, 276 (1974). doi:10.1016/0550-3213(74)90486-6

[2] A. M. Polyakov, JETP Lett. **20**, 194 (1974) [Pisma Zh. Eksp. Teor. Fiz. **20**, 430 (1974)].

[3] S. Baek, P. Ko and W. I. Park, JCAP **10**, 067 (2014) doi:10.1088/1475-7516/2014/10/067 [arXiv:1311.1035 [hep-ph]].

[4] V. V. Khoze and G. Ro, JHEP **10**, 061 (2014) doi:10.1007/JHEP10(2014)061 [arXiv:1406.2291 [hep-ph]].

[5] M. Tanabashi *et al.* [Particle Data Group], Phys. Rev. D **98**, no. 3, 030001 (2018). doi:10.1103/PhysRevD.98.030001

[6] E. Witten, Phys. Lett. B **86**, 283 (1979) [Phys. Lett. **86B**, 283 (1979)]. doi:10.1016/0370-2693(79)90838-4

[7] G. Aad *et al.* [ATLAS], Phys. Lett. B **716**, 1-29 (2012) doi:10.1016/j.physletb.2012.08.020 [arXiv:1207.7214 [hep-ex]].

[8] S. Chatrchyan *et al.* [CMS], Phys. Lett. B **716**, 30-61 (2012) doi:10.1016/j.physletb.2012.08.021 [arXiv:1207.7235 [hep-ex]].

[9] N. Aghanim *et al.* [Planck], [arXiv:1807.06209 [astro-ph.CO]].

[10] B. Abbott *et al.* [LIGO Scientific and Virgo], Phys. Rev. Lett. **116**, no.6, 061102 (2016) doi:10.1103/PhysRevLett.116.061102 [arXiv:1602.03837 [gr-qc]].

[11] F. Englert and R. Brout, Phys. Rev. Lett. **13**, 321 (1964). doi:10.1103/PhysRevLett.13.321

[12] P. W. Higgs, Phys. Rev. **145**, 1156 (1966). doi:10.1103/PhysRev.145.1156

[13] G. S. Guralnik, C. R. Hagen and T. W. B. Kibble, Phys. Rev. Lett. **13**, 585 (1964). doi:10.1103/PhysRevLett.13.585

[14] J. Christenson, J. Cronin, V. Fitch and R. Turlay, Phys. Rev. Lett. **13**, 138-140 (1964) doi:10.1103/PhysRevLett.13.138

[15] M. Kobayashi and T. Maskawa, Prog. Theor. Phys. **49**, 652-657 (1973) doi:10.1143/PTP.49.652

[16] B. Pontecorvo, Sov. Phys. JETP **7**, 172-173 (1958)

[17] Z. Maki, M. Nakagawa and S. Sakata, Prog. Theor. Phys. **28**, 870-880 (1962) doi:10.1143/PTP.28.870

[18] P.A. Zyla et al. (Particle Data Group), to be published in Prog. Theor. Exp. Phys. 2020, 083C01 (2020).

[19] E. W. Kolb and M. S. Turner, Front. Phys. **69**, 1-547 (1990)

[20] P. F. de Salas and S. Pastor, JCAP **07**, 051 (2016) doi:10.1088/1475-7516/2016/07/051 [arXiv:1606.06986 [hep-ph]].

[21] T. Yanagida, Prog. Theor. Phys. **64**, 1103 (1980) doi:10.1143/PTP.64.1103

[22] A. Sakharov, Sov. Phys. Usp. **34**, no.5, 392-393 (1991) doi:10.1070/PU1991v034n05ABEH002497

[23] M. B. Gavela, P. Hernandez, J. Orloff and O. Pene, Mod. Phys. Lett. A **9**, 795-810 (1994) doi:10.1142/S0217732394000629 [arXiv:hep-ph/9312215 [hep-ph]].

[24] M. B. Gavela, P. Hernandez, J. Orloff, O. Pene and C. Quimbay, Nucl. Phys. B **430**, 382-426 (1994) doi:10.1016/0550-3213(94)00410-2 [arXiv:hep-ph/9406289 [hep-ph]].

[25] P. Huet and E. Sather, Phys. Rev. D **51**, 379-394 (1995) doi:10.1103/PhysRevD.51.379 [arXiv:hep-ph/9404302 [hep-ph]].

[26] V. A. Kuzmin, V. A. Rubakov and M. E. Shaposhnikov, Phys. Lett. B **155**, 36 (1985) doi:10.1016/0370-2693(85)91028-7

[27] W. Buchmuller, R. Peccei and T. Yanagida, Ann. Rev. Nucl. Part. Sci. **55**, 311-355 (2005) doi:10.1146/annurev.nucl.55.090704.151558 [arXiv:hep-ph/0502169 [hep-ph]].

[28] M. Fukugita and T. Yanagida, Phys. Lett. B **174**, 45-47 (1986) doi:10.1016/0370-2693(86)91126-3

[29] V. Rubakov and M. Shaposhnikov, Usp. Fiz. Nauk **166**, 493-537 (1996) doi:10.1070/PU1996v039n05ABEH000145 [arXiv:hep-ph/9603208 [hep-ph]].

[30] B. Graner, Y. Chen, E. Lindahl and B. Heckel, Phys. Rev. Lett. **116**, no.16, 161601 (2016) doi:10.1103/PhysRevLett.116.161601 [arXiv:1601.04339 [physics.atom-ph]].

[31] R. Peccei and H. R. Quinn, Phys. Rev. Lett. **38**, 1440-1443 (1977) doi:10.1103/PhysRevLett.38.1440

[32] R. Peccei and H. R. Quinn, Phys. Rev. D **16**, 1791-1797 (1977) doi:10.1103/PhysRevD.16.1791

[33] G. Jungman, M. Kamionkowski and K. Griest, Phys. Rept. **267**, 195-373 (1996) doi:10.1016/0370-1573(95)00058-5 [arXiv:hep-ph/9506380 [hep-ph]].

[34] N. Arkani-Hamed, A. Cohen, E. Katz and A. Nelson, JHEP **07**, 034 (2002) doi:10.1088/1126-6708/2002/07/034 [arXiv:hep-ph/0206021 [hep-ph]].

[35] E. W. Kolb and R. Slansky, Phys. Lett. B **135**, 378 (1984) doi:10.1016/0370-2693(84)90298-3

[36] C. Amole *et al.* [PICO Collaboration], Phys. Rev. D **100**, no. 2, 022001 (2019) doi:10.1103/PhysRevD.100.022001 [arXiv:1902.04031 [astro-ph.CO]].

[37] S. Weinberg, Phys. Rev. Lett. **40**, 223-226 (1978) doi:10.1103/PhysRevLett.40.223

[38] F. Wilczek, Phys. Rev. Lett. **40**, 279-282 (1978) doi:10.1103/PhysRevLett.40.279

[39] S. Borsanyi *et al.*, Nature **539**, no. 7627, 69 (2016) [arXiv:1606.07494 [hep-lat]].

[40] E. Berkowitz, M. I. Buchoff and E. Rinaldi, Phys. Rev. D **92**, no. 3, 034507 (2015) [arXiv:1505.07455 [hep-ph]].

[41] P. Petreczky, H. P. Schadler and S. Sharma, Phys. Lett. B **762**, 498 (2016) [arXiv:1606.03145 [hep-lat]].

[42] J. Frison, R. Kitano, H. Matsufuru, S. Mori and N. Yamada, JHEP **1609**, 021 (2016) [arXiv:1606.07175 [hep-lat]].

[43] Y. Taniguchi, K. Kanaya, H. Suzuki and T. Umeda, Phys. Rev. D **95**, no. 5, 054502 (2017) [arXiv:1611.02411 [hep-lat]].

[44] G. Grilli di Cortona, E. Hardy, J. Pardo Vega and G. Villadoro, The QCD axion, precisely, JHEP **1601**, 034 (2016) doi:10.1007/JHEP01(2016)034 [arXiv:1511.02867 [hep-ph]].

[45] J. Preskill, M. B. Wise and F. Wilczek, Phys. Lett. B **120**, 127 (1983).

[46] L. F. Abbott and P. Sikivie, Phys. Lett. B **120**, 133 (1983).

[47] M. Dine and W. Fischler, Phys. Lett. B **120**, 137 (1983).

[48] T. Hiramatsu, M. Kawasaki, K. Saikawa and T. Sekiguchi, Phys. Rev. D **85**, 105020 (2012) Erratum: [Phys. Rev. D **86**, 089902 (2012)] [arXiv:1202.5851 [hep-ph]].

[49] M. Kawasaki, K. Saikawa and T. Sekiguchi, Phys. Rev. D **91**, no. 6, 065014 (2015) [arXiv:1412.0789 [hep-ph]].

[50] L. Fleury and G. D. Moore, JCAP **1601**, 004 (2016) [arXiv:1509.00026 [hep-ph]].

[51] V. B. Klaer and G. D. Moore, JCAP **1711**, no. 11, 049 (2017) [arXiv:1708.07521 [hep-ph]].

[52] M. Gorghetto, E. Hardy and G. Villadoro, JHEP **1807**, 151 (2018) [arXiv:1806.04677 [hep-ph]].

[53] M. Kawasaki, T. Sekiguchi, M. Yamaguchi and J. Yokoyama, arXiv:1806.05566 [hep-ph].

[54] G. Ballesteros, J. Redondo, A. Ringwald and C. Tamarit, JCAP **1708**, no. 08, 001 (2017) [arXiv:1610.01639 [hep-ph]].

[55] R. Mayle, J. R. Wilson, J. R. Ellis, K. A. Olive, D. N. Schramm and G. Steigman, Phys. Lett. B **203**, 188 (1988).

[56] G. Raffelt and D. Seckel, Phys. Rev. Lett. **60**, 1793 (1988).

[57] M. S. Turner, Phys. Rev. Lett. **60**, 1797 (1988).

[58] T. Kobayashi, R. Kurematsu and F. Takahashi, JCAP **1309**, 032 (2013) [arXiv:1304.0922 [hep-ph]].

[59] A. Arvanitaki, S. Dimopoulos, S. Dubovsky, N. Kaloper and J. March-Russell, Phys. Rev. D **81**, 123530 (2010) [arXiv:0905.4720 [hep-th]].

[60] B. S. Acharya, K. Bobkov and P. Kumar, JHEP **1011**, 105 (2010) [arXiv:1004.5138 [hep-th]].

[61] M. Cicoli, M. Goodsell and A. Ringwald, JHEP **1210**, 146 (2012) [arXiv:1206.0819 [hep-th]].

[62] T. Higaki and F. Takahashi, JHEP **1407**, 074 (2014) [arXiv:1404.6923 [hep-th]].

[63] T. Higaki and F. Takahashi, Phys. Lett. B **744**, 153 (2015) [arXiv:1409.8409 [hep-ph]].

[64] N. Kitajima and F. Takahashi, JCAP **1501**, no. 01, 032 (2015) [arXiv:1411.2011 [hep-ph]].

[65] D. Cadamuro and J. Redondo, JCAP **1202**, 032 (2012) [arXiv:1110.2895 [hep-ph]].

[66] P. Arias, D. Cadamuro, M. Goodsell, J. Jaeckel, J. Redondo and A. Ringwald, JCAP **1206**, 013 (2012) [arXiv:1201.5902 [hep-ph]].

[67] S. J. Asztalos *et al.* [ADMX Collaboration], Phys. Rev. D **69**, 011101 (2004) [astro-ph/0310042].

[68] S. J. Asztalos *et al.* [ADMX Collaboration], Phys. Rev. Lett. **104**, 041301 (2010) [arXiv:0910.5914 [astro-ph.CO]].

[69] G. Carosi, A. Friedland, M. Giannotti, M. J. Pivovaroff, J. Ruz and J. K. Vogel, arXiv:1309.7035 [hep-ph].

[70] V. Anastassopoulos *et al.* [CAST Collaboration], Nature Phys. **13** (2017) 584 [arXiv:1705.02290 [hep-ex]].

[71] https://indico.in2p3.fr/event/16579/contributions/60840/attachments/47276/59399/Moriond.pdf

[72] E. Petrakou [CAPP/IBS Collaboration], EPJ Web Conf. **164**, 01012 (2017) [arXiv:1702.03664 [physics.ins-det]].

[73] A. Caldwell *et al.* [MADMAX Working Group], Phys. Rev. Lett. **118**, no. 9, 091801 (2017) [arXiv:1611.05865 [physics.ins-det]].

[74] Y. Kahn, B. R. Safdi and J. Thaler, Phys. Rev. Lett. **117**, no. 14, 141801 (2016) [arXiv:1602.01086 [hep-ph]].

[75] R. Bähre *et al.*, JINST **8**, T09001 (2013) [arXiv:1302.5647 [physics.ins-det]].

[76] E. Armengaud *et al.*, JINST **9**, T05002 (2014) [arXiv:1401.3233 [physics.ins-det]].

[77] A. Ayala, I. Domínguez, M. Giannotti, A. Mirizzi and O. Straniero, Phys. Rev. Lett. **113**, no. 19, 191302 (2014) [arXiv:1406.6053 [astro-ph.SR]].

[78] J. E. Kim, Phys. Rev. Lett. **43**, 103 (1979).

[79] M. A. Shifman, A. I. Vainshtein and V. I. Zakharov, Nucl. Phys. B **166**, 493 (1980).

[80] M. Dine, W. Fischler and M. Srednicki, Phys. Lett. **104B**, 199 (1981).

[81] A. R. Zhitnitsky, Sov. J. Nucl. Phys. **31**, 260 (1980) [Yad. Fiz. **31**, 497 (1980)].

[82] S. Y. Ho, K. Saikawa and F. Takahashi, JCAP **10**, 042 (2018) doi:10.1088/1475-7516/2018/10/042 [arXiv:1806.09551 [hep-ph]].

[83] S. Y. Ho, F. Takahashi and W. Yin, JHEP **04**, 149 (2019) doi:10.1007/JHEP04(2019)149 [arXiv:1901.01240 [hep-ph]].

[84] Y. Hochberg, E. Kuflik, T. Volansky and J. G. Wacker, Phys. Rev. Lett. **113**, 171301 (2014) doi:10.1103/PhysRevLett.113.171301 [arXiv:1402.5143 [hep-ph]].

[85] S. Y. Ho, T. Toma and K. Tsumura, JHEP **07**, 101 (2017) doi:10.1007/JHEP07(2017)101 [arXiv:1705.00592 [hep-ph]].

[86] P. Hut and K. A. Olive, Phys. Lett. **87B**, 144 (1979). doi:10.1016/0370-2693(79)90039-X

[87] S. Nussinov, Phys. Lett. **165B**, 55 (1985). doi:10.1016/0370-2693(85)90689-6

[88] K. M. Zurek, Phys. Rept. **537**, 91-121 (2014) doi:10.1016/j.physrep.2013.12.001 [arXiv:1308.0338 [hep-ph]].

[89] Ya.B. Zel'dovich and I.D. Novikov, Sov. Astron. **10**, 602 (1967).

[90] S.W. Hawking, Nature (London) **248**, 30 (1974).

[91] T. Harada, C. M. Yoo and K. Kohri, Phys. Rev. D **88**, no.8, 084051 (2013) doi:10.1103/PhysRevD.88.084051 [arXiv:1309.4201 [astro-ph.CO]].

[92] B. Carr, K. Kohri, Y. Sendouda and J. Yokoyama, [arXiv:2002.12778 [astro-ph.CO]].

[93] H. Niikura, M. Takada, N. Yasuda, R. H. Lupton, T. Sumi, S. More, T. Kurita, S. Sugiyama, A. More, M. Oguri and M. Chiba, Nature Astron. **3**, no.6, 524-534 (2019) doi:10.1038/s41550-019-0723-1 [arXiv:1701.02151 [astro-ph.CO]].

[94] W. Hu, R. Barkana and A. Gruzinov, Phys. Rev. Lett. **85**, 1158-1161 (2000) doi:10.1103/PhysRevLett.85.1158 [arXiv:astro-ph/0003365 [astro-ph]].

[95] T. W. B. Kibble, J. Phys. A **9**, 1387 (1976). doi:10.1088/0305-4470/9/8/029

[96] E. J. Weinberg, doi:10.1017/CBO9781139017787

[97] P. Goddard and D. I. Olive, Rept. Prog. Phys. **41**, 1357 (1978). doi:10.1088/0034-4885/41/9/001

[98] L. H. Ryder, Quantum Field Theory

[99] E. B. Bogomolny, Sov. J. Nucl. Phys. **24**, 449 (1976) [Yad. Fiz. **24**, 861 (1976)].

[100] M. Prasad and C. M. Sommerfield, Phys. Rev. Lett. **35**, 760-762 (1975) doi:10.1103/PhysRevLett.35.760

[101] J. S. Schwinger, Science **165**, 757 (1969). doi:10.1126/science.165.3895.757

[102] W. Fischler and J. Preskill, Phys. Lett. **125B**, 165 (1983). doi:10.1016/0370-2693(83)91260-1

[103] W. H. Zurek, Nature **317**, 505 (1985). doi:10.1038/317505a0

[104] H. Murayama and J. Shu, Phys. Lett. B **686**, 162 (2010) doi:10.1016/j.physletb.2010.02.037 [arXiv:0905.1720 [hep-ph]].

[105] G. Belanger, F. Boudjema, A. Pukhov and A. Semenov, Comput. Phys. Commun. **180**, 747 (2009) doi:10.1016/j.cpc.2008.11.019 [arXiv:0803.2360 [hep-ph]].

[106] F. Brummer and J. Jaeckel, Phys. Lett. B **675**, 360 (2009) doi:10.1016/j.physletb.2009.04.041 [arXiv:0902.3615 [hep-ph]].

[107] F. Brummer, J. Jaeckel and V. V. Khoze, JHEP **0906**, 037 (2009) doi:10.1088/1126-6708/2009/06/037 [arXiv:0905.0633 [hep-ph]].

[108] K. Kadota, T. Sekiguchi and H. Tashiro, arXiv:1602.04009 [astro-ph.CO].

[109] A. Stebbins and G. Krnjaic, arXiv:1908.05275 [astro-ph.CO].

[110] B. von Harling and K. Petraki, JCAP **12**, 033 (2014) doi:10.1088/1475-7516/2014/12/033 [arXiv:1407.7874 [hep-ph]].

[111] M. A. Buen-Abad and J. Fan, JHEP **12**, 161 (2019) doi:10.1007/JHEP12(2019)161 [arXiv:1911.05737 [hep-ph]].

[112] D. E. Kaplan and R. Rattazzi, Phys. Rev. D **93**, no.8, 085007 (2016) doi:10.1103/PhysRevD.93.085007 [arXiv:1511.01827 [hep-ph]].

[113] M. E. Peskin and D. V. Schroeder, An Introduction to quantum field theory,

[114] K. R. Dienes, J. Kumar, B. Thomas and D. Yaylali, Phys. Rev. D **90**, no. 1, 015012 (2014) doi:10.1103/PhysRevD.90.015012 [arXiv:1312.7772 [hep-ph]].

[115] E. Behnke *et al.* [COUPP Collaboration], Phys. Rev. D **86**, no. 5, 052001 (2012) Erratum: [Phys. Rev. D **90**, no. 7, 079902 (2014)] doi:10.1103/PhysRevD.86.052001, 10.1103/PhysRevD.90.079902 [arXiv:1204.3094 [astro-ph.CO]].

[116] https://indico.cern.ch/event/660187/contributions/2888067/attachments/1624996/2587371/Aspen_2018_Levine_PICO.pdf

[117] F. Bergsma *et al.* [CHARM], Phys. Lett. B **157**, 458-462 (1985) doi:10.1016/0370-2693(85)90400-9

[118] S. Alekhin, *et al.* [SHiP], Rept. Prog. Phys. **79**, no.12, 124201 (2016) doi:10.1088/0034-4885/79/12/124201 [arXiv:1504.04855 [hep-ph]]. LaTeX (US)

[119] M. J. Dolan, F. Kahlhoefer, C. McCabe and K. Schmidt-Hoberg, JHEP **1503**, 171 (2015) Erratum: [JHEP **1507**, 103 (2015)] doi:10.1007/JHEP07(2015)103, 10.1007/JHEP03(2015)171 [arXiv:1412.5174 [hep-ph]].

[120] A. Djouadi, Phys. Rept. **457**, 1 (2008) doi:10.1016/j.physrep.2007.10.004 [hep-ph/0503172].

[121] R. Ammar *et al.* [CLEO Collaboration], Phys. Rev. Lett. **87**, 271801 (2001) doi:10.1103/PhysRevLett.87.271801 [hep-ex/0106038].

[122] G. G. Raffelt, Phys. Rept. **198**, 1 (1990). doi:10.1016/0370-1573(90)90054-6

[123] G. G. Raffelt, Lect. Notes Phys. **741**, 51 (2008) [hep-ph/0611350].

[124] N. Bar, K. Blum and G. D'amico, arXiv:1907.05020 [hep-ph].

[125] F. D'Eramo, R. Z. Ferreira, A. Notari and J. L. Bernal, JCAP **1811**, 014 (2018) doi:10.1088/1475-7516/2018/11/014 [arXiv:1808.07430 [hep-ph]].

[126] A. G. Riess, S. Casertano, W. Yuan, L. M. Macri and D. Scolnic, Astrophys. J. **876**, no. 1, 85 (2019) doi:10.3847/1538-4357/ab1422 [arXiv:1903.07603 [astro-ph.CO]].

[127] F. Takahashi and M. Yamada, JCAP **1907**, no. 07, 001 (2019) doi:10.1088/1475-7516/2019/07/001 [arXiv:1904.12864 [astro-ph.CO]].

[128] J. Preskill, Ann. Rev. Nucl. Part. Sci. **34**, 461 (1984). doi:10.1146/annurev.ns.34.120184.002333